TABLE OF CONTENTS

TABLE OF CONTENTS (Continued)

18 AG

OVERPRESSURED MARINE SEDIMENTS

VOLUME I: THE PREDICTION OF HYDROFRACTURE AND K_o DURING DRILLING

Final Report for Phase III
for
U. S. Department of Interior
U. S. Geological Survey
U. S. G. S. Grant No. 14-08-0001-G-444

A report from the

Texas A&M Research Foundation
College Station, Texas
Project No. RF 3956

by

Louis J. Thompson
and
Michael Joseph Callanan
Texas A&M University
College Station, Texas
77843

May 5, 1981

This work was sponsored by the
U. S. G. S. as a part of the Research
Program in OSC Oil and Operations
Conservation Division
12201 Sunrise Valley Drive
Reston, Va. 22092
John Gregory - Program Manager

LIST OF TABLES

LIST OF TABLES (Continued)

LIST OF FIGURES (Continued)

LIST OF FIGURES

LIST OF FIGURES (Continued)

INTRODUCTION

Statement of the Problem

Abnormally high pore pressure zones in earth are found world wide. Such pressure occurs when pore fluid in the formation begins to support more of the overburden than just the fluid, i.e., not all the mineral weight above the formation is transmitted through the mineral matrix.

It has been thought that the pore pressure could not exceed the stress produced by the total weight of the overburden. However, experience in certain areas (Mississippi, Middle East, U.S.S.R., etc.) has shown that pore water pressures can exceed the overburden pressure, and are thought to be the major cause of blowouts and stuck drill stem (14).

When a well is drilled into a porous formation and its pore fluid pressure is greater than the bottom hole drilling fluid pressure, the formation pore water runs into the well bore. Dissolved gases in the pore water may come out of solution, mix with drilling fluid, and expand due to the reduced pressure. This reduces the specific gravity of the drilling fluid and further lowers the bottom hole drilling fluid pressure which permits even higher flow rates into the well bore. If the well is not quickly shut in by closing the blowout preventers a catastrophic blowout may occur.

Blowouts occur only from porous formations that have high

The style and format of this thesis follows that used by the Journal of the Geotechnical Engineering Division, American Society of Civil Engineers.

permeability. The shales or clays that lie above the high pressured formation may have an even higher pore fluid pressure than those in formation below them, but their permeability is so low that they pose no threat. If the high pressured shale formation can be recognized before the interbedded high pressured formations are penetrated, and the pore water pressure estimated, a blowout may be prevented.

It has been noticed that the shale formation on top of over-pressured sand formation usually has a low porosity and a high temperature. However, these indicators give no direct information for the pore pressure.

Condition of equilibrium may be used to estimate pore pressure. For a geostatic state of stress, the total vertical force on a plane must be in equilibrium with the vertical force in the mineral matrix plus the force in the water on that plane. It is known that a power law function of porosity can be used to represent the force in the mineral matrix. Furthermore, it is known that the force in the water is equal to the water pressure in the pore times the area of the water filled pore on the plane. This being the case, it appears reasonable to assume that the power law function, along with careful estimates of temperature and total geostatic vertical force, can be used to get a good estimate of pore pressure. To be used in this way, methods must be developed for finding the compressibility coefficients in the functions, and for determining the ratio of water area to total area on the plane. Since the compressibility of soil is related to other properties of the material, it might be possible to develop a relationship between it and Atterberg limits, porosity, percent clay and

temperature. It also appears reasonable to expect that these same parameters are related to the soil permeability and area ratio of water on the plane. If these relationships can be found, the pore pressure can be found from the power law function.

Objective

The purpose of the research is to determine how the compressibility and permeability of clays is related to the Atterberg limits, percent clay, and porosity, and how these relationships are affected by temperature.

Stresses in Overpressured Formations

The primary requirement for the existence of the overpressure formation is the existence of a seal. Normally, the seal formation is a thick layer of impermeable shale which acts as a pressure barrier which prevents the removal of the pore water and restricts the dissipation of the pore pressure. According to Costley (9), under such conditions the abnormal pore pressure will support a larger portion of the overburden and will reduce the compression pressure acting on the shale. The porosity of shale in the overpressure zone will be higher than that of the shale which is normally consolidated under the same depth of overburden. It has been suggested by Ruby and Hubbert (37), in accordance with Terzaghi's effective stress principle, that the compression pressure of the sediment can be determined by subtracting the water pressure from the total overburden pressure.

As cited by Bjerrum, Casagrande, Peck and Skemption (5), the classic effective stress definition was given by Terzaghi in 1923. The definition, analogous to the partial pressure in gases is:

$$\bar{\sigma} = \sigma - u \quad \ldots\ldots\ldots\ldots\ldots\ldots\ldots\ldots \quad (1)$$

where $\bar{\sigma}$ = the effective normal stress acting on a plane

σ = the total normal stress acting on a plane

u = the pore water pressure acting at the point of consideration

Essentially he assumed that the two stress fields can be superimposed even though they do not act on the same materials. Terzaghi contended that it was the effective stress that controlled the shear strength and density changes in soil. Many have assumed that the limiting case developed when the effective vertical stress is zero and that it is impossible for the pore pressure to exceed the geostatic or overburden stress (44). However, field tests and consideration of static equilibrium do not show this to be true.

Four different sets of field measurements in ocean bottom sediments made by different observer groups indicated that the pore water pressure may exceed the overburden so that the vertical effective stress is negative (4), (11), (16), (17). Some of these tests have been conducted for periods up to two years. Many measurements in oil wells in the Gulf of Mexico area show that the pore pressure may exceed the overburden stress over great areas, hundred of miles in extent. Pore pressures that exceed the overburden stress are not confined to the Gulf Coast area (13).

$\bar{\sigma}$ = the effective stress,

σ = the total stress,

and u = the pore pressure

From the geometry of the Mohr-Coulomb's failure envelope λ is defined as:

$$\lambda = \frac{(1 - \sin \phi_a')(\sin \phi_b')}{(1 - \sin \phi_b')(\sin \phi_a')}$$

ϕ_a' = the angle of shearing resistance obtained from the normal consolidated undrained test,

and ϕ_b' = the angle of shearing resistance obtained from the test with negative pore pressure.

Based on a model consisting of elastic and isotropic aggregate, Nur and Byerlee (33), in 1971, defined a new expression for effective stress:

$$\bar{\sigma} = \sigma - Mu \quad \ldots\ldots\ldots\ldots\ldots\ldots\ldots\ldots \quad (5)$$

where $\bar{\sigma}$ = the stress acting on the solid,

σ = the total stress,

M = parameter defined below,

and u = the pore water pressure.

By assuming that the strains of the rocks are linearly related to the pressures, the parameter, M, was derived as $(1 - \frac{H_c}{H_m})$, where H_c = the bulk modulus of the dry aggregate and, H_m = the intrinsic bulk modulus of the solid.

Nur and Byerlee's (33) simple compression and pore pressure tests

on Weber sandstone and Westerley granite found that the experimental result is better described by their effective stress expression. However, their effective stress expression is limited to elastic strain conditions; it does not include inelastic processes such as failure.

It has been shown that over any area of a saturated porous material equilibrium requires that (44):

$$F = F_m + F_w$$

also $$\sigma = f_m + un^E \quad \ldots\ldots\ldots\ldots\ldots\ldots\ldots\ldots \quad (6)$$

where F = the total force,

F_m = the force acting on the mineral,

F_w = the force acting on the water,

σ = the total stress acting on the total area of the sediment,

f_m = the force acting on the mineral grain per unit total cross-sectional area of the sediment,

u = the pore water pressure,

n = the porosity ratio,

and E = an area ratio parameter.

Under the extreme condition that the force acting on the mineral grain approaches zero and the water carries most of the load Eq. 6 becomes (44):

Upon re-examination it can be seen that the limiting case will develop when the force in the water is equal to the total overburden force (44). The force in the water is equal to the product of the water pressure and the area of the water space. When the force in the mineral matrix is zero, the force in the water is equal to the total stress divided by the area of the water. Since the sum of the area of the mineral and the area of the water must equal the total area and at no point in the soil is the water area as large as the total area, then the pore pressure must exceed the total overburden stress.

It is believed that the classic effective stress definition is not, in general, true for real rock because it does not consider the contact area of the mineral grain. Many have recognized this, and there have been several attempts to redefine the effective stress concept.

From the view of intergranular stress concept, Skempton (41), in 1961, theoretically derived two expressions for effective stress in fully saturated materials that govern the shear strength and the volume changes.

For shear strength:

$$\bar{\sigma} = \sigma - \left(1 - \frac{a \tan \psi}{\tan \phi}\right) u \quad \ldots\ldots\ldots\ldots\ldots\ldots \quad (2)$$

For volume change:

$$\bar{\sigma} = \sigma - \left(1 - \frac{C_s}{C_p}\right) u \quad \ldots\ldots\ldots\ldots\ldots\ldots \quad (3)$$

$\bar{\sigma}$ = the effective stress,

σ_t = the total stress,

u = the pore pressure,

a = the area ratio: $\frac{\text{area of grain to grain contact}}{\text{total area}}$

ψ = the angle of intrinsic shearing resistance,

ϕ' = the angle of shearing resistance of the porous material,

C_s = the compressibility of solid substance,

and C_p = the compressibility of porous material.

Based on the derived equation, Skempton (41) stated that "if the material is incompressible and purely cohesive, where $C_s = 0$ and $\psi = 0$ then Terzaghi's equation is rigorously true. However, Terzaghi's equation may not be generally applied to saturated rocks and concrete".

In 1970, Evan and Lewis (12) studied the effect of negative pore pressure on the shear strength of saturated clay, and two series of triaxial compression tests on a saturated silty soil were performed. First, the normally consolidated undrained test was performed and pore pressure was measured. Second, the same soil was tested with a negative pressure induced in the sample. Different values of cohesion, and the angle of shearing resistance were obtained. Based on the principle that the shear strength parameter of the soil should be the same regardless of the value of the pore pressure, a new expression for the effective stress was given for the negative pore pressure regime, that is:

$$\bar{\sigma} = \sigma - \lambda u \quad \ldots\ldots\ldots\ldots\ldots\ldots\ldots\ldots \quad (4)$$

$$u = \frac{1}{n^E} \quad \ldots\ldots\ldots\ldots\ldots\ldots\ldots\ldots\ldots\ldots \quad (7)$$

As n is always less than unity, n^E must always be less than unity. Consequently, the pore pressure can exceed the overburden stress while equilibrium is still maintained.

Since the total overburden force depends on the depth of the formation, it can be estimated by integrating the weight of sediment above the formation. Thus, if the area ratio parameter E in Eq. 6 is known, and if the force acting on the mineral can be estimated, the pore water pressure of the formation can be predicted by simply measuring the porosity of the sediment in the formation.

The change in the force acting on the sediment causes the decrease in the volume of the sediment. Initially when a load is applied to a soil-water mixture, the consolidation load is almost completely supported by the pore water. With the passage of time, the pore water dissipates and the force is transferred from the water to the soil structure. The flow of water from the voids results in the volumetric change (49).

Compressibility of the Sediment

Many researchers have related the consolidation stress to the pore space of the sediments and their stress and strain relationships are herein given.

In 1940, Macey (28) investigated the properties of the plastic mixture of clay and he suggested that the compression pressure can be described by an exponential function in terms of the equilibrium

moisture content of the clay sample.

$$\bar{\sigma} = \alpha e^{-\beta w} \quad \ldots\ldots\ldots\ldots\ldots\ldots\ldots\ldots\ldots\ldots \quad (8)$$

$\bar{\sigma}$ = the compression pressure,

w = the moisture content,

α and β are the experimental constants.

In defining their consolidation theory in 1948, Terzaghi and Peck (47) used the plot of void ratio (e) versus the logarithm of effective stress ($\bar{\sigma}$) to represent the stress-strain behavior of soil. It is illustrated in Fig. 1 that the relationship between e and log $\bar{\sigma}$ for the "virgin" compression is linear. The slope of the straight line is defined as the compression index (C_c), in which

$$C_c = \frac{\Delta e}{\Delta \log \bar{\sigma}} \quad \ldots\ldots\ldots\ldots\ldots\ldots\ldots\ldots\ldots\ldots \quad (9)$$

where Δe = the change in void ratio,

and $\Delta \log \bar{\sigma}$ = the change in the logarithm of the effective stress corresponding to Δe.

In 1960, Akagi (1) showed that the e-log $\bar{\sigma}$ curves were linear, even up to a pressure of about 28,000 psi (193,000 kN/m^2). For the non-marine sediments represented in his tests. Through examination of hundreds of curves and various high pressure consolidation tests on marine sediment, Katherman and Bryant (18), in 1978, found that at pressures approaching 7,000 to 10,000 psi (48,300 to 69,000 kN/m^2) the e-log $\bar{\sigma}$ curve will become asymototic with respect to the log $\bar{\sigma}$ axis at zero void ratio.

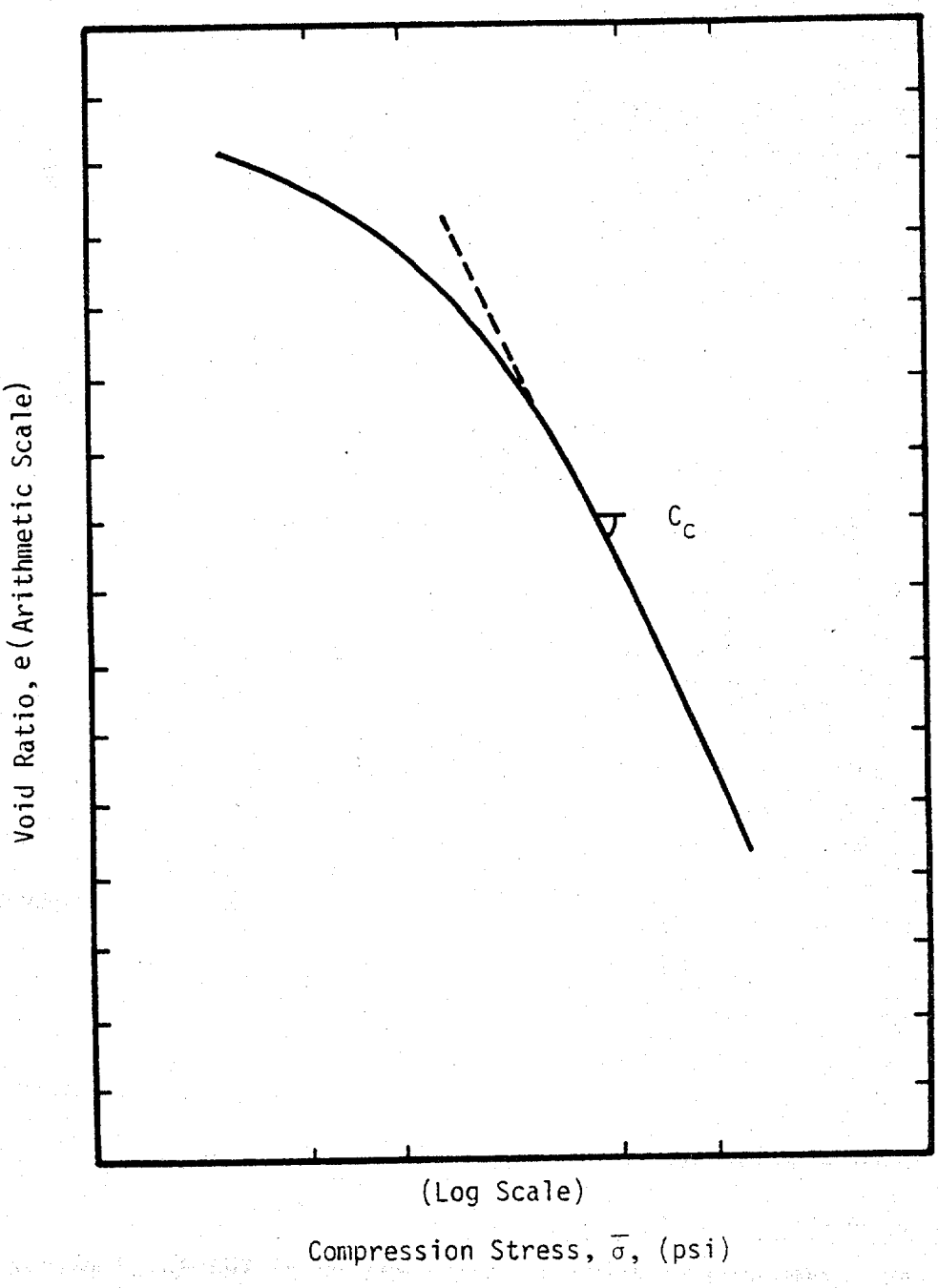

Fig. 1 - Typical Results of Consolidation Test

To overcome the difficulties inherent with the e-log $\bar{\sigma}$ plot for compressibility, other relationships involving porosity and compressive load have been tried. In 1927, Rubey (38) re-examined the data published by Hedberg and found that the laboratory determination of load and porosity follows a hyperbolic equation.

$$\sigma n^F = G \quad \ldots\ldots\ldots\ldots\ldots\ldots\ldots\ldots \quad (10)$$

σ = corresponds to the applied vertical compressive stress,

n = the observed porosity ratio,

F and G = constants reflecting the compressibility.

In 1959, Rubey and Hubbert (37) have theorized that the compression pressure acting on the soil matrix is a function of its porosity.

In 1979, both Thompson (46) and Miller (30) used a "power law" to relate the force acting on the mineral matrix and the porosity ratio of the sediment. Such relationship is identical to the one suggested by Rubey. The equation is given below:

$$f_m = An^B \quad \ldots\ldots\ldots\ldots\ldots\ldots\ldots\ldots \quad (11)$$

where f_m = the compression force acting on the solid matrix per unit total area,

n = the porosity ratio,

and A and B are the compressibility coefficients.

Thus, if Eq. 11 is substituted into Eq. 6 a relationship between

the pore pressure acting on the sediment and its porosity and total overburden stress is developed.

$$\sigma = An^B + un^E$$

to give

$$u = \frac{\sigma - An^B}{n^E} \quad \ldots\ldots\ldots\ldots\ldots\ldots\ldots\ldots \quad (12)$$

If the compressibility coefficients A and B can be related to the Atterberg limits of the sediment, the force acting on the mineral matrix can be estimated. If the parameter E can also be related to some mineral descriptors Eq. 12 will allow the downhole pore pressure, u, to be estimated.

SUMMARY OF PREVIOUS WORK

Relationship Between Compressibility and Atterberg Limits

The Atterberg limits are moisture contents of the remolded soil as determined by arbitrary tests. The tests supposedly differentiate between the liquid and plastic state (liquid limit), the plastic and the semisolid state (plastic limit), and the semisolid static and the solid state (shrinkage limit). As the amount of clay or the type of clay changes, these limits change. They give no indication of the condition of the material. They only indicate how much water is attracted to the surface of the soil particles. They have been used to classify clay soils since the time of World War II.

With a knowledge of both the percentage of clay and the Atterberg limits, the activity of the clay fraction can be calculated (25). The activity is a measure of the specific surface area of the clay which depends primarily on the type of clay mineral present in the soil.

For years engineers have tried to relate many of soil characteristics to the Atterberg limits. One of these characteristics is the compression index C_c as given by Eq. 9 and illustrated in Fig. 1. Because many people have empirically related the compression index, C_c, to the liquid limit, it seems reasonable that the compressibility coefficients A and B in the power law function of the porosity should also be related to the Atterberg limits. Some of the history of various attempts to relate the compression index and liquid limit is herein given.

Based on the information obtained from the field test and laboratory data, Skempton (42) in 1943, developed an empirical relationship

between the compression index and the liquid limit of clay which is expressed as follows:

$$C_c = 0.009\ (w_\ell - 10) \quad \ldots\ldots\ldots\ldots\ldots\ldots \quad (13)$$

w_ℓ is the liquid limit of the clay.

With the experimental data on samples from the Mississippi River, Sherman and Hadjidakis (40), in 1962, suggested that the compressibility index is related approximately to the liquid limit, with values generally increasing in direct proportion to the liquid limit. However, the discrepancy of the relationship increases at high liquid limits. The line of regression in the graph of compressibility index versus liquid limit is represented by:

$$C_c = 0.011\ (w_\ell - 16) \quad \ldots\ldots\ldots\ldots\ldots\ldots \quad (14)$$

During the same year regression analysis of test data by Cozzoline (10) also indicated that the compressibility indices of two Brazilian clays were related to their liquid limits by the following empirical equations:

$$C_c = 0.0046\ (w_\ell - 9) \pm 0.086 \quad \ldots\ldots\ldots\ldots\ldots \quad (15)$$

for motley clays from Sao Panlo City and

$$C_c = 0.0186\ (w_\ell - 30) \pm 0.41 \quad \ldots\ldots\ldots\ldots\ldots \quad (16)$$

for the soft silty clay from the lowlands of Santos.

In 1976, Azzouz, et al. (3) statistically analyzed the experimental data from more than 700 consolidation tests on a large variety of undisturbed samples. They established a regression equation in terms of liquid limit, w_ℓ, to predict the compressibility index, in which,

$$C_c = 0.006\ (w_\ell - 9) \quad \ldots\ldots\ldots\ldots\ldots\ldots \quad (17)$$

In the same year, Krizek and Salem (21), indicated that the compression indices of the dredged materials fall within a fairly narrow range even though the samples are quite diversified. It was observed that most of the examples have void ratios of nearly the same magnitude for the last three load increments of 8 psi (55 kN/m^2), 16 psi (110 kN/m^2) and 32 psi (220 kN/m^2). The values of the compressibility index for the different materials for this loading range are quite close together despite a large range of initial void ratios. This suggested to them that the observed homogeneity in consolidation response is related to the relative uniformity in general chemical composition and the grain size of the different dredging specimens.

It is evident that the compressibility characteristic of clay is related to its Atterberg limits; however, all the correlations are based on the experimental data on relatively low pressure consolidation tests. Many of the empirical relationships are found on rather homogeneous specimens, or samples obtained from a specific origin. Thus, an investigation of high pressure consolidation for samples that have widely different Atterberg limits is needed.

The Effect of Mineral Composition on Permeability of Clay

No direct relationship between the permeability of clay and its Atterberg limits has been established. Nevertheless, the influence of mineral composition of clay on its permeability has been investigated. In 1954, Lambe (22) compared previous measurements on the permeability of soil with different minerals and various exchangeable cations. He indicated that the magnitude of permeability varies widely with soil composition. As shown in Fig. 2, the permeability of the minerals are in the following order: montmorillonite < attapulgite < kaolinite. Also, the permeability of the clay minerals varies with different types of exchangeable ions. According to Smith and Stallman (43), the ion exchange capacity of clay samples has a significant effect on their permeability. On the other hand, Mitchell (31) suggests that the liquid limit of clay greatly depends on the type of cation that surrounds the clay particles. It is noted by Terzaghi (44) that "The results of the simplified soil tests (Atterberg limits) depend precisely on the same physical factors which determine the resistance and the permeability of soil (shape of particles; effective size, and uniformity) only in a far more complex manner." Hence, it seems that permeability of the sediment may be related to its Atterberg limits.

Permeability as a Function of the Porosity Ratio

The permeability of soil is the property that describes the resistance to the flow of a liquid through soil. The rate of flow

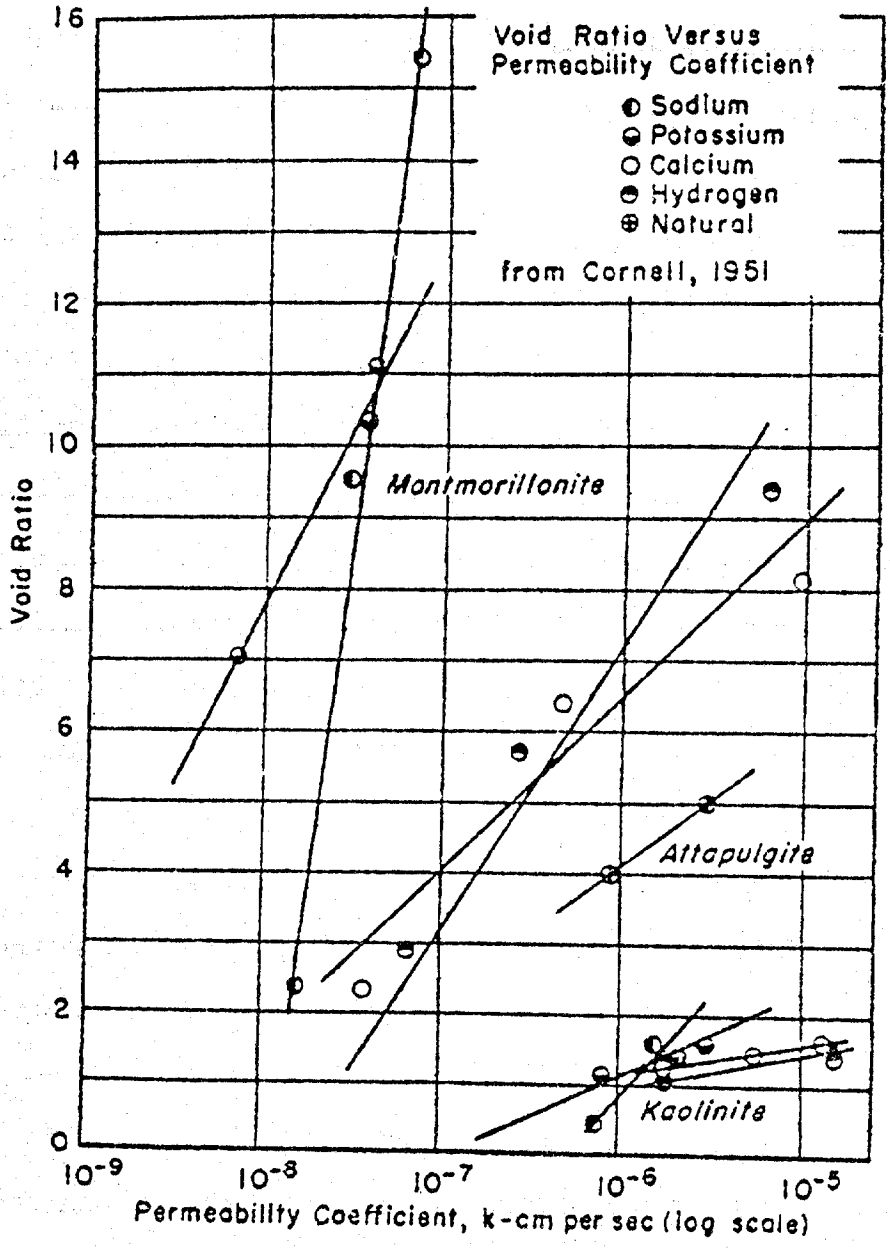

Fig. 2 - Void Ratio Versus Permeability - Refer to Lambe (22).

through the soil is given by Darcy's law (49). It is

$$q = kiA_t \quad \ldots\ldots\ldots\ldots\ldots\ldots\ldots\ldots \quad (18)$$

where q = flow rate through the soil,

i = hydraulic gradient. It is defined as the last in total head per unit length of microscopic flow path.

k = coefficient of permeability

A_t = total area of soil and water.

Since the flow rate depends on the size of the void, many researchers (19, 25) have recognized that porosity has a substantial influence on the permeability. Since moisture content, void ratio and porosity are all directly related for saturated soils, many have chosen to represent their results in terms of moisture content or void ratio.

In 1940, Macey (28) compared the permeability of clay at different moisture contents and suggested that the permeability of clay can also be represented by an exponential function in terms of its moisture content.

$$k = A_o e^{wB_o} \quad \ldots\ldots\ldots\ldots\ldots\ldots\ldots\ldots \quad (19)$$

where k is the permeability

w is the moisture content

A_o, B_o are the experimental constants

In 1950, Archie (2) published the relationship between the

permeability and porosity for various rock formations. Straight line relationships were shown for different formations when the permeability and porosity data were plotted on semi-log paper.

As cited by Wu (49), Carman in 1956 improved the equation proposed by Kozeny and established the Kozeny-Carman equation.

$$k = C_k \frac{n^3}{(1-n)^2} \quad \ldots\ldots\ldots\ldots\ldots\ldots\ldots\ldots \quad (20)$$

k is the permeability

C_k is a factor depending on the pore shape, specific surface area and the ratio of length of actual flow path to soil bed thickness.

n is the porosity ratio.

Although this equation works very well for the description of permeability in cohesionless soil, it is less successful for clays.

In 1977, Thompson et al. (47) empirically established a "power law" relationship between the porosity and permeability for the marine sediments, in which

$$k = Cn^D \quad \ldots\ldots\ldots\ldots\ldots\ldots\ldots\ldots \quad (21)$$

where k is the permeability

n is the porosity ratio

C and D are the permeability constants

The Effect of Temperature on the Compressibility of Clay

Temperature increases with depth from the surface of the earth to its center. The temperature gradient with depth may vary from different geological locations. Lewis and Rose (27) suggested that the temperature gradient along the Texas Gulf coast ranged from 1.6 to 2.2^{o}F/100 ft (2.7 to 3.7^{o}C/100 m). Thus, the temperature of the sediment at great depth is much higher than the normal temperature on the earth surface. In order to simulate the field conditions in the laboratory a study on the effect of temperature on the consolidation of the soil sample is necessary.

In 1949, Burmister (7) noted that " . . . appreciable temperature variations affect the slope of the pressure-void ratio curve, making the slope flatter for temperature effects."

Based on test results from the investigation of temperature effect on the consolidation characteristic of clay, Finn (15) in 1951, stated that for a specific pressure increment, the amount of compression of a clay stratas is independent of temperature.

From experiments performed on the Boston blue clay, T. W. Lambe (24), in 1958 concluded that, under constant load, the clay shrank with a temperature increase and expanded with the temperature decrease. The volume changes were exactly those expected from the effect of temperature on the double layer, since an increase in temperature will depress the double layer and a decrease will expand it.

From consolidation tests performed at constant temperature, Paaswell (35), in 1965, concluded that a significant increase in temperature (about 86^{o}F (30^{o}C)) is necessary to produce a noticeable change in the amount of consolidation.

In 1968, direct measurement of changes in particle spacing with variations in temperature in a monmorillonite slurry subjected to low stresses were reported by Yong et al. (50). They observed volume increases in sodium montmorillonite as the temperature increased. The externally applied pressure of less than one atmosphere was held constant.

Triaxial consolidation tests on saturated remolded illite have been performed by Campanella and Mitchell (8) in the same year. These show significant volume decrease with an increase in temperature. The results also indicate that the compression index of remolded illite is essentially independent of temperature. However, as in Boyle's law, the higher the temperature of the clay, the lower the porosity at any given consolidation pressure.

During the next year, Plum and Esrig (36) suggested that the behavior of soil under a particular temperature is governed by the applied effective stress and the stress history; altering the temperature of a soil specimen can produce an effect similar to the change in stress history. From consolidation tests performed at various temperatures on new field clay and illite, they concluded that the compressibility changes are most notable in soft soils consolidated under small stress. However, at applied stresses in excess of about 30 psi, an increase in temperature appeared to produce insignificant changes in compressibility.

Therefore, it seems that thermal effect on the consolidation characteristics of clay arouses different opinions. In general, most researchers agree that a temperature increase causes a decrease in

volume of soil if it can drain. However, all of the experiments were performed under relatively low consolidation pressures. The temperature effect on the compressibility characteristics of clay under high pressure consolidation is still unknown. Such knowledge would be beneficial to the study of the engineering properties of the progressive burial sediments.

Effect of Temperature on the Permeability of Clay

Temperature affects the viscosity of fluid which controls the flow rate. Hence, the permeability of the sediment is also affected by the change in temperature.

In 1962, Leonards (26) compared Darcy's law of permeability with the Hagen-Poisenilles equation of flow. He pointed out that the fluid's influence can be expressed by the ratio of its unit weight to its absolute viscosity. He credits Notting (32) for suggesting the use of absolute permeability, in which,

$$K = k \frac{\mu}{\gamma} \quad \ldots\ldots\ldots\ldots\ldots\ldots\ldots\ldots\ldots\ldots \quad (22)$$

K is the absolute permeability and has dimensions of $(\text{length})^2$,

γ is the unit weight of the fluid,

μ is the viscosity of the fluid,

and k is the coefficient of permeability based on Darcy's law, and has dimensions of (lenght/time).

Others (25), (49) corrected the coefficient of permeability for the change of viscosity at various temperature and reported at $68^{o}C$ ($20^{o}C$)

by the multiplication of a conversion factor.

$$K_{20} = k_T \left(\frac{\mu_{20}}{\mu_T}\right) \quad \ldots\ldots\ldots\ldots\ldots\ldots\ldots\ldots\ldots\ldots \quad (23)$$

where K_{20} is the coefficient of permeability at 68^oF (20^oC),

μ_{20} is the viscosity of water at 68^oF (20^oC),

k_T is the coefficient of permeability at T^oC,

and μ_T is the viscosity of water at T^oC.

Such conversion eliminates the effect of temperature on the permeant and allows the measured permeability data between different type of soils to be compared. However, thermal effects on the mineral matrix of the sediment are not eliminated by this correction.

The overpressured marine sediment is located not only in a high pressure and temperature environment; it is also associated with sea water so that there can be chemical interaction between the salt water and the mineral particles.

In 1976, Kharaka and Smalley (20) investigated the effect on permeability of clay under different compaction pressures and temperatures. They used chloride solutions of alkali and alkali earth metals as the permeant. The permeability of bentonite compacted to 7,000 psi (48,300 kN/m^2) and 10,000 psi (68,000 kN/m^2) at 77^oF (25^oC) was found to be 4.0×10^{-13} cm/sec and 1.6×10^{-13} cm/sec respectively. At 122^oF (50^oC) and 176^oF (80^oC), the permeability of the bentonite compacted to 7,000 psi (48,300 kN/m^2) was found to be 6.1×10^{-13} cm/sec and 8.0×10^{-13} cm/sec respectively. The results showed the permeability decreasing with increasing compaction pressure, but

Permeability

The coefficient of permeability depends upon the size and extent of the path of the fluid flow and the reluctance of the fluid to move (i.e. viscosity). The smaller the void and the higher the viscosity of the fluid in the pore, the greater the resistance to the flow. Since the viscosity of the water in the clay is influenced by the interacting force between the water molecules and the clay particles, the permeability is also affected by the electrostatic force produced by the clay particles.

Atterberg Limits

Atterberg limits are the water contents at which soil consistency changes from one state to another. Liquid limit is the water content at which the soil on two sides of a groove flows together after the dish which contains the soil has been dropped 25 times through the distance of 0.39 in. (1 cm) (25). In a microscopic point of view, Wankentin (48), in 1961, noted the "liquid limit can be regarded as the water content at which sufficient free water is present to allow clay particles to slip past one another under a certain applied force. It can also be explained as the distance between the structural units of the particles at which the interacting force between the clay particles becomes weak enough to allow easy movement of particles related to each other." Therefore, liquid limit may be used to describe the interacting force between the clay particles, or the electrostatic force produced by the clay particles.

Plastic limit is the water content at which a soil begins to

crumble when it is rolled into a one-eighth in. (0.31 cm) diameter thread. Other than a lower boundary of the range of water contents within which soil exhibits plastic behavior, the physical significance of the plastic limit is not as apparent as that of the liquid limit (39). It was suggested by Terzaghi that, "for moisture contents equal to or smaller than the plastic limit the physical properties of the water are no longer identical with those of free or ordinary water" (44). Nevertheless, the plastic limit is a good indication of the clay-mineral composition of a soil and the amount of clay content in the soil sample.

The compressibility characteristics, permeability and the liquid limit of clay are influenced by the electrostatic force of clay particles. Thus, it seems that both the compressibility characteristic and the permeability of clay may be related to their Atterberg limits.

The Effect of Temperature on the Compressibility and Permeability of Clay

An increase in temperature causes an increase in the internal energy of the soil system. Additional energy to the system will reduce the affinity of water molecules in the pore to the clay particles. The electrostatic force attracting the different types of water in the pore space decreases, and the water in the pore becomes less viscous. Thus, the internal resistance to the flow of water out of the soil system under a given consolidation pressure also decreases. As a result, an increase in temperature may cause a larger volumetric compression.

The effect of temperature on the permeability of clay seems to be

increasing with increasing temperature.

By comparing the filtration ratio (which is the ratio of the concentration of alkali and alkaline earth metals of the input solution to that of the output solution) with the flow rate at different temperatures, they concluded that the increase in permeability with temperature is equal to that expected from decrease in kinematic viscosity of water.

Kharaka and Smalley's (20) data are valuable in the study of marine sediment. However the data are given to describe the permeability of marine clay at various pressures and temperatures. Thus, a more thorough investigation is needed so that the permeability of marine clays at various porosities and temperatures can be better described.

PHYSICO-CHEMICAL THEORIES FOR BEHAVIOR OF CLAY

Compressibility

In the "Physico-chemical Analysis of the Compressibility of Pure Clay," Bolt (6) in 1956, stated that the compressibility of pure clay suspensions and pastes can be explained very well by the interaction between the electric double layer formed on the clay particles. In 1970, Olson and Mesic (34) suggested that the compressibility characteristics of clay are influenced by both the mechanical and physico-chemical effect. However, the degree of influence of both the mechanical effect and physico-chemical effect on the compressibility characteristics depends on the mineral composition of the clay. Clay minerals carry net negative charges which create an electric field around the clay sheets. These negative charges are balanced by cations, such as Na^{+} and Ca^{++}, which are held to the clay particles by electrostatic attraction. The dipole action of the water molecules provides positive and negative charged ends, and the molecules are attracted to the clay particles and cations.

It is theorized that this electromagnetic field causes the water molecules to turn into a viscous fluid. The viscosity depends on the distance of the water molecule from the clay particle and the concentration of the electrical charges on the clay particles. Water tends to be more viscous when the water molecules are held close to the clay particle, and when there is high concentration of electric charges on the clay particles (23).

On the basis of the relative magnitude of force between water and

more obvious. Permeability of clay depends on the rate of flow through the clay sample. With an increase in temperature the permeant becomes less viscous, hence, there is less resistance to the flow through the sample. The clay mineral at a given porosity becomes more permeable in a higher temperature environment.

EXPERIMENTAL PROGRAM

Equipment

Abnormally pressured formations are usually situated in relatively high temperature and pressure environments. To study the characteristics of different clay sediments, a high pressure consolidation system with a temperature control unit was built. The overall schematic of the system is illustrated in Fig. 4.

The system contains the following elements: consolidometer, loading device, heating unit, back pressure system and volume measuring device, and permeameter.

Consolidometer. - This unit is shown in Fig. 5. The fixed ring consolidometer was designed to withstand pressure in excess of 10,000 psi (69,000 kN/m^2). It is corrosion resistant, stainless steel having a diameter of 2-1/2 in. (6.35 cm). Lateral movement of the test specimen during consolidation is prevented by a 1/2 in. (1.27 cm) thick chamber wall. Friction is minimized by a machine-smoothed inside chamber. The load is applied through the piston which is sealed by a U-shaped teflon seal which can withstand high pressure and temperature (up to 392^oF (200^oC)). It produces less friction than an ordinary O-ring. Top and bottom drainage are provided by porous stones located in the piston and the base. Filter papers are used between the porous stones and the specimen to prevent the fine clay particles from entering the porous stone. A dial extensometer is attached to the piston to record the change in sample height while the consolidation test is in progress.

Loading device. - Consolidation pressure is provided by dead

soil, Kezdi (19) arbitrarily divided the water in clay into four types, as shown in Fig. 3. The four types of water are as follows:

a. Pore water. - Water that has the same physical and chemical properties of ordinary water. It is capable of moving under a hydraulic gradient.

b. Solvate water or double layer water. - Water that is attracted to the soil, and is subject to electrostatic, polar and ionic binding forces. The viscosity and density of water inside the double layer are greater than those of ordinary water.

c. Absorbed water. - Thin layer of water held as interlayer water by the clay minerals with an expanding-lattice structure. Since the absorption forces are extremely large, the absorbed water cannot be moved by normal hydrodynamic force.

d. Structural water. - Such water refers to the hydroxyl groups that constitute parts of the crystal structure. The structural water can only be removed by temperature that is high enough to cause the destruction of crystal structure.

When pressure is applied to a layer of saturated clay particles, water from between particles is forced out until the clay particles are separated by water of high enough viscosity to resist the applied stress (29). The clay mineral compressibility therefore depends on the resistance or viscosity of the double layer water which is controlled by the attractive force produced by the clay particles and the cations. Consequently, the compressibility of clay relies on the electrostatic force produced by the clay particles.

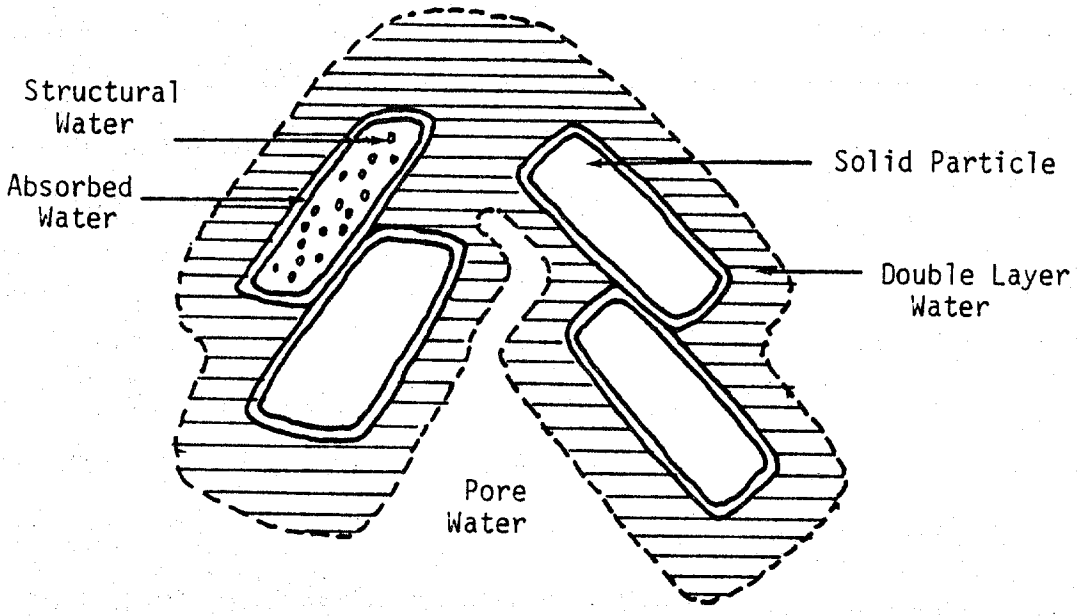

Fig. 3 - Classification of Water in Soil
(as taken from Kezdi (19))

weights acting through a lever system. The compound lever has a mechanical advantage or ratio of 1 to 100 which enables a small weight to produce a relatively high pressure. The dead weight lever system is inexpensive, simple and accurate, because 1) it does not require any high-capacity regulator, accumulator or pressure gauges; and 2) the applied pressure can be measured directly from the dead load on the hanger, no precalibration is required. A compensating lever at the top of the frame is used to counterbalance the weight of the lower lever beams. Therefore, the beams are in a free and balanced condition when there is no weight applied to the lever and the applied loads on the hanger are transferred to the soil specimen without any corrections.

Heating unit. - This unit is shown in Fig. 6. A one inch thick insulating fabric separates the steel double wall of the heating oil bath. Heat was applied by two electrical heating elements, enclosed in copper cases. One of the elements was bent in a circular shape which easily fits around the consolidometer. The other was located at the side of the oil bath to generate additional heat for test temperatures higher than 158°F (70°C). The heating elements were connected to rheostats to control the current passing through the elements. By adjusting the current the temperature of the oil bath was controlled. An electric motor-operated stirrer was used to maintain a uniform temperature inside the oil bath. The temperature was monitored throughout tests by means of a thermometer.

Back pressure and volume measuring device. - The top and bottom drainage pipe of the consolidometer were connected to a Wykeham-Farrance water and mercury pot back pressure device. This equipment is shown

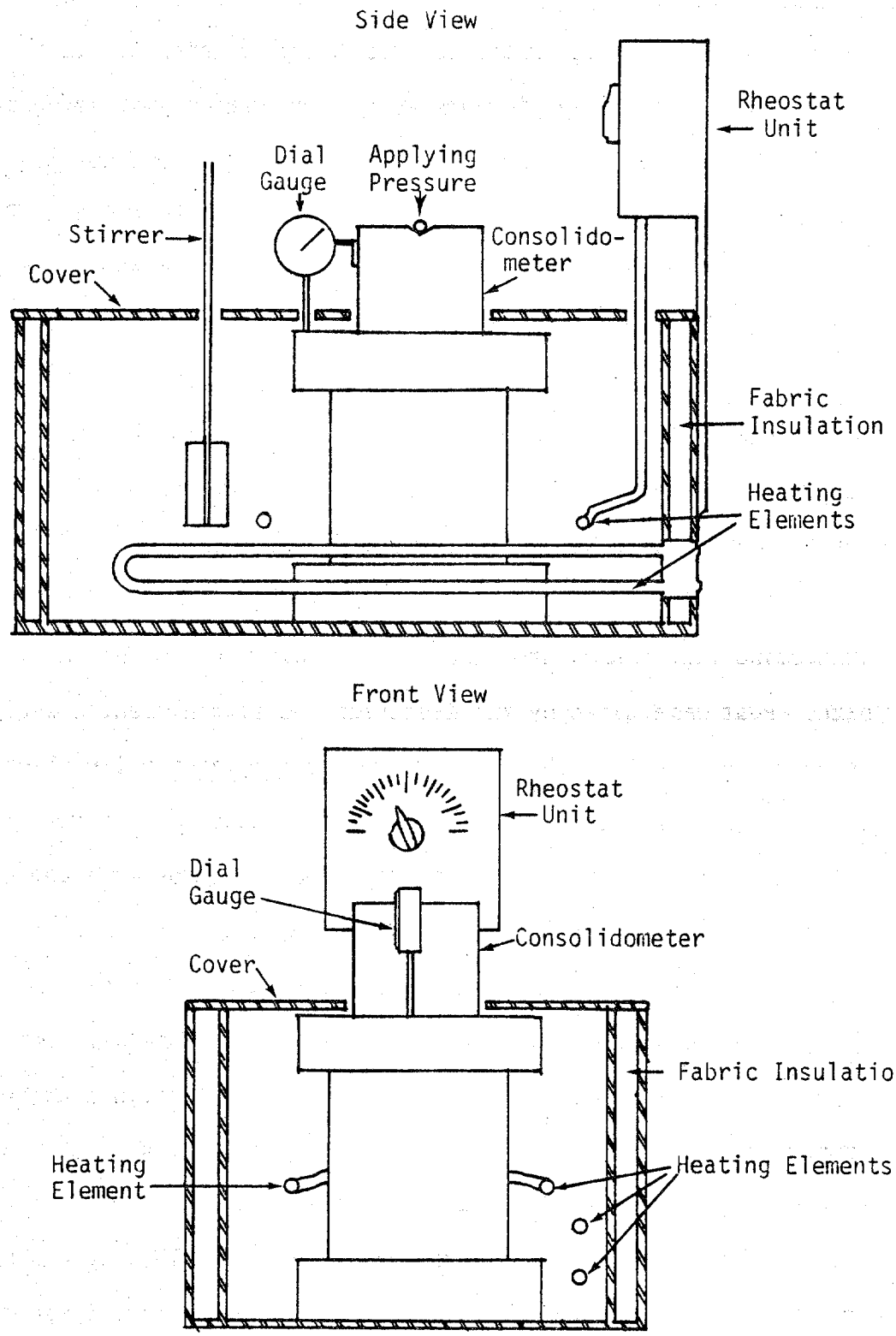

Fig. 6 - Heating Unit

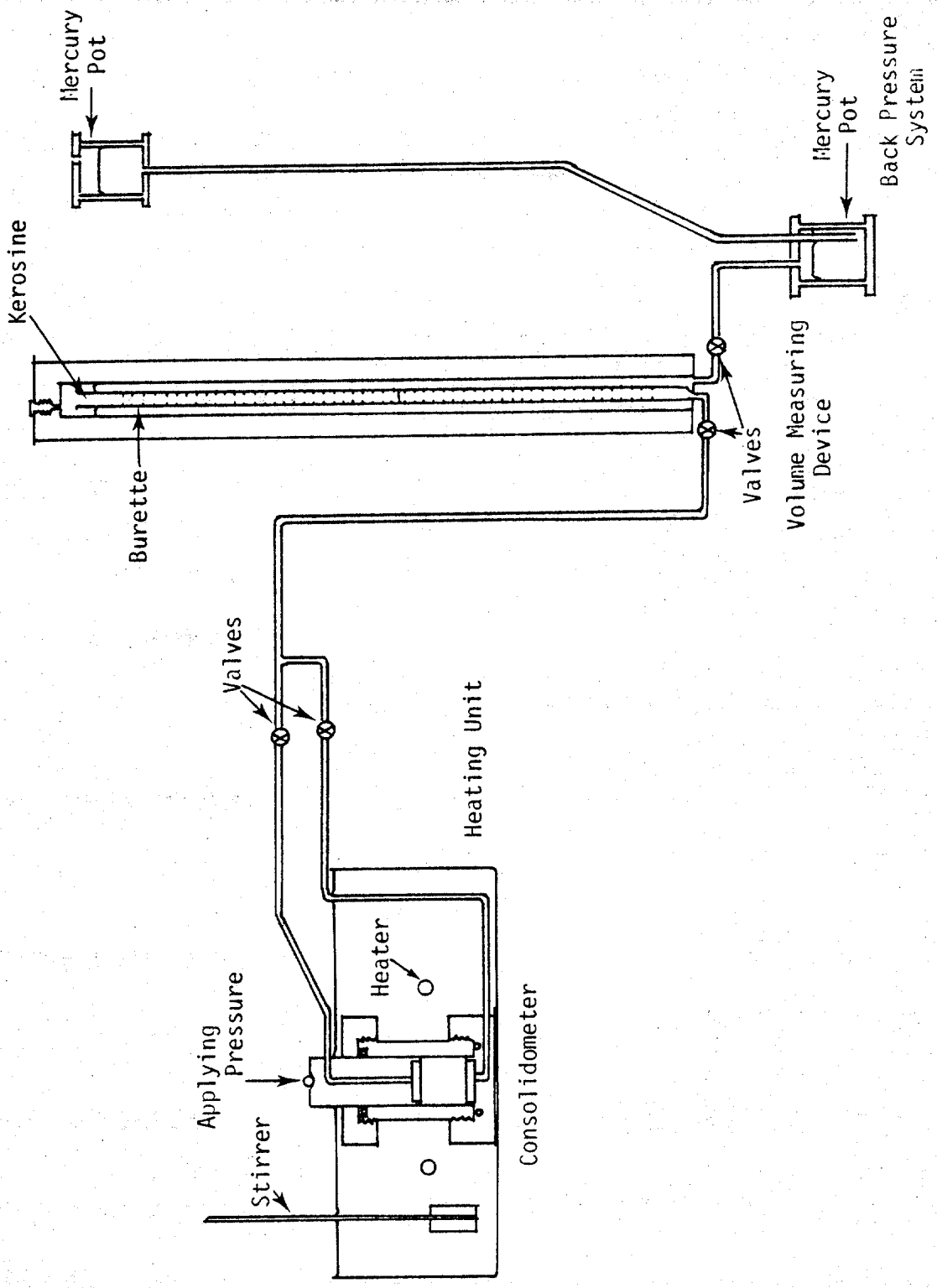

Fig. 4 - Consolidation Test Apparatus

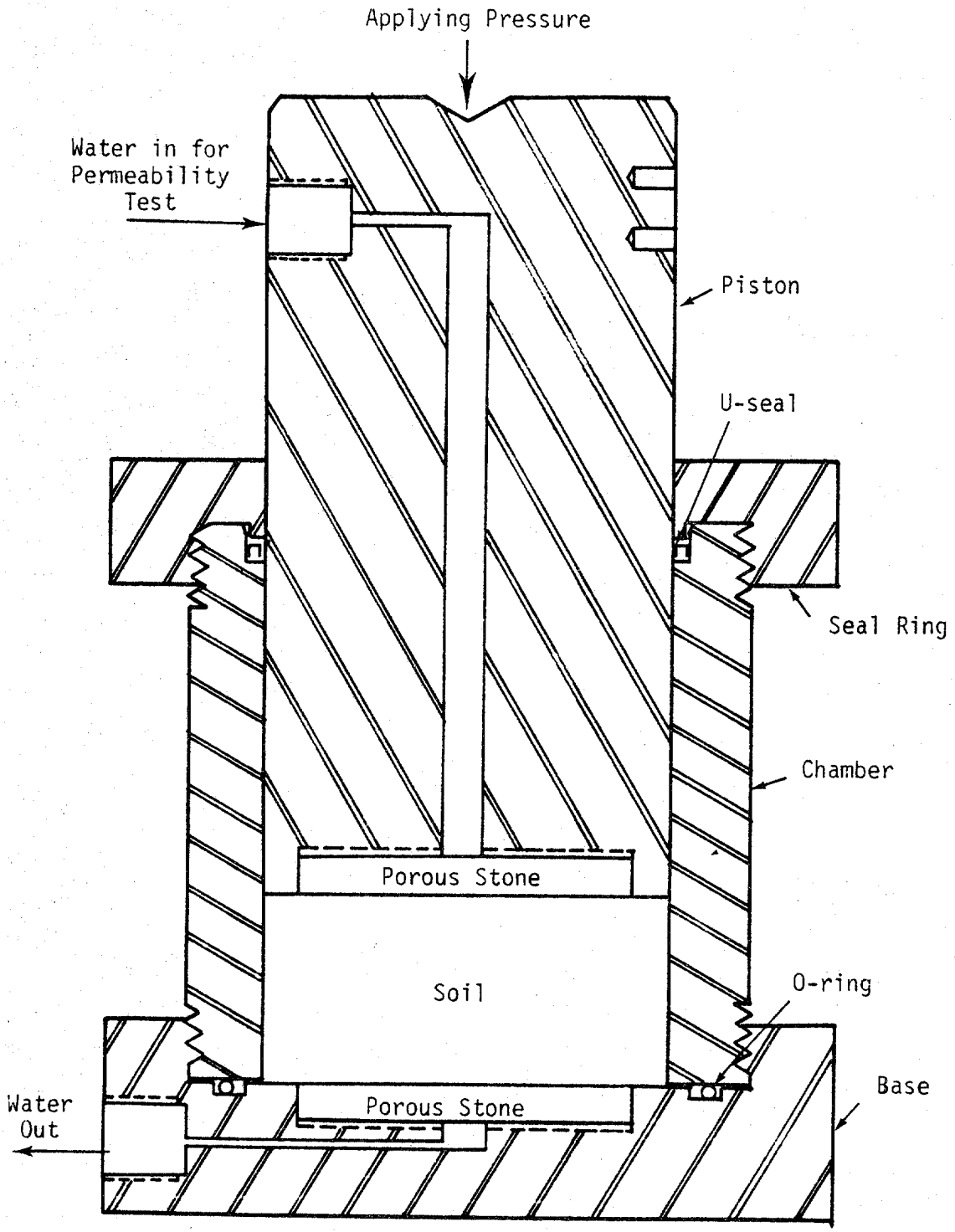

Fig. 5 - Stainless Steel Consolidometer/Permeameter

schmematically in Fig. 7. When the consolidometer was heated above room temperature, a thermal gradient was established between the sediment and water in the consolidometer and the water in the volume-measuring device. The mercury back pressure system produced a pressure gradient in opposition to the thermal gradient to prevent water flow from the consolidating sediment. The device was calibrated at various temperatures, and the calibration curve is shown in Fig. 8.

During the process of consolidation or unloading of the sample and during the measurement of the permeability of the sample, the height of the water in the volume-measuring device experienced a substantial change. The mercury pot, which hangs on a spring of appropriate stiffness, automatically adjusts to its own level as the height of the water changes so that a constant back pressure head is maintained throughout the test.

The change in volume was indicated by the meniscus between the red-dyed kerosene and water inside the inner graduate tube of the volume-measuring unit.

Permeameter. - A piston cylinder mechanism and dead weight lever system, identical to the consolidation unit, was used to produce the hydraulic pressure for the permeability tests. Sea water was forced from the permeameter through the soil sample, and the volume of flow was measured by the volume measuring device.

All the tubing, valves and fittings connected to the consolidometer and the permeameter were designed to withstand pressure greater than 10,000 psi (69,000 kN/m^2). The high pressure valves and fittings were manufactured by Highpressure Equipment Company, Erie, Pennsylvania. A

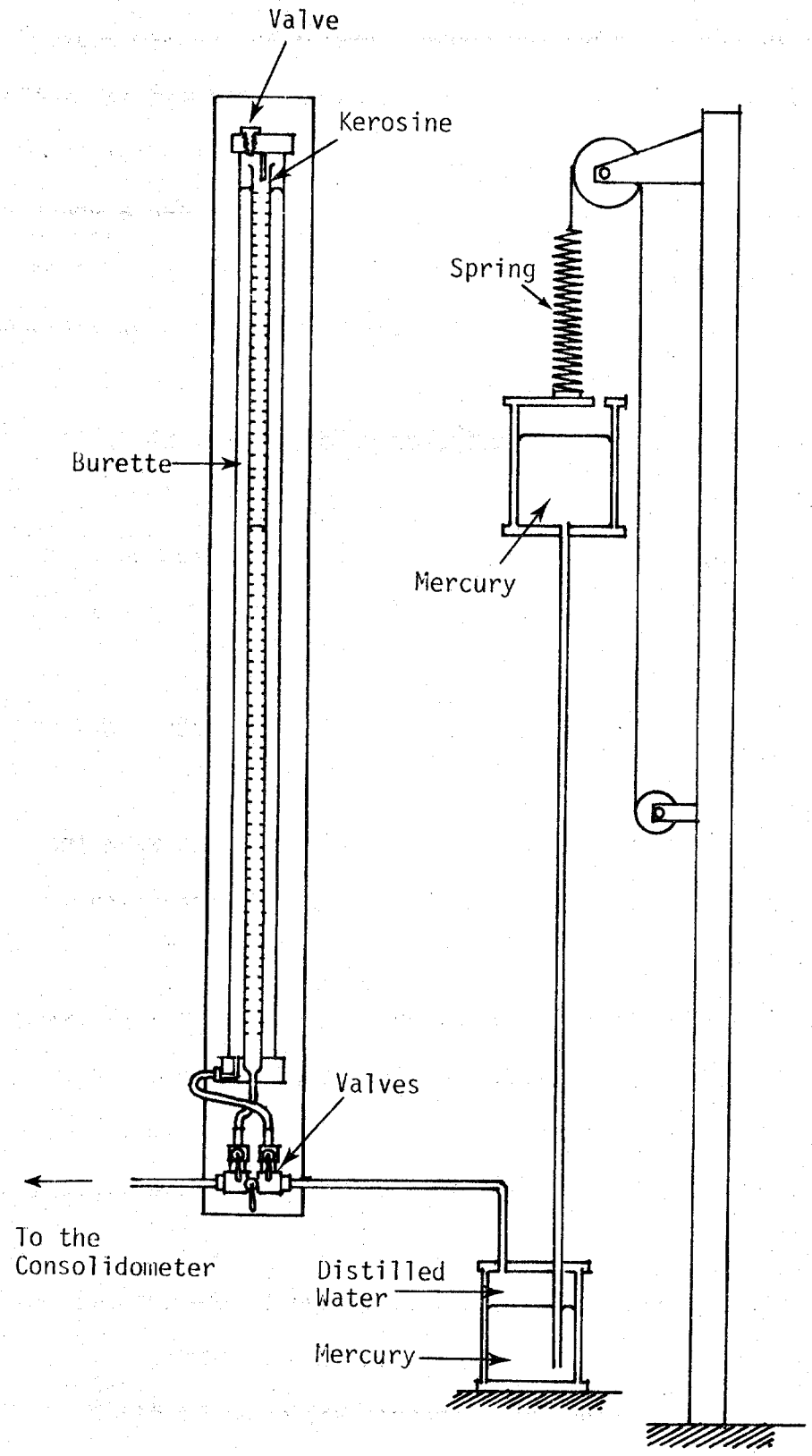

Fig. 7 - Wykeham-Farrance Back Pressure System and Volume Measuring Device

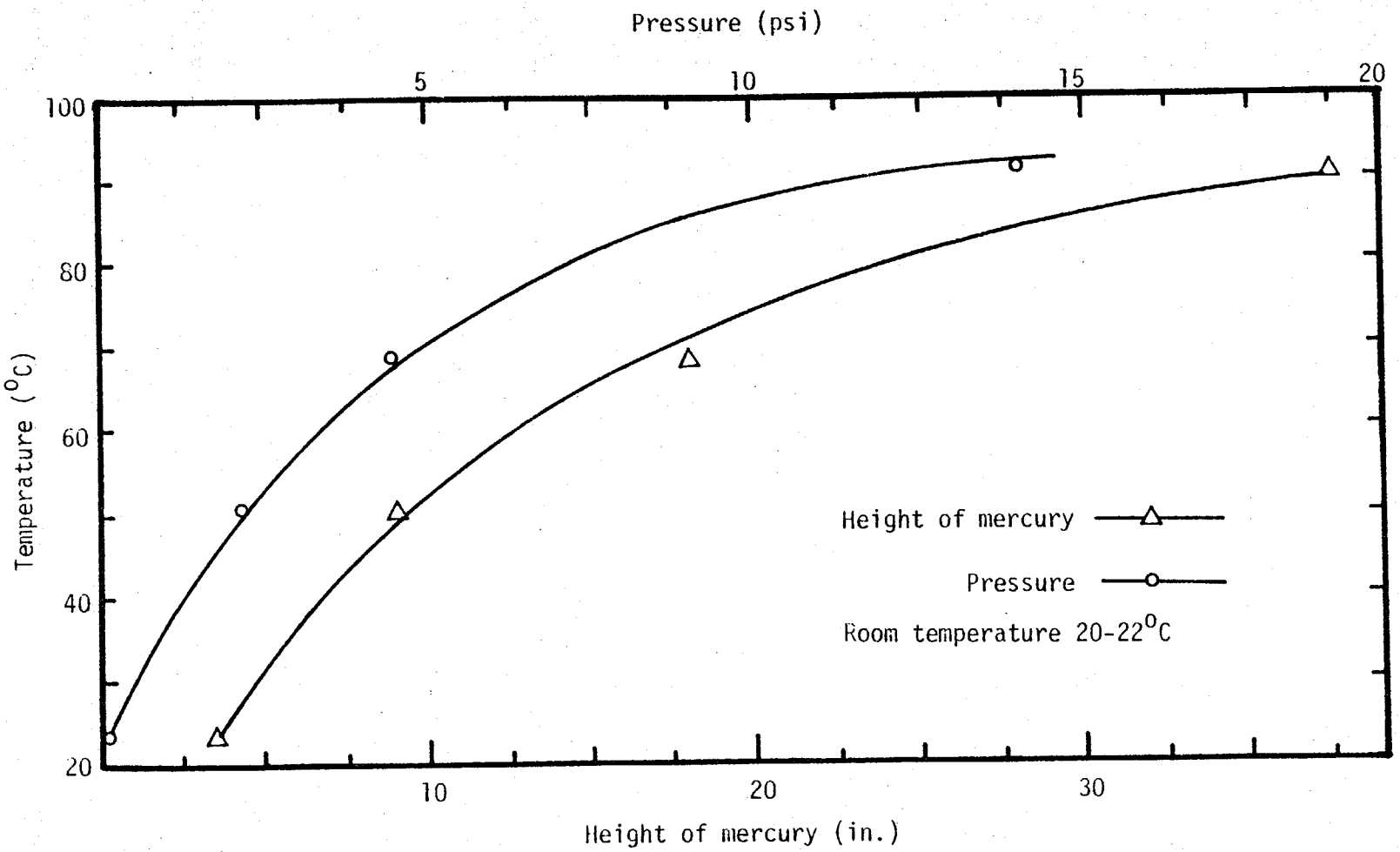

Fig. 8 - Calibration Graph of Temperature versus Mercury Head Required to Prevent Water Flow from Consolidometer When it was Heated Above Room Temperature

picture of the equipment in operation is shown in Fig. 9.

Description of Samples

The effect of temperature on the compressibility and permeability of clay sediments can be best be studied with uniform homogeneous test samples. To minimize the effect of the difference in cores, the bulk of the consolidation and permeability tests were performed on samples identically prepared from single batches of commercial clay mineral powders.

Dr. William Bryant, Oceanography Department, Texas A&M University, made available an undisturbed marine core. It was taken by the deep ocean drillship "Glomar Challenger". The core was taken from a depth of 690 ft (229 m) below the mudline in the Angola Basin in the Atlantic Ocean. The water depth was 1500 ft (4570 m). The core number was Leg 41, Site 369A, Section 20-4, 134-150 cm. A core adjacent to the undisturbed sample core was ground up in a blender and was used to prepare the remolded sample which was tested in the same was as the commercial clay samples were prepared and tested. The engineering indices of all samples are given in Table 1. The mineralogical analysis, as determined by X-ray defraction is given in Table 2.

Experimental Procedure

The progressive burial process of a marine sediment starts with a very high porosity slurry and it takes thousands of years for the overburden to accumulate to a depth where overpressure zones are normally found. Since it is impossible for a laboratory test to

TABLE 2 - Mineralogical Analysis of the Materials Tested*

Sample	Minerals				
	Montomorillonite	Illite	Kaolinite	Chlorite	Quartz
Kaolinite	-	4%	95%	1%	trace
Illite	5%	85%	10%	-	-
Bentonite	100%	-	-	-	trace
Marine Core (Angola Basin)	22%	37%	36%	5%	-

*100% of the material tested passed through the No. 200 sieve

operate over such a long period of time, the soil samples were subjected to incremental constant stresses, and the change in volume due to secondary consolidation was ignored.

Experiments performed on different samples at various constant temperatures are given in Table 3. The experimental procedures are as follows:

1. Preparation of samples.
   a. Remolded sample - Ground dry clay that passed a No. 40 sieve was mixed with synthetic sea water to form a slurry. The slurry was deaired by shaking and applying vacuum to the containing flask for approximately 8 hours. After the slurry was transferred to the consolidometer, vacuum was applied to the slurry for another 12 hours (to further assure the system was totally deaired and saturated).
   b. Undisturbed sample - The sample core was trimmed directly into the consolidation chamber. The entrapped air in the pore water was redissolved by the application of a back pressure of about 1 atm. pressure. After consolidation under the first load of 45 psi (300 kN/m^2), the back pressure was not needed and was removed.
2. Temperature adjustment.

   For consolidation tests at elevated temperatures the consolidometer was placed in a hot oil bath. By heating the oil the desired testing temperature was maintained constantly throughout the test. The back pressure used to prevent thermal gradient flow is shown in Fig. 8.

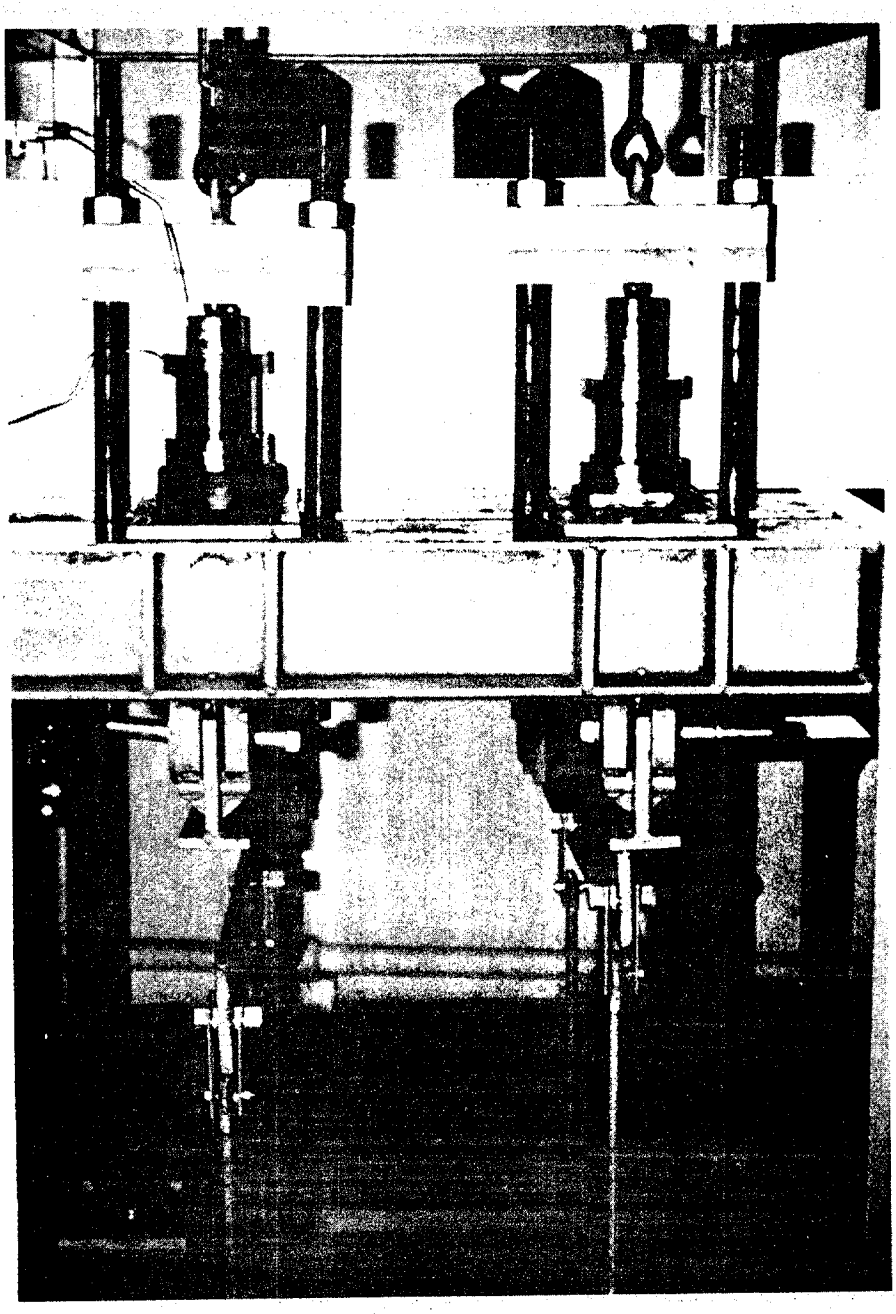

Fig. 9 - Consolidation Test in Operation

TABLE 1 - Engineering Indices of Samples Tested*

Sample	Admixture	Liquid Limit (%)	Plastic Limit (%)	Plastic Index (%)	Specific Gravity	% Clay Size
Kaolinite	Distilled Water	55.0	34.8	20.2	2.63	99
	Sea Water	57.0	33.7	23.3		
Illite	Distilled Water	45.6	23.5	21.2	2.79	77
	Sea Water	43.2	23.4	19.8		
Bentonite	Distilled Water	388.0	32.5	355.5	2.75	85
	Sea Water	123.5	31.6	91.9		
Marine Clay (Angola Basin)	Distilled Water	72.0	25.8	46.2	2.93	98
	Sea Water	62.5	21.6			

*The Atterberg limits were determined for the sample with distilled water and sea water.

TABLE 3 - Experiments Performed at Various Temperatures

Test No.	Mineral or Core	Temperature
K-20	Kaolinite	20°C
K-60	Kaolinite	60°C
K-90	Kaolinite	90°C
I-20	Illite	20°C
I-60	Illite	60°C
I-90	Illite	90°C
B-20	Bentonite	20°C
B-60	Bentonite	60°C
B-90	Bentonite	90°C
M-U	Marine Core (Undisturbed)	20°C
M-R	Marine Core (Remolded)	20°C

3. Consolidation test.

Samples were consolidated under a constant load until they reached 100% primary consolidation. The change in volume was measured by both the dial extensometer and the volume-measuring unit. The time between each reading was twice the preceding time interval between readings. For each test the change in sample height or the "dial reading" was plotted as a function of the log of time. These curves were used to compute the time to 100% primary consolidation (25). A sample dial reading-log of time curve is given in Fig. 10. The 100 percent primary consolidation is located by extending the straight line portion of the curve representing secondary consolidation back to its intersection with a tangent drawn to the curve at its point of inflection (25). When 100% primary consolidation was complete and the sample height had stabilized under the load, the consolidation load was doubled and the measurements of height change due to drainage were repeated. This process was continued until the stress on the sample was approximately 10,000 psi (69,000 kN/m^2).

The same procedure was used for unloading and reloading. Example calculation for the change in porosity (or void ratio) as determined by the change in the sample height are given in the Appendix.

The consolidation tests were performed at three different temperatures; 68°F (20°C), 140°F (60°C) and 194°F (90°C) for each of the three clay minerals. Both tests on the undisturbed and remolded marine core samples were performed at

DISCUSSION OF THE TEST RESULTS

Consolidation

Ordinarily in a consolidation test, the final void ratio (when drainage is complete) is plotted against the log of total vertical load on the sample (45). It is called the "e-log $\overline{\sigma}$" curve. Tables 9 through 18 in Appendix III gives the final void ratio, e, that resulted from each total load on each sample. Fig. 11 and Figs. 25 through 34 in Appendix IV show the plots of the results for loading, unloading and reloading. These plots show that the slope of the e-log $\overline{\sigma}$ curve tends to flatten as the load is increased. Obviously there is no linear relationship between the void ratio, after complete drainage, and the log of the load. These results were expected because the load, to cause zero void ratio, must be enormous. Katherman and Bryant (18) observed similar phenomena with their consolidation tests on marine core samples.

Tables 9 through 18 in Appendix III also show the sample porosity ratio that corresponds to each of the consolidation loads when the pore pressure is zero. When the log of load is plotted against the log of the porosity ratio as illustrated in Fig. 12, and also shown in Figs. 35 through 42 in Appendix IV, it is seen that a straight line fits the data very well. These straight lines represent the "power law" function for the force in the mineral structure only. The slope of the lines corresponds to the constant B and the intercept of the line at the porosity ratio of one corresponds to the constant A in Eq. 11.

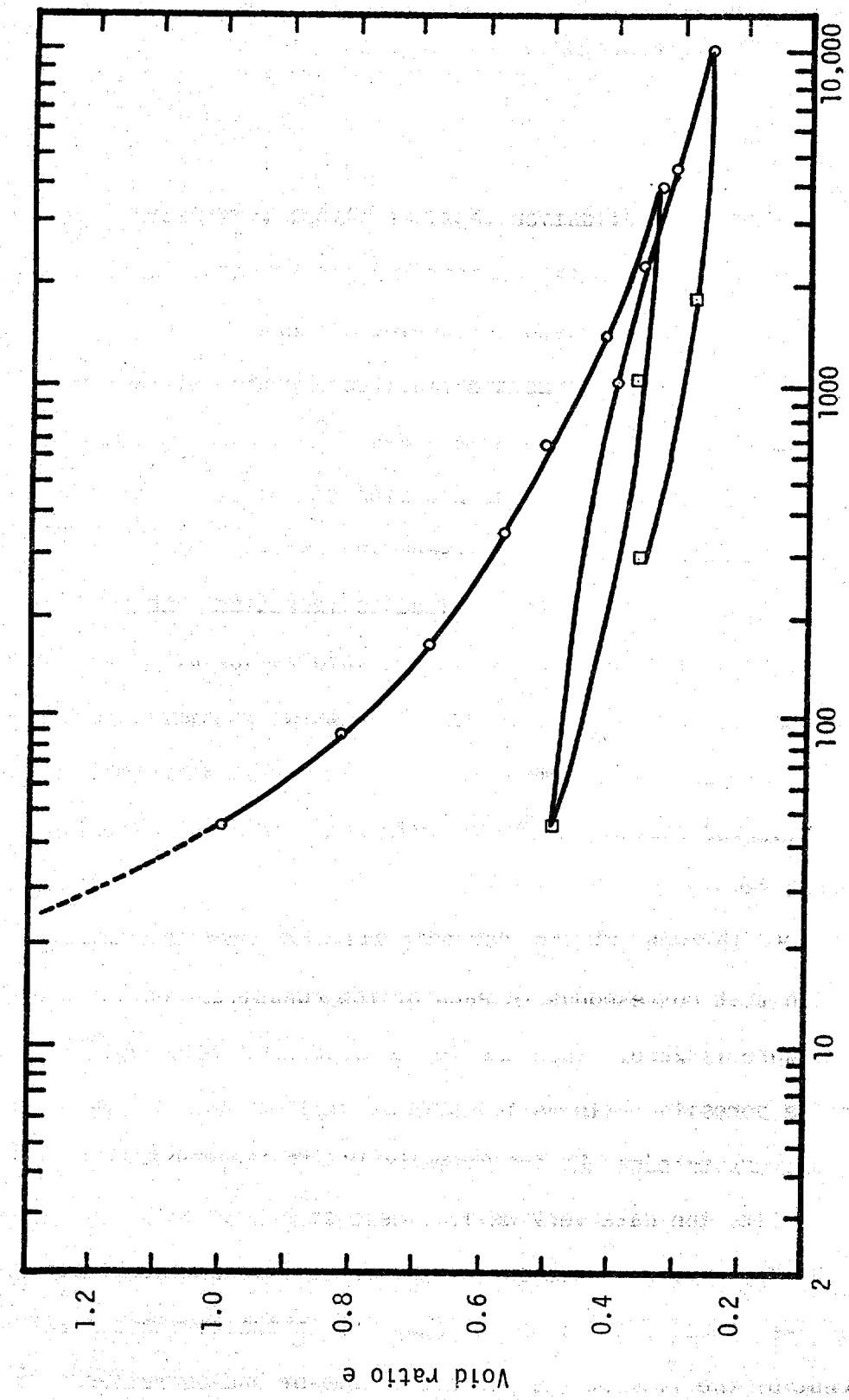

Fig. 11 - Graph of Void Ratio versus Consolidation Pressure for Illite Tested at 20°C

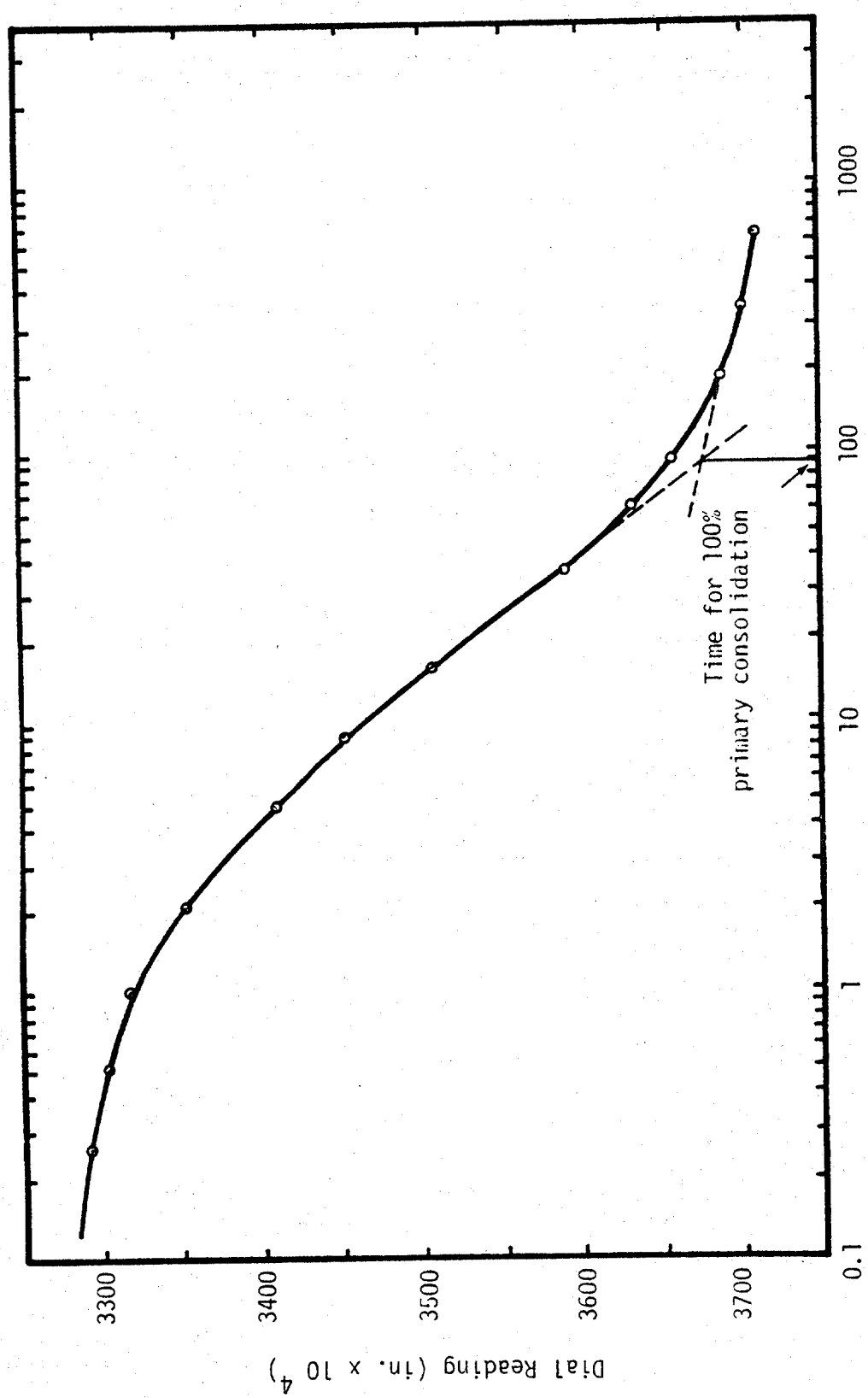

Fig. 10 - Graph of Dial Reading versus Time for Illite Tested at 20°C Under the Consolidation Load of 1520 psi

temperature 68°F. (20°C)).

4. Permeability test.

When the consolidation was completed for a given load on a sample, its permeability was measured by forcing sea water through it. An hydraulic gradient was applied across the sample to cause the flow through the sample. A sufficient hydraulic pressure was selected so that a measurable rate of flow would result. Care was also taken to keep the hydraulic pressure below the consolidation pressure at all times during the permeability tests. The flow of sea water was measured by the volume-measuring device. With the measured amount of flow and the applied hydraulic gradient, the permeability of the sample was calculated by using Darcy's law. Details of this calculation are shown in Appendix V. Table 8 in the appendix gives the test data used to compute the permeabilities for each sample at the various temperatures.

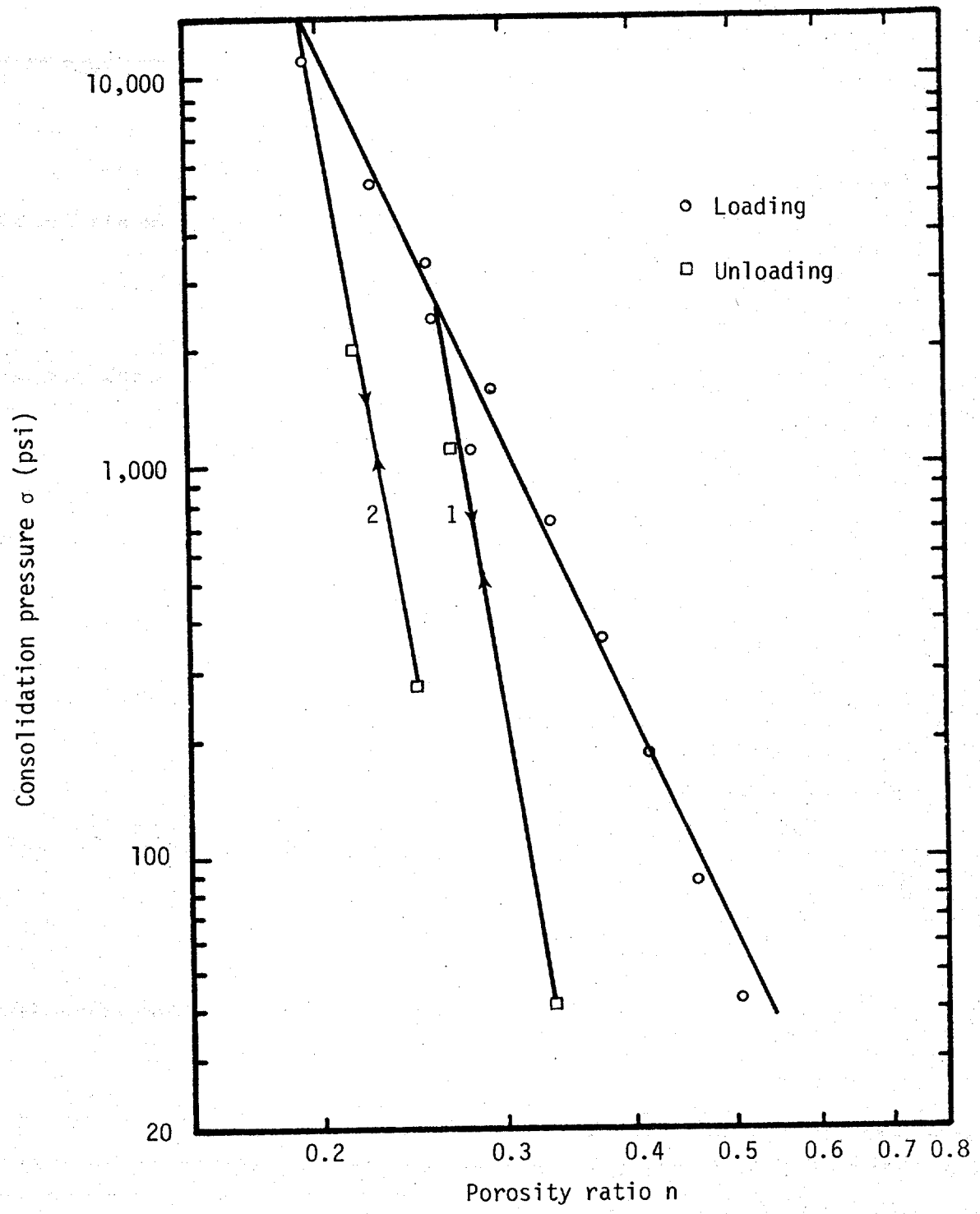

Fig. 12 - Graph of Consolidation Pressure versus Porosity Ratio for Illite Tested at 20°C

The compressibility coefficient A and B for each sample for both loading and unloading is shown in Table 4. These results were obtained by linear regression analysis. As can be seen in Table 4, the correlation coefficients are excellent. The plot of compressibility coefficients versus different temperatures are shown in Figs. 13 and 14. The results of tests on illite and bentonite indicate that an increase in temperature does not have any significant effect on the compressibility. However, the test results on kaolinite, as shown in Figs. 35, 36 and 37 in Appendix IV, show that the compressibility of the mineral increases slightly with an increase in temperature.

Experiments on the marine core as shown in Fig. 15 show that at pressures below 700 psi (4,830 kN/m^2) the undisturbed sample had a higher compressibility than the remolded sample. However, the difference in the porosity ratios between the remolded and undisturbed samples decreases and finally vanishes when the pressure reachs 1500 psi (10,250 kN/m^2).

Permeability

Tables 9 through 18 in Appendix III give the permeability for each sample at the different temperatures and porosities. The calculated values of absolute permeability are shown, also.

Because of the previous work by Thompson et al. (47), the log of the permeability was plotted against the log of the porosity ratio. Figs. 16 through 18 show that these permeability data at each temperature can be represented by a power law function of porosity

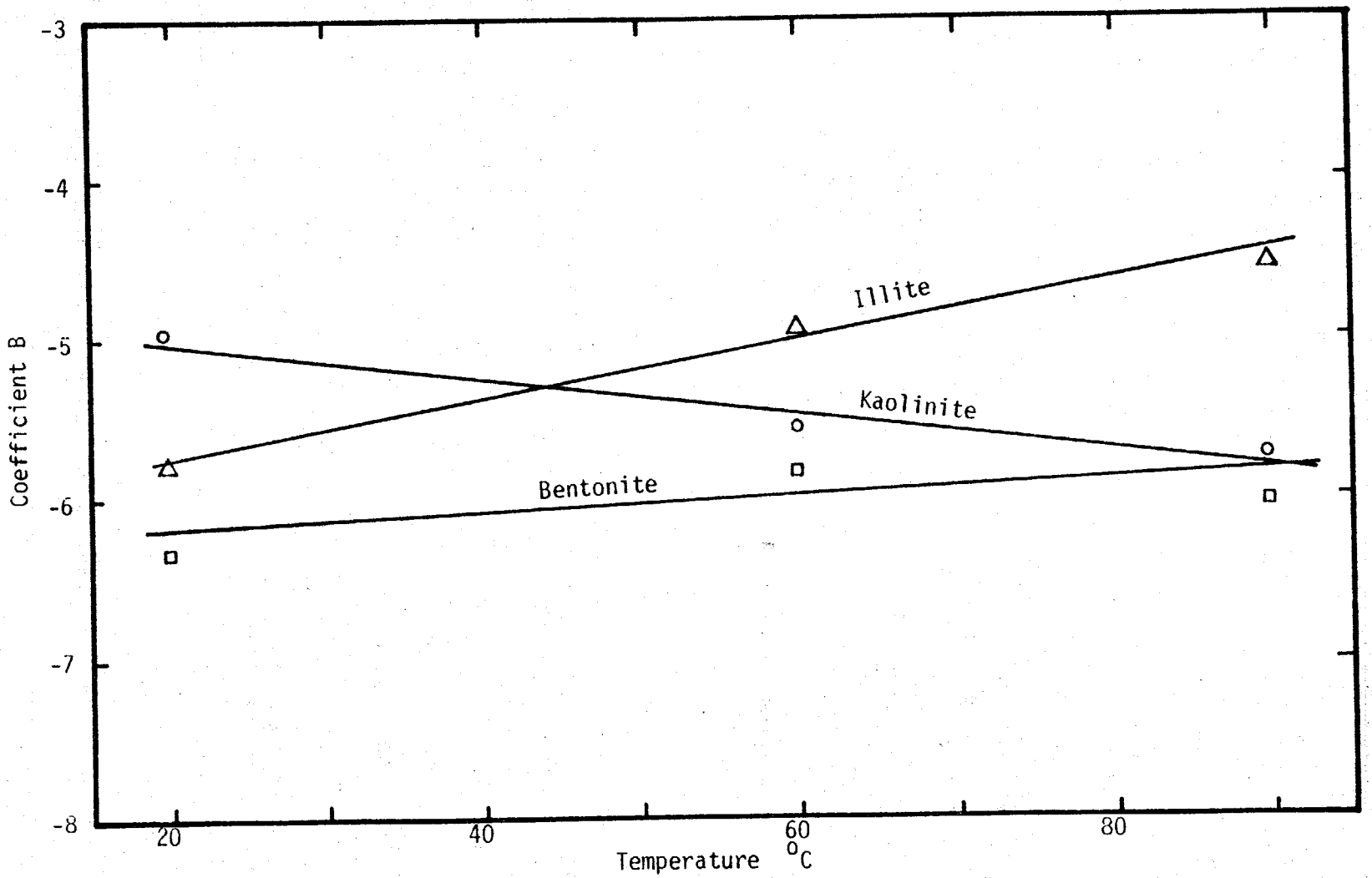

Fig. 14 - Graph of Coefficient B versus Temperature

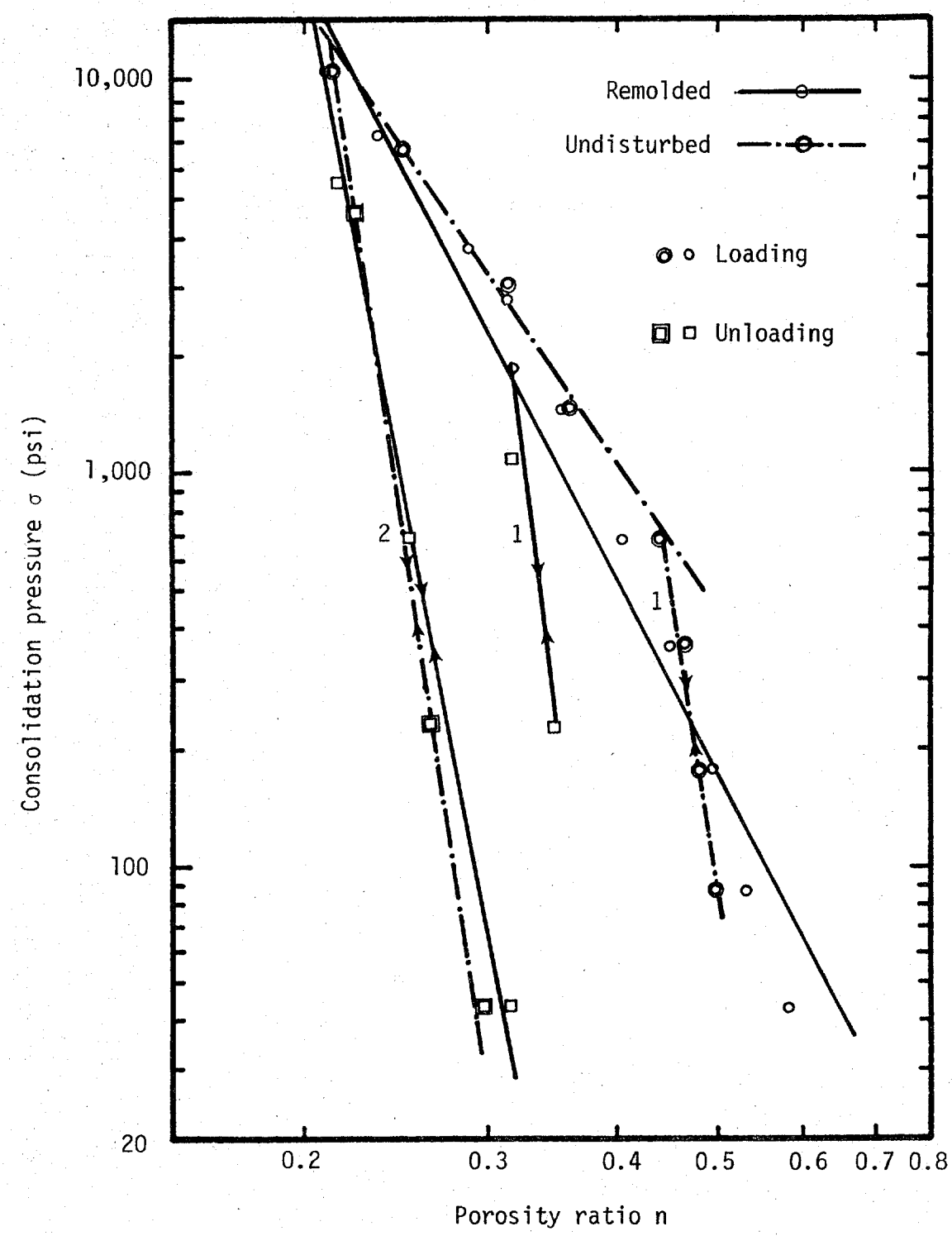

Fig. 15 - Graph of Consolidation Pressure versus Porosity Ratio for Marine Core from Angola Basin Tested at 20°C

TABLE 4 - Coefficients A&B for the "Power Law" Equation

Sample	Test Temperature	Virgin Curve			Rebound Curve 1			Rebound Curve 2		
		A*	B	R^2	A*	B	R^2	A*	B	R^2
Kaolinite	20°C	15.17	-4.99	0.98				3.23×10^{-2}	-12.88	0.92
Kaolinite	60°C	6.33	-5.50	0.97	9.84×10^{-5}	-16.00	0.93	2.09×10^{-4}	-12.54	0.99
Kaolinite	90°C	2.81	-5.79	0.97	1.61×10^{-7}	-20.50	0.91	2.30×10^{-8}	-17.98	0.99
Illite	20°C	1.06	-5.78	0.99	2.22×10^{-5}	-13.60	0.90	1.80×10^{-7}	-18.30	0.92
Illite	60°C	2.94	-4.97	0.99	2.48×10^{-7}	-16.80	0.95	4.80×10^{-8}	-15.58	0.89
Illite	90°C	5.22	-4.55	0.99	2.60×10^{-5}	-13.50	0.93	1.62×10^{-3}	-11.80	0.99
Bentonite	20°C	4.48	-6.32	0.99	4.17×10^{-9}	-29.98	0.95	5.24×10^{-7}	-19.45	0.98
Bentonite	60°C	6.79	-5.88	0.99	1.01×10^{-7}	-24.01	0.89	6.13×10^{-9}	-22.60	0.99
Bentonite	90°C	5.09	-6.07	0.99	1.29×10^{-9}	-27.98	0.96	1.73×10^{-7}	-19.60	0.99
Marine Core (undisturbed)	20°C	28.41	-3.94	0.99	1.24×10^{-3}	-15.80	0.98	7.12×10^{-9}	-18.20	0.99
Marine Core (remolded)	20°C	3.47	-5.54	0.97	6.00×10^{-4}	-12.67	0.81	4.73×10^{-7}	-15.45	0.97

*The dimension is in psi.

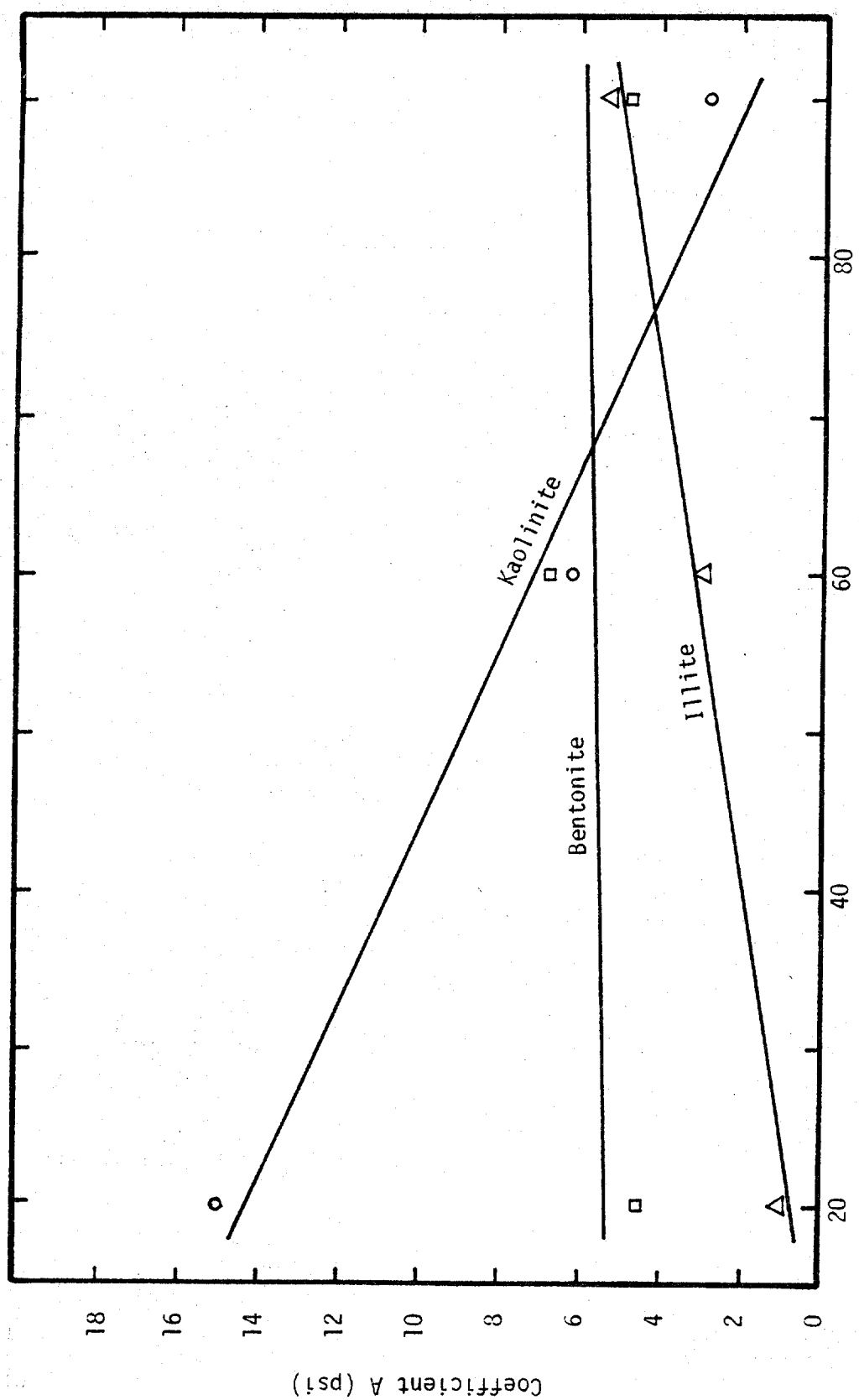

Fig. 13 - Graph of Coefficient A versus Temperature

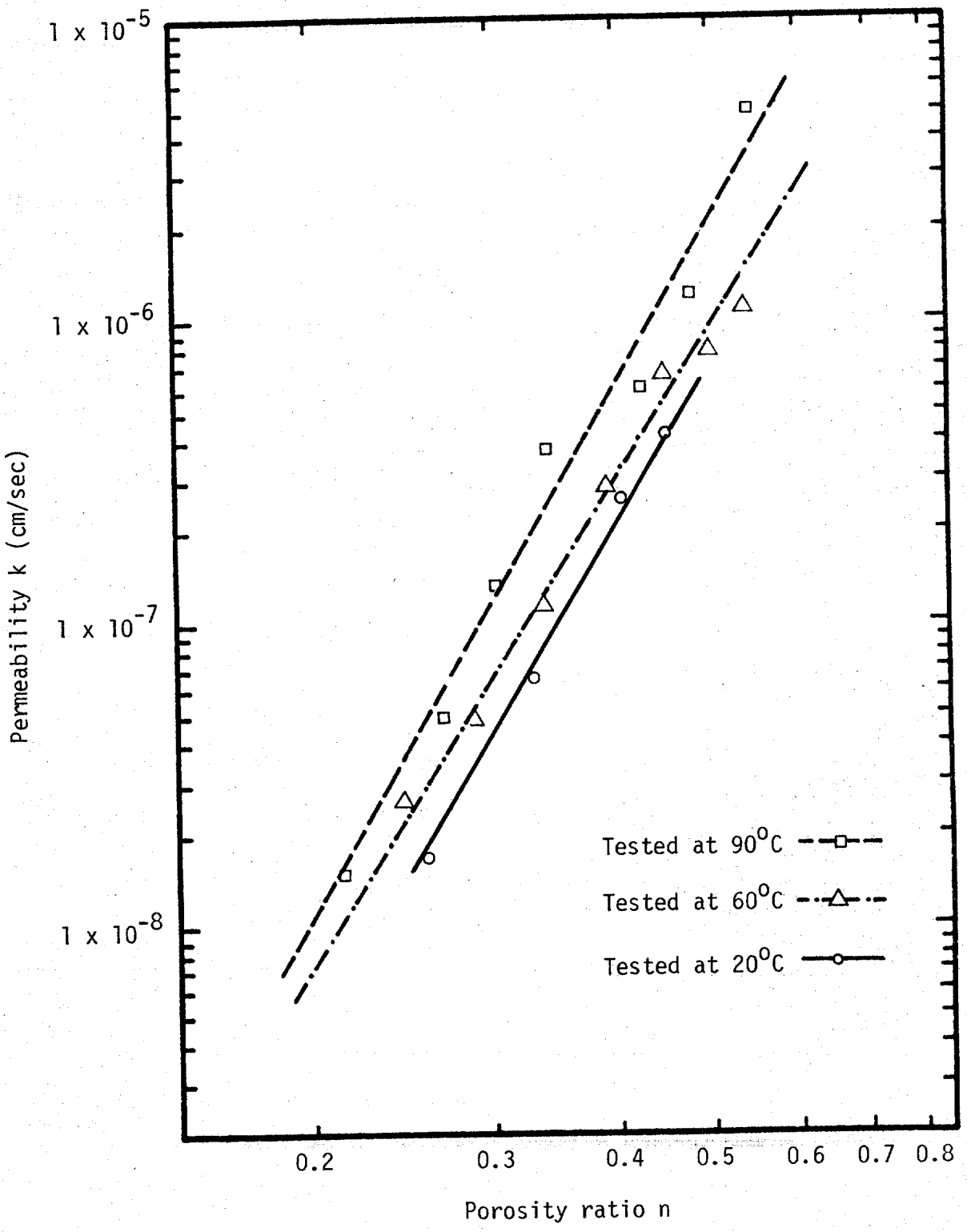

Fig. 16 - Graph of Permeability versus Porosity Ratio for Kaolinite

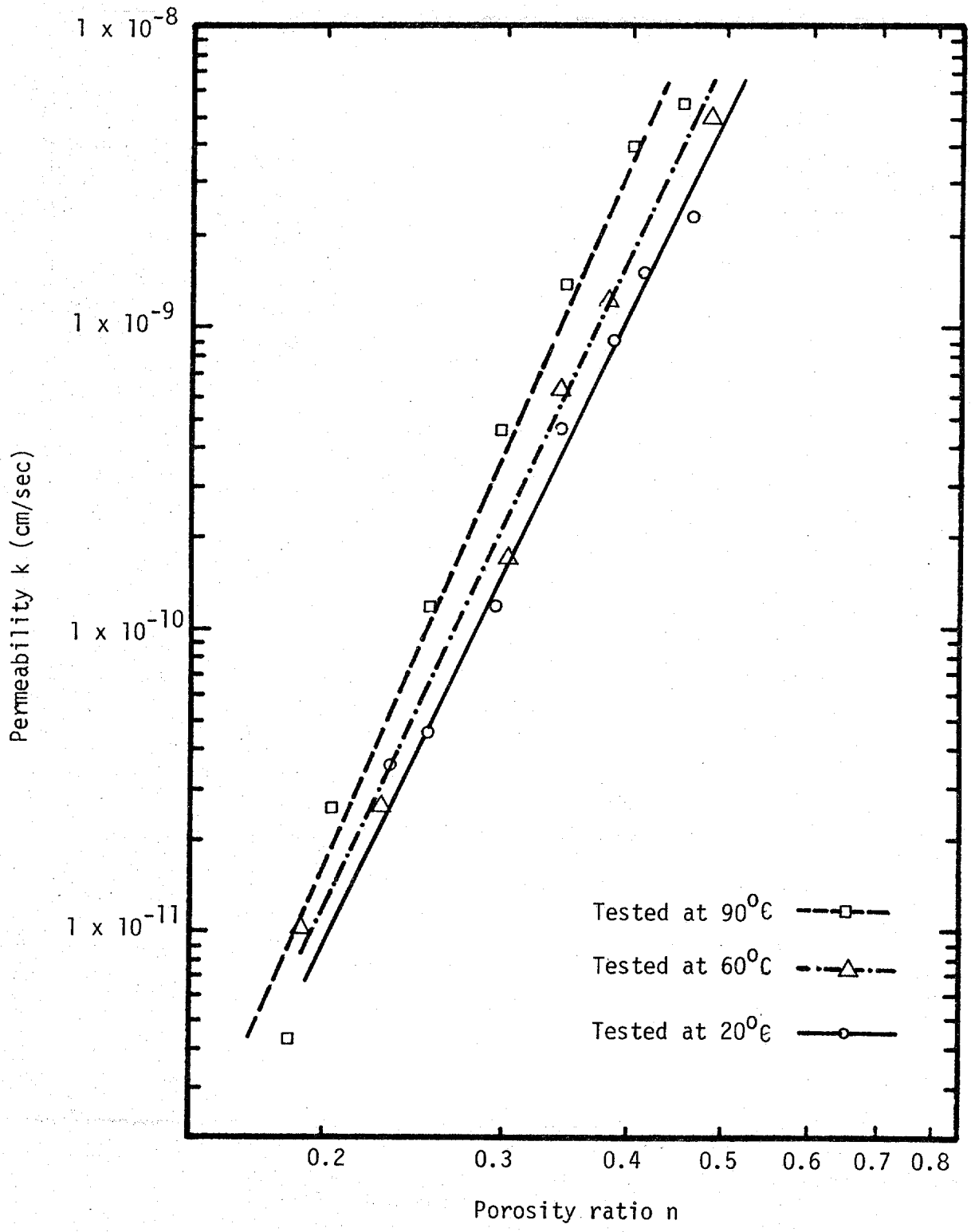

Fig. 17 - Graph of Permeability versus Porosity Ratio for Illite

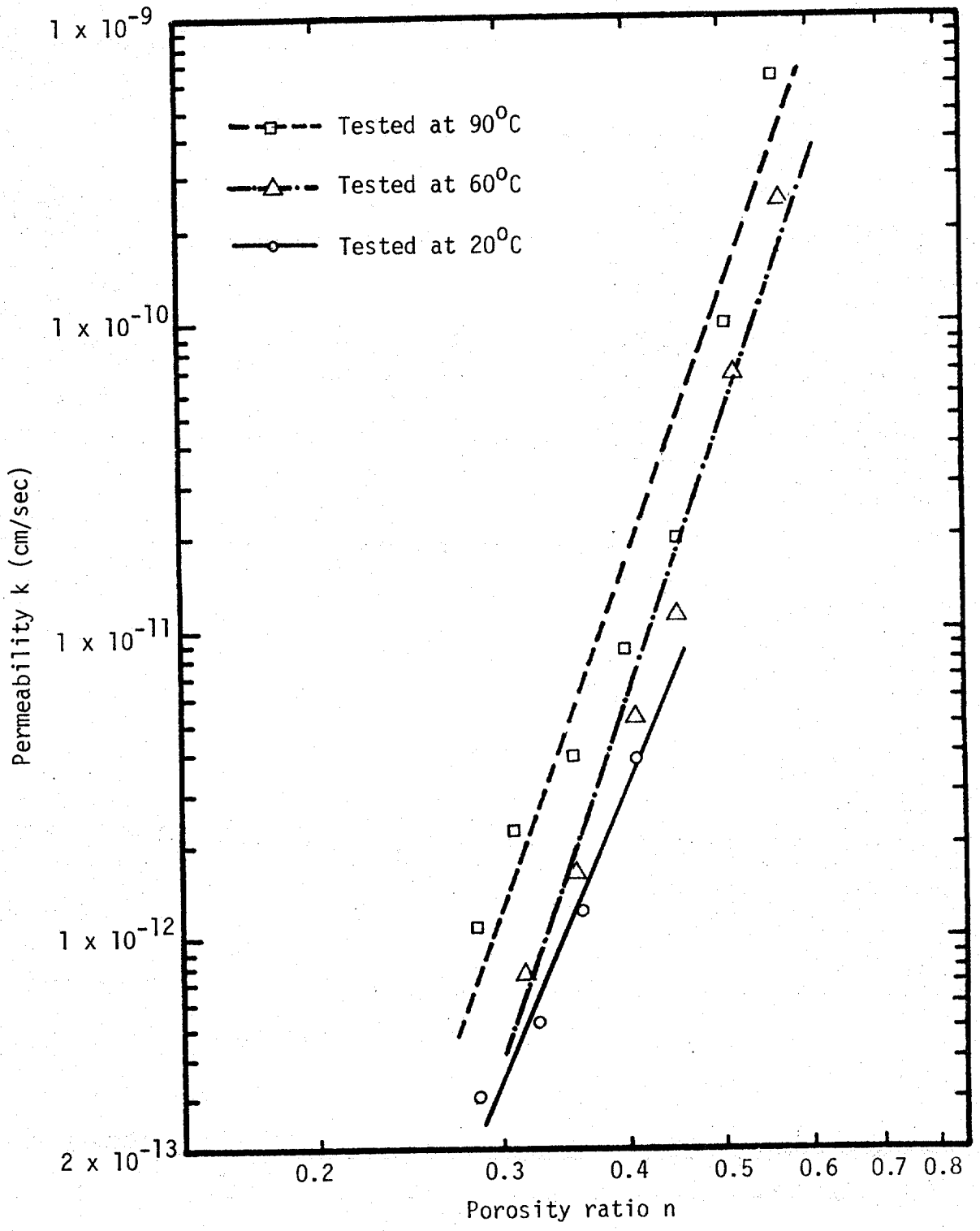

Fig. 18 - Graph of Permeability versus Porosity Ratio for Bentonite

ratio as given by Eq. 21. The test results indicated that the permeability increases with temperature. Similar plottings of the absolute permeability and porosity ratio shows that a power law can represent all the data for each material. This is shown in Figs. 19 through 21. The absolute permeability is the permeability times the water viscosity divided by the water density. Thus, the constant C becomes a function of temperature for the absolute permeability and the constant D is the same for both the permeability and the absolute permeability. The plot of constants C and D versus temperature are shown in Figs. 22 and 23.

The best fit of these data was found by linear regression analysis. Table 5 gives both the permeability and absolute permeability constants C and D for each material tested. The excellent corresponding correlation coefficients are also given in the same table. When all of the absolute permeabilities for each material were used to get the best fit it was found that

$k = 0.296\ n^{5.71}$ for kaolinite $\quad R^2 = \underline{0.96}$

$k = 0.836\ n^{7.34}$ for illite $\quad R^2 = \underline{0.97}$

and $k = 0.0098\ n^{8.64}$ for bentonite $\quad R^2 = \underline{0.92}$

where k is the absolute permeability in millidarcies.

In general, the experimental results agree with previous measurements on the permeability of clay. The direct measurements performed on the bentonite samples consolidated under the pressure of 10,000 psi (69,000 kN/m^2), indicated that the permeability of the clay mineral

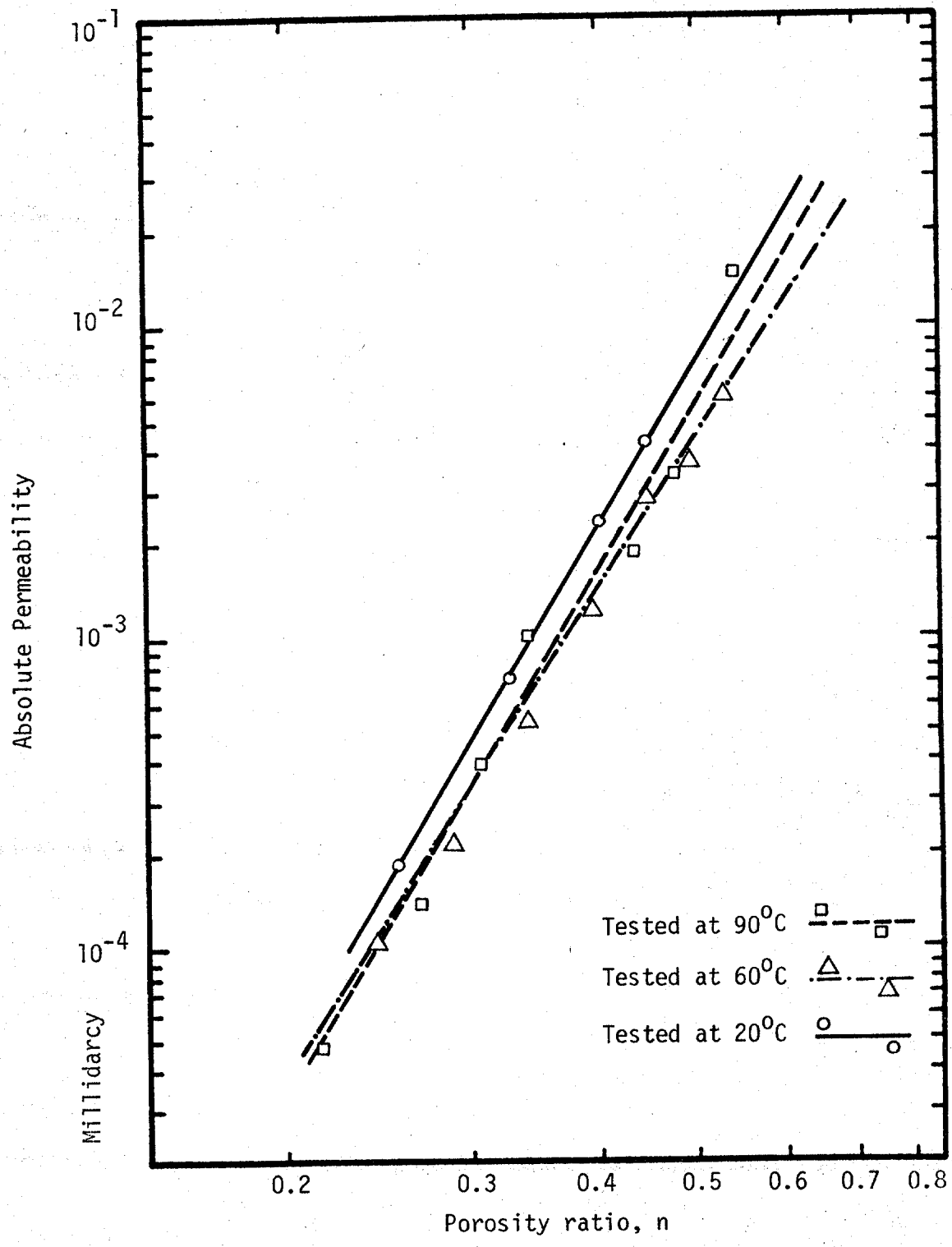

Fig. 19 - Graph of Absolute Permeability versus Porosity Ratio for Kaolinite

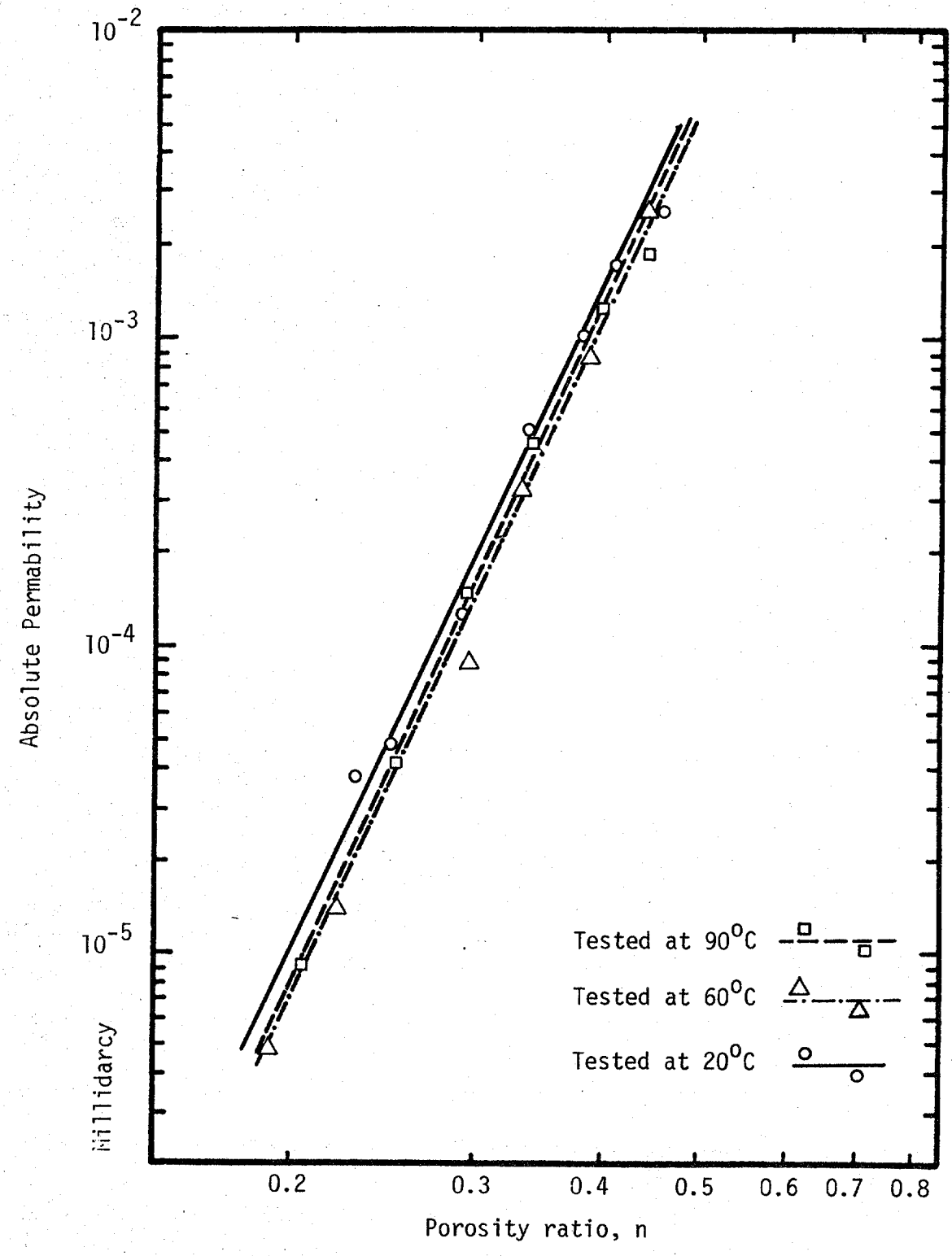

Fig. 20 - Graph of Absolute Permeability versus Porosity Ratio for Illite

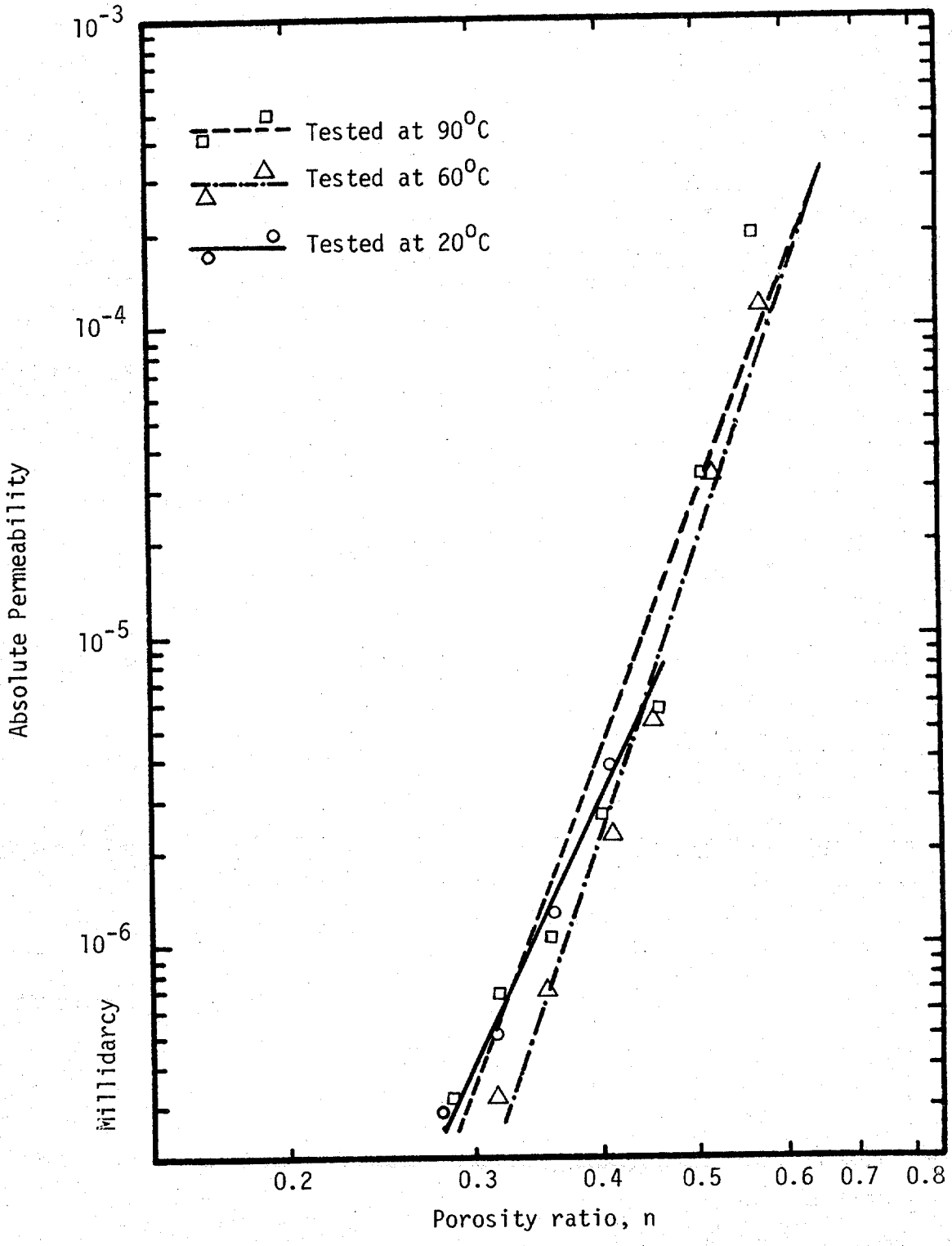

Fig. 21 - Graph of Absolute Permeability versus Porosity Ratio for Bentonite

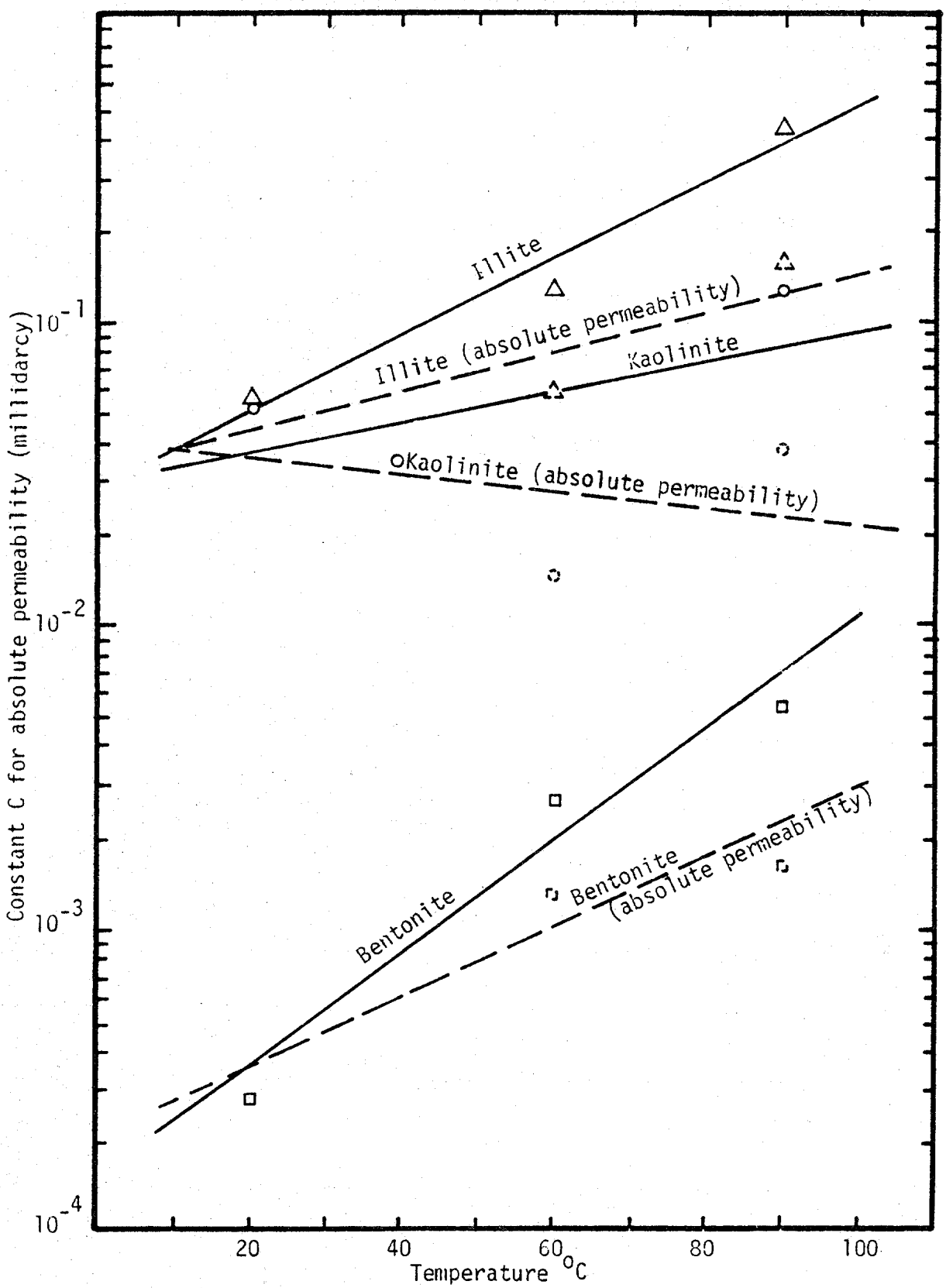

Fig. 22 - Graph of Constant C versus Temperature

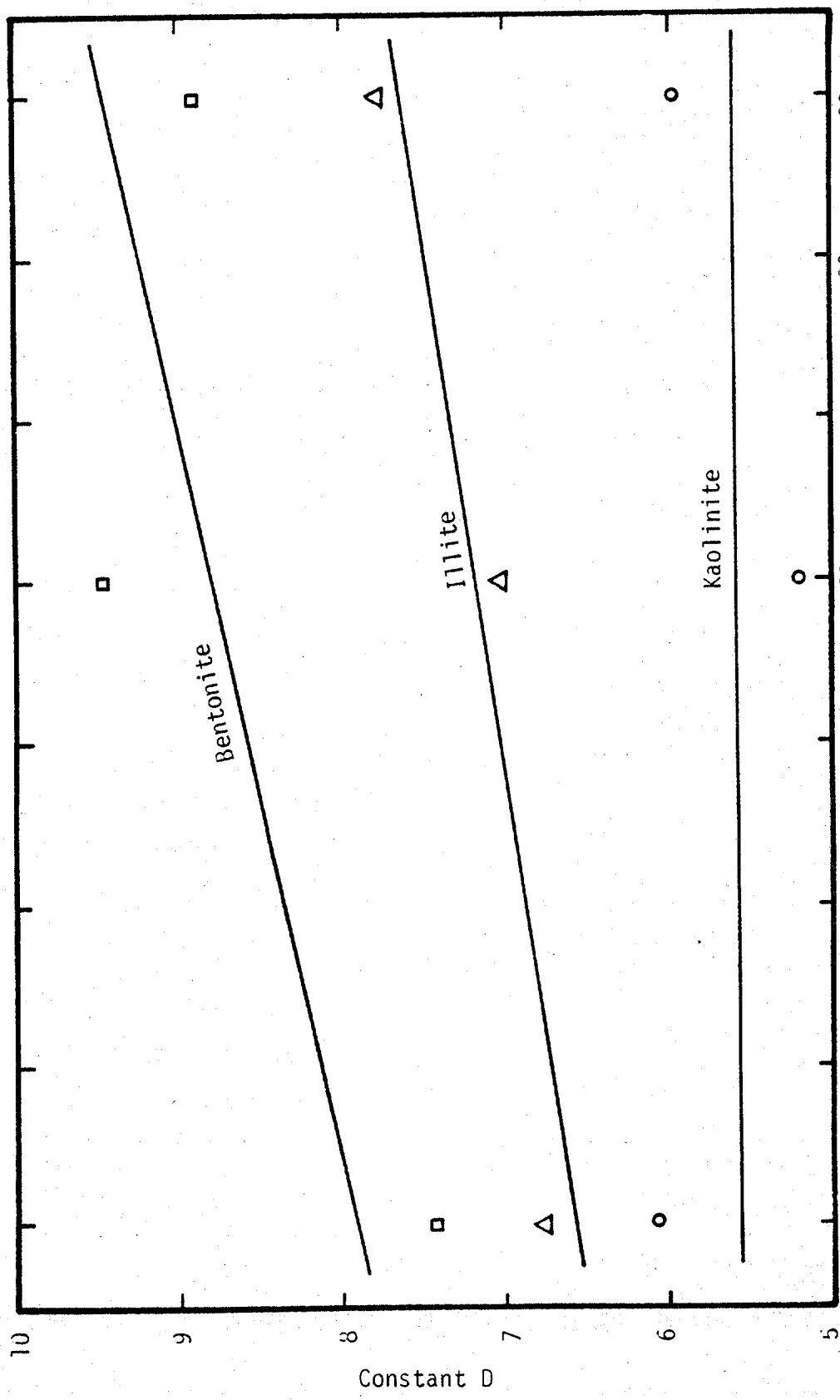

Fig. 23 - Graph of Constant D versus Temperature

TABLE 5 - Constants for Permeability "Power Law" Equations

Sample	Test Temperature	Permeability Coefficient			Permeability Coefficient on Absolute Permeability		
		C*	D	R^2	C**	D	R^2
Kaolinite	20°C	0.52×10^{-6}	6.07	0.99	0.528	6.08	0.99
Kaolinite	60°C	0.33×10^{-6}	5.20	0.99	0.158	5.20	0.99
Kaolinite	90°C	0.124×10^{-5}	5.95	0.96	0.406	5.95	0.97
Illite	20°C	0.546×10^{-6}	6.79	0.98	0.431	6.73	0.94
Illite	60°C	0.126×10^{-5}	7.02	0.99	0.598	7.02	0.99
Illite	90°C	0.463×10^{-5}	7.77	0.96	1.60	7.93	0.99
Bentonite	20°C	0.273×10^{-8}	7.44	0.95	0.0027	7.43	0.95
Bentonite	60°C	0.275×10^{-7}	9.45	0.96	0.0131	9.45	0.96
Bentonite	90°C	0.522×10^{-7}	8.89	0.93	0.0171	8.89	0.93
Marine Core (undisturbed)	20°C	0.163×10^{-7}	8.63	0.97	1.644	8.63	0.96
Marine Core (remolded)	20°C	0.291×10^{-8}	7.11	0.99	0.292	7.11	0.99

*The dimension is in cm/sec.

**The dimension is in millidarcy.

at the temperature of 68°F (20°C), and 194°F (90°C) are 3.1×10^{-13} cm/sec and 1.1×10^{-12} cm/sec respectively. These measurements coincide with the results published by Kharaka and Smalley (20).

The permeabilities of different clays vary by two orders of magnitude. At a porosity ratio equal to 0.3, the permeability of kaolinite is equal to 2.3×10^{-10} cm/sec, that of illite is equal to 8.1×10^{-10} cm/sec, and for bentonite, the permeability is equal to 5.1×10^{-13} cm/sec. The permeability of kaolinite, illite and bentonite decrease in that order. These results also agree with the results suggested by Lambe (22).

Experiments on the marine core (see Fig. 24) indicate no significant change in the permeability between the undisturbed and remolded samples.

Effect of Salinity on the Atterberg Limits

When sea water was substituted for distilled water, the liquid limit of bentonite changed substantially from 288% to 123.5%. The liquid limit of the marine clay sample changed from 72% to 62.5%. Illite had an insignificant change of about 2%. A 2% increase of liquid limit was observed for kaolinite. The saline water seemed to have no significant influence on the plastic limit. These results are given in Table 1.

Bentonite consists predominately of sodium montmorillonite. An increase in salinity results in an increase in the electrolyte concentration. Warkentin (48) has shown that the liquid limit of sodium montmorillonite decreases when the electrolyte concentration increases. His

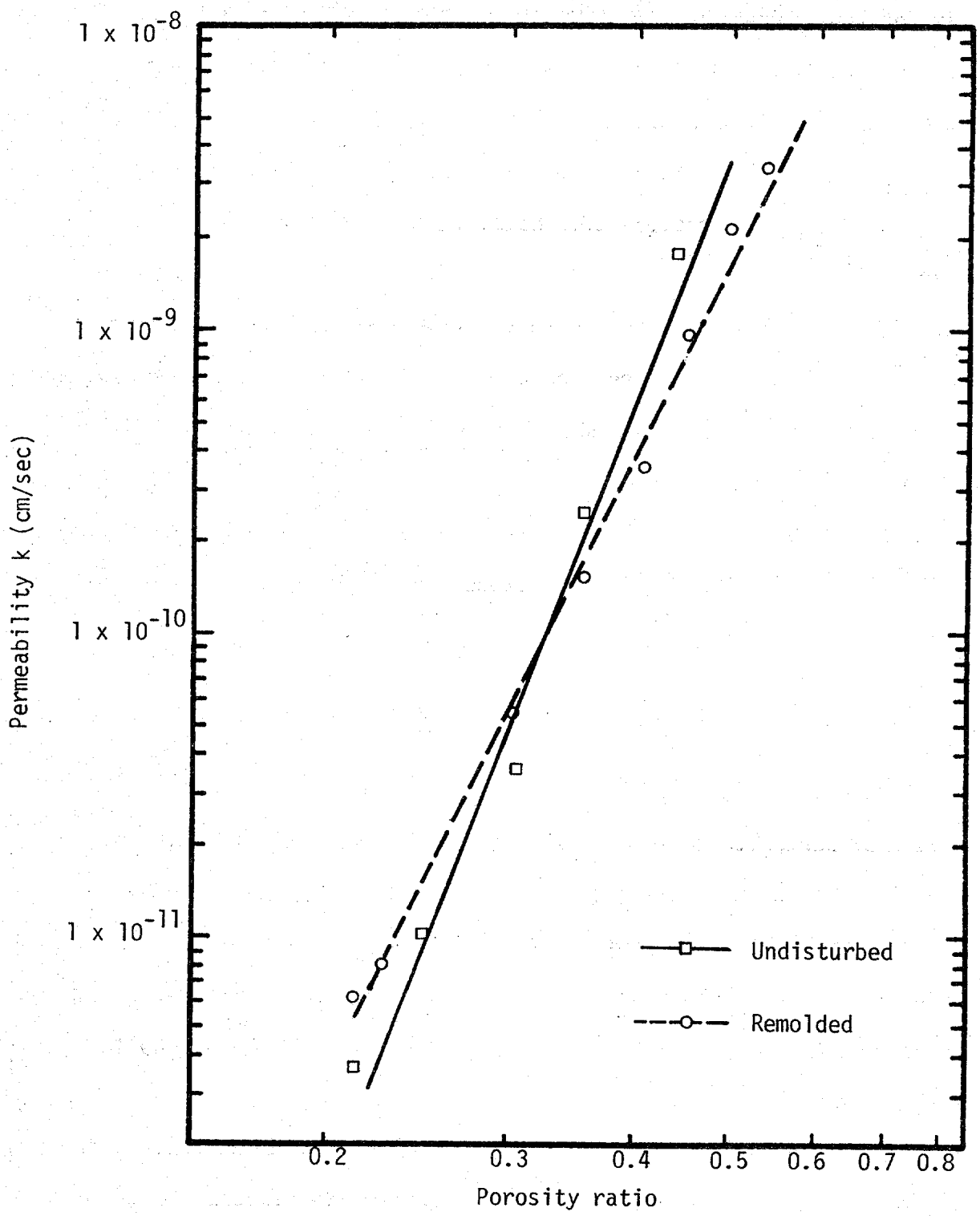

Fig. 24 - Graph of Permeability versus Porosity Ratio for Marine Core from Angola Basin Tested at 20°C

interpretation may be used to explain the phenomenon.

> . . . It (liquid limit) also can be interpreted as the distance between particles or between structural units of particles at which forces of interaction between the clay particles become sufficiently weak to allow easy movement of particles or units relative to each other . . . . An increasing salt concentration, which results in a decrease in interparticle repulsion decreases the liquid limit. The repulsion between particles can be considered to determine the interaction volume, keeping the particles in a fixed configuration with respect to each other and preventing free movement. As the repulsion is decreased, the particles become free to move at lower water contents or lower interparticle distances, and the liquid limit decreases.

Correlation of the Compressibility and Permeability with Soil Indices

Consolidation. - An attempt was made to relate the compressibility coefficients A and B to the liquid limit, plastic limit and the percent clay of each sample. In order to get a better spread of materials, additional consolidation data were obtained from both the Oceanography Department and the Geology Department at Texas A&M University. Table 20 in Appendix III lists the fifty sets of consolidation data with the corresponding compressibility coefficients, liquid limits, plastic limits and the percent clay for each sample.

A simple multiple regression analysis computer program was used to analyze the data. It is written in FORTRAN language and given in Appendix III.

It was assumed that the compressibility constants could be expressed by a generalized power series of the three variables liquid limit (w_ℓ), the plastic limit (w_p) and the percent clay (%C). It was also assumed that various terms in these series would dominate and

that the other terms could be ignored. By trial and error, various terms of the power series were selected to express the compressibility coefficients as a polynomial of the three variables. The 50 sets of data then were used to compute the unknown constants. Table 6 shows the different polynomials tried and the computed constants. The coefficient of determination (R^2) is also shown. R^2, the measure of the goodness of fit of the data, has a value of unity when the fit is perfect.

For the compressibility coefficient A, the best polynomial of the variables yielded is $R^2 = 0.84$. However, there are 17 terms and it is doubtful that such a complicated function could have much practical use.

For the compressibility coefficient B, the best polynomial of the variables yielded an $R^2 = 0.41$. It also has 17 terms. The correlation is unsatisfactory and the function is much too complicated for practical use.

The maximum consolidation stress and the minimum porosity developed during the tests are also shown in Table 20 in Appendix III. It can be seen that the results from other studies, with nine exceptions, are for tests at much lower maximum pressures than the test performed during this study. Most of the data are limited to a very low pressure range. Even though all the correlations for the compressibility coefficients are excellent the compressibility coefficients computed for all the data do not correspond to the same pressure range. The large difference in the pressure range may have affected the correlation.

It has been suggested by R. L. Lytton that the shrinkage limit may be a better index because the porosity at the shrinkage limit

TABLE 6 - Functions of the Compressibility Coefficients A and B in Terms of the Material Properties

Compressibility Coefficient	Function	Coefficient of Determination R^2
A	$5.7 \times 10^3 \, w_\ell^{0.805}$	0.02
A	$1.44 \, w_p^{-0.56}$	0.01
A	$6.67 \times 10^6 \, \%C^{2.48}$	0.14
A	$0.017 \, w_\ell^{3.09} \, w_p^{-3.13}$	0.15
A	$1.0 \times 10^{-5} \, w_\ell^{-0.23} \, \%C^{2.63}$	0.14
A	$6.86 \times 10^5 \, w_p^{-1.97} \, \%C^{3.61}$	0.23
A	$1.15 \times 10^{-5} \, w_\ell^{2.24} \, w_p^{-3.60} \%C^{3.10}$	0.30
A	$- 6.27 + 0.104 \, w_\ell^{0.8} + 2.68 \, w_p^{-0.56} - 0.394$ $\%C^{2.48} - 0.0787 \, w_\ell^{3.09} w_p^{-3.13} + 0.629 \times 10^{-3}$ $w_\ell^{-0.234} w_p^{2.63} + 0.888 \times 10^{-4} w_\ell^{2.24} w_p^{-3.64}$ $\%C^{3.09} - 0.668 \times 10^{-3} w_p^{4.98} \%C^{3.61}$	0.79
A	$-2.26 - 0.05 \, w_\ell - 0.02 \, w_p + 64.0 \log w_\ell -$ $32.1 \log w_p - 30 \log \%C + 0.1 \, \%C$	0.18
A	$- 2.31 + 0.0037 \, w_\ell - 0.71 \, w_p + 0.17 \, \%C +$ $25.9 \frac{w_p}{w_\ell} - 8.1 \frac{\%C}{w_\ell} + 6.3 \frac{w_p}{\%C} + 0.002 \, w_\ell \cdot w_p +$	

TABLE 6 - (Continued)

Compressibility Coefficient	Function	Coefficient of Determination R^2
	$8 \times 10^{-4} w_p \cdot \%C$	0.55
A	$2.6 + 8.4 \times 10^5 \frac{w_\ell}{w_p \%C^3} - 131 \cdot (\frac{w_p}{w_\ell})^2 +$ $138 (\frac{w_p}{w_\ell})^3 - 2691 \frac{\%C}{w_p \%C} - 4.15 \times 10^4 \frac{w_\ell}{w_p \%C^2} +$ $4032 \frac{w_p}{w_\ell^2} - 1.4 \times 10^5 \frac{w_p}{w_\ell^3} - 907 \frac{\%C}{w_\ell^2} + 4.3 \times$ $10^4 \frac{\%C}{w_\ell^3}$	0.58
A	$- 51 + 0.5 w_\ell - 4.0 w_p + 0.4 \%C + 433 \frac{w_p}{w_\ell}$ $- 32 \frac{\%C}{w_\ell} + 40 \frac{w_p}{\%C} - 8414 \frac{w_p}{w_\ell^3} - 222 \frac{\%C}{w_\ell^2} -$ $1.3 \frac{w_p \%C}{w_\ell} - 4780 \frac{w_p}{w_\ell \%C} + 6.8 \frac{w_p^2}{w_\ell} - 910$ $(\frac{w_p}{w_\ell})^2 + 423 (\frac{w_p}{w_\ell})^3 + 0.008 \frac{w_p \%C^2}{w_\ell}$	0.78
A	$- 21.2 + 0.97 (\frac{w_\ell}{w_p})^3 - 62.5 (\frac{w_\ell}{w_p})^2 + 36 \frac{w_p}{w_\ell} +$	

TABLE 6 (continued)

Compressibility Coefficient	Function	Coefficient of Determination R^2
	$+ 59.7 \frac{w_\ell}{w_p} + 382 \frac{w_\ell}{w_p^2} - 1.0 \times 10^5 \frac{w_\ell}{w_p^2} - 660$	
	$\frac{w_p}{w_\ell^2} + 7.8 \times 10^5 \frac{w_p}{w_\ell^3} + 7.3 \times 10^5 \frac{w_\ell}{w_p^4} -$	
	$- 2.5 \times 10^5 \frac{w_p}{w_\ell^4} - 9.6 \times 10^4 (\frac{w_p}{w_\ell^2})^2 + 2.1 \times$	
	$10^4 \frac{w_p}{w_\ell^2 \%C})^2 + 2.1 \times 10^4 \frac{w_p}{w_\ell^2 \%C} - 4.78 \frac{w_p}{w_\ell \%C}$	0.70
A	$- 51.5 + 13.3\ w_p - 2.11\ w_\ell + 0.53\ \%C + 71.1$	
	$\frac{w_\ell}{w_p} - 18.6 \frac{\%C}{w_p} + 23.8 \frac{w_\ell}{\%C} + 2037 \frac{w_\ell}{w_\ell^2} - 98.73$	
	$\frac{w_\ell}{w_p^3} - 78 \frac{\%C}{w_\ell^2} - 0.59 \frac{w_\ell \%C}{w_p} - 1610 \frac{w_\ell}{w_p \%C} + 1.1$	
	$\frac{w_\ell^2}{w_p} - 0.062 \frac{w_\ell^3}{w_p} - 43 (\frac{w_\ell}{w_p})^2 + 2.95 (\frac{w_\ell}{w_p})^3 +$	
	$0.003 \frac{w_\ell \%C^2}{w_p}$	0.84
A	$- 10 + 15 \frac{\%C}{w_\ell} - 225.8 \frac{\%C}{w_\ell^2} - 0.27 \frac{w_\ell^2}{\%C} + 1.7 \times$	
	$10^4 \frac{\%C}{w_p^3} - 22 \frac{\%C}{w_\ell} + 16 \frac{w_p}{\%C} + 0.002 \frac{w_p^3}{\%C} - 0.6$	

TABLE 6 (continued)

Compressibility Coefficient	Function	Coefficient of Determination R^2
	$\frac{\%C}{w_\ell^2} + 930 \frac{w_\ell}{\%C} - 1.2 \times 10^5 \frac{\%C}{w_\ell^3}$	0.55
A	$- 23.9 + 0.06\ w_\ell - 0.148\ w_p + 60 \log w_\ell -$ $23.1 \log w_p - 316 \log (w_\ell - w_p) - 2.7 \frac{w_\ell - w_p}{\%C}$	0.55
B	$- 198\ w_\ell^{0.34}$	0.08
B	$- 1.06\ w_p^{0.60}$	0.23
B	$- 14.42\ \%C^{-0.119}$	0.006
B	$- 1.5\ w_\ell^{-0.25}\ w_p^{0.8}$	0.24
B	$- 6.0\ w_\ell^{0.52}\ \%C^{-0.46}$	0.15
B	$- 5.42\ w_\ell^{0.83}\ \%C^{-0.59}$	0.35
B	$- 5.75\ w_\ell^{-0.09}\ w_p^{0.9}\ \%C - 0.57$	0.35
B	$- 8.42 + 111.6\ w_\ell^{0.34} - 79.5\ w_p^{0.6} + 1129.3$ $\%C^{-0.12} + 97.5\ w_\ell^{-0.25}\ w_p^{0.8} - 195.4\ w_\ell^{0.52}$	

TABLE 6 (continued)

Compressibility Coefficient	Function	Coefficient of Determination R^2
	$\%C^{-0.46} - 902\, w_\ell^{-0.09}\, w_p^{0.89}\, \%C^{0.57} +$ $856.2\, w_p^{0.83}\, \%C^{-0.59}$	0.33
B	$+ 5.55 + 0.074\, w_\ell - 0.27\, w_p - 10.58 \log w_\ell - 17.5 \log w_p + 15.8 \log \%C - 0.026\, \%C$	0.31
B	$- 0.25 + 0.14\, w_\ell - 0.33\, w_p - 0.31\, \%C - 7.04 \frac{w_p}{w_\ell} + 8.8 \frac{\%C}{w_\ell} - 5.6 \frac{w_p}{\%C} - 0.0017\, w_\ell \cdot w_p + 0.0055\, w_p\, \%C$	0.34
B	$+ 74.7 - 0.4\, w_\ell + 3.6\, w_p - 0.06\, \%C - 522.7 \frac{w_p}{w_\ell} - 1.5 \times 10^5 \frac{\%C}{w_\ell} - 33 \frac{w_p}{\%C} - 4102 \frac{w_p}{w_\ell^2} - 8 \times 10^4 \frac{w_p}{w_\ell^3} + 1.6 \times 10^4 \frac{\%C}{2^w} - 0.21 \frac{w_p}{w_\ell^2} + 1.4 \times 10^4 \frac{w_p}{w_\ell \%C} - 5.8 \frac{w_p}{w_\ell} + 0.015 \frac{w_p^3}{w_\ell} + 1.6 \times 10^4 \left(\frac{w_p}{w_\ell}\right)^2 - 997 \left(\frac{w_p}{w_\ell}\right)^3 + 0.01 \frac{w_p \%C^2}{w_\ell}$	0.38
B	$+ 120 - 2.1\, w_p + 3.6\, w_\ell - 1.3\, \%C - 122 \frac{w_\ell}{w_p} +$	

TABLE 6 (continued)

Compressibility Coefficient	Function	Coefficient of Determination R^2
	$+ 36 \frac{\%C}{w_p} - 37 \frac{w_\ell}{\%C} - 4516 \frac{w_\ell}{w_p^2} + 2.4 \times 10^4 \frac{w_\ell}{w_p^3} + 139 \frac{\%C}{w_p^2} + 1.1 \frac{w_\ell \%C}{w_p} + 2.9 \times 10^3 \frac{w_\ell}{w_p \%C} - 2.1 \frac{w_\ell^2}{w_p} + 0.004 \frac{w_\ell^3}{w_p} + 86.3 \left(\frac{w_\ell}{w_p}\right)^2 - 6.05 \left(\frac{w_\ell}{w_p}\right)^3 - 0.005 \frac{w_\ell \%C^2}{w_p}$	0.41
B	$- 5.62 - 77924 \frac{w_\ell}{w_p \%C^2} - 55.5 \left(\frac{w_p}{w_\ell}\right)^2 + 58.9 \left(\frac{w_p}{w_\ell}\right)^3 - 7861.8 \frac{\%C}{(w_p)^4} 0\ 70.4 \frac{w_\ell}{w_p \%C} + 6962 \frac{w_\ell}{w_p \%C^2} - 1824 \frac{w_p}{w_\ell^2} + 65034 \frac{w_p}{w_\ell^3} + 9874 \frac{\%C}{w_\ell^2} - 28114.2 \frac{\%C}{w_\ell^3}$	0.35
B	$- 235 + 1.25 \left(\frac{w_\ell}{w_p}\right)^3 - 23.3 \left(\frac{w_\ell}{w_p}\right)^2 + 103 \frac{w_p}{w_\ell} + 129 \frac{w_\ell}{w_p} - 833 \frac{w_\ell}{w_p^2} + 22555 \frac{w_\ell}{w_p^3} + 4810 \frac{w_p}{w_\ell^2} -$	

TABLE 6 (continued)

Compressibility Coefficient	Function	Coefficient of Determination R^2
B	$-214712 \frac{w_p}{w_\ell^3} - 179988 \frac{w_\ell}{w_p^4} + 76177 \left(\frac{w_p}{w_\ell^2}\right)^2 + 7296 \frac{w_p}{u^2 \%C} - 444 \frac{w_p}{w_\ell \%C}$	0.36
	$-11.3 - 18.3 \frac{\%C}{w_p} + 427 \frac{\%C}{w_p^2} - 0.44 \frac{w_p^2}{\%C} - 3318 \frac{\%C}{w_p^3} + 43 \frac{\%C}{w_p} - 0.33 \frac{w_p}{\%C} + 0.003 \frac{w_p^3}{\%C} - 2010 \frac{\%C}{w_\ell^2} + 5.31 \frac{w_\ell}{\%C} + 32463 \frac{\%C}{w_\ell^3}$	0.33
B	$-2.0 + 0.01\, w_\ell - 0.07\, w_p + 23.6 \log w_\ell - 20.9 \log w_p - 10.3 \log (w_\ell - w_p) - 2.2 \frac{w_\ell - w_p}{\%C}$	0.26

w_ℓ is the liquid limit

w_p is the plastic limit

%C is the % clay content

resembles the porosity developed under high pressure consolidation. However, the suggestion was made too late to be included in this study.

Permeability. - The same technique was used in the attempt to relate the permeability constants C and D to the Atterberg limits. The results of nine different permeability tests, tabulated in Table 21, in Appendix III, were used for the analysis. Table 7 shows the function for C and D and the coefficient of determination. The R^2 of the best fit functions for C and D are 0.36 and 0.35 respectively. These functions indicate that no good correlation could be found between the liquid limit, plastic limit and the permeability constants.

However, the data had a very limited range. A more thorough study could have been performed if more experimental data had been available. It may be that the percent clay and the shrinkage limit would have been additional indices of value. When these indices were suggested there was not time to include them in the study.

TABLE 7 - Functions of the Permeability Constants C & D in Terms of the Material Properties

Permeability Constant	Function	Coefficient of Determination (R^2)
C	$0.0033 - 0.23 \times 10^{-4} w_\ell + 0.77 \times 10^{-5} w_p + 0.14 \times 10^{-5} (w_\ell - w_p)$	0.04
C	$- 0.05 + 0.56 \times 10^{-3} w_\ell + 0.16 \times 10^{-2} w_p - 0.18 \times 10^{-4} w_p \cdot w_\ell$	0.35
C	$0.36 \times 10^{-2} w_\ell^{-3.1}$	0.19
C	$- 5.11 w_p^{-0.524}$	0.01
C	$0.38 w_\ell^{-3.06} w_p^{-0.28}$	0.20
C	$0.015 + 28643 w_\ell^{-3.1} + 0.087 w_p^{-0.524} - 59017 w_\ell^{-3.06} w_p^{-0.28}$	0.36
D	$11.1 - 0.017 w_\ell + 0.002 w_p + 0.012 (w_\ell - w_p)$	0.06
D	$- 30.3 + 0.45 w_\ell + 1.29 w_p - 0.014 (w_\ell \cdot w_p)$	0.35
D	$0.922 w_\ell^{0.0167}$	0.001
D	$1.09 w_p^{-0.085}$	0.03
D	$1.04 w_\ell^{0.029} w_p^{-0.087}$	0.03
D	$18166 - 16645 w_\ell^{0.0167} - 14072 w_p^{-0.025} + 12185 w_\ell^{0.029} w_p^{-0.087}$	0.14

w_ℓ is the liquid limit
w_p is the plastic limit
%C is the % clay content

CONCLUSIONS AND RECOMMENDATIONS

In an effort to aid in the development of a method to estimate downhole or formation pore pressure in overpressured marine sediments a sequence of consolidation and permeability tests have been performed on the major types of clay minerals. The pressures ranged from 46 psi (0.32 kN/m^2) to 10,000 psi (69,000 kN/m^2) and the temperatures ranged from 69°F (20°C) to 194°F (90°C). An effort was made to relate the compressibility coefficients and permeability constants to the liquid limit, plastic limit and percent clay. Based on the results obtained, conclusions are drawn as follows:

1. With high pressure consolidation, temperature does not seem to affect the compressibility of bentonite and illite. However, the compressibility of kaolinite increases slightly with an increase in temperature.

2. The compressibility of clay can be very well described by the power law function of porosity ratio.

3. It was found that the coefficients of the power law representation for compressibility could be related to the liquid limit, plastic limit and percent clay. However, 17 terms were required to get a R^2 of 0.84 for A and 17 terms were required to get a R^2 of 0.38 for B. These functions indicate that liquid limit, plastic limit and percent clay are not the best parameters for the description of high pressure compressibility.

4. The compressibility of the remolded sample for Angola Basin is lower than that of the undisturbed sample.

5. The liquid limit of bentonite is much lower if sea water is

used instead of distilled water. It is believed that the concentration of exchangeable cations affects the liquid limit of bentonite.

6. The permeability of the clays can be described by a power law of the porosity ratio. As the temperature was increased the permeability increased.

7. No good relationship could be found between the permeability constants and the liquid limit and plastic limit. The R^2 of the best fit functions for C and D are 0.36 and 0.35 respectively. This indicates that the liquid limit and plastic limit alone are not the preferable parameters for the description of permeability.

In order to understand more about the behavior of the marine sediments, new investigations are suggested. These are:

1. Development of the relationship between the compressibility and permeability coefficients A, B, C and D and the mineralogy of sediments. The shrinkage limit may also be a good indicator of these descriptions.

2. Further experiments on the compressibility of both remolded and undisturbed samples of various types of marine sediments are needed to validate the application of lab test data to actual field conditions.

APPENDIX I

References

REFERENCES

1. Akagi, T., "Effect of Desiccation and Ring Friction on the Apparent Preconsolidation Load and Clay," thesis presented to the University of Illinois, Urbana, Illinois, in 1960 in partial fulfillment of the requirement for the degree of Master of Science.

2. Archie, G. E., "Introduction to Petrophysics of Reservoir Rocks," Bulletin of AAPG, Vol. 34, No. 5, 1950, pp. 943-961.

3. Azzouz, A. S., Krizek, R. J., and Corotis, R. B., "Regression Analysis of Soil Compressibility," Soils and Foundations, Japanese Society of Soil Mechanics and Foundation Engineering, Vol. 16, No. 2, June 1976, pp. 19-29.

4. Bennett, R. H., "Piezometer Data and Instrumentation of 1975," presented at the workshop on Pore Pressures in Submarine Sediments, NOAA, Atlantic Oceanographic and Meteorological Laboratories, 15 Richenbacker Causeway, Miami, Florida, 33149, February 1979.

5. Bjerrum, L., Casagrande, A., Peck, R. B., and Skempton, A. W., From Theory to Practice in Soil Mechanics, Selection from the writings of Karl Terzaghi, John Wiley and Sons, Inc., Publisher, New York, N. Y., 1960.

6. Bolt, G. H., "Physico-Chemical Analysis of the Compressibility of Pure Clay," Geotechnique, Vol. 6, No. 2, 1956, pp. 86-93.

7. Burmister, D. M., "Strain Rate Behavior of Clay and Organic Soil," Special Technical Publication 254, ASTM, 1949, pp. 88-105.

8. Campanella, R. G., and Mitchell, J. K., "Influence of Temperature Variation on Soil Behavior," Journal of Soil Mechanics and Foundation Division, ASCE, Vol. 94, No. SM3, May 1968, pp. 709-734.

9. Costley, R. D., "Hazards and Costs Cut by Planned Drilling Programs," World Oil, October 1967, pp. 92-96.

10. Cozzoline, E. V. M., "Statistical Forecasting of Compression Index," Proceedings of the 5th International Conference of Soil Mechanics and Foundations Engineering, Vol. 1, 1961, pp. 51-53.

11. Dunlap, W. A., Bryant, W. R., Williams, G. N., and Sudayda, J. N., "Storm Wave Effects on Deltaic Sediments - Results of SEASWAB I and II," Proceedings of the Fifth International Conference of Port and Ocean Engineering Under Arctic Conditions, at the Norwegian Institute of Technology, August 1979, pp. 899-933.

12. Evans and Lewis, "Effective Stress Principle in Saturated Clay," Journal of Soil Mechanics and Foundation Division, ASCE, Vol. 96, No. SM2, March 1970, pp. 671-683.

13. Fertl, W. H., Abnormal Formation Pressure, Elsevier Scientific Publishing Co., New York, N.Y.

14. Fertl, W. H., and Timko, D. J., "How Downhole Temperature, Pressure Affect Drilling," An Engineering Practices Report: Part I, World Oil, Vol. 174, No. 7, pp. 67-70.

15. Finn, F. N., "The Effect of Temperature on the Consolidation Characteristics of Remolded Clay," Special Publication No. 126, ASTM, 1951, pp. 65-71.

16. Franklin, A. G., Personal Communication, Corps of Engineers, Waterways Experiment Station, Vicksburg, Mississippi, 1980.

17. Hamilton, T. K., Personal Communication, Fugro Gulf Co., Houston, Texas, 1979.

18. Katherman, C., and Bryant, W. R., "Variations in Porosity with Depth for Marine Sediments," Department of Oceanography, Texas A&M University, Technical Report 78-11-T, November 1978.

19. Kezdi, A., Handbook of Soil Mechanics, Soil Physics, Elsevier Scientific Publishing Co., New York, N. Y., 1974.

20. Kharaka, Y. K., and Smalley, W. C., "Flow of Water and Solutes Through Compacted Clays," Bulletin of AAPG, Vol. 60, No. 6, June 1976, pp. 973-980.

21. Krizek, R. I., and Salam, A. M., "Behavior of Dredged Material in Diked Containment Areas," E.P.A. Grants 15070-GCK and R-800948, Technical Report No. 5, Environmental Protection Agency, Northwestern University, Evanston, Illinois, September 1974.

22. Lambe,T. W., "The Permeability of Compacted Fine-Grained Soils," Symposium on Permeability of Soils, ASTM, Special Technical Publication No. 163, 1954, pp. 56-67.

23. Lambe, T. W., "The Structure of Compacted Clay," Journal of Soil Mechanics and Foundation Division, ASCE, Vol. 84., No. SM2, May 1958, pp. 1654-1 - 1654-33.

24. Lambe, T. W., "The Engineering Behavior of Compacted Clay," Journal of Soil Mechanics and Foundation Division, ASCE, Vol. 84, No. SM2, May 1958, pp. 1655-1 - 1655-38.

25. Lambe, T. W., and Whitman, R. V., Soil Mechanics, John Wiley and Son, Inc., New York, 1969.

26. Leonards, G. A., Foundation Engineering, McGraw-Hill Co., Inc., New York, N. Y., 1962.

27. Lewis, C. R., and Rose, S. C., "A Theory Relating High Temperature and Overpressures," Journal of Petroleum Technology, Vol. 22, January 1970, pp. 11-16.

28. Macey, H. H., "Clay-Water Relationship," The Proceedings of Physical Society of London, Vol. 52, No. 293, September 1940.

29. Means, R. E., and Parcher, J. V., Physical Properties of Soils, Charles E. Merrill Books, Inc., Columbus, Ohio, 1963.

30. Miller, J. W., "The Thermal Conductivity of Sediments as a Function of Porosity," Thesis presented to Texas A&M University, College Station, Texas, August 1979, in partial fulfillment of the requirements for the degree of Master of Science.

31. Mitchell, J. K., Fundamentals of Soil Behavior, John Wiley and Son, Inc., New York, N.Y., 1976.

32. Notting, P. G., "Physical Analysis of Oil Sands," Bulletin of AAPG, Vol. 14, No. 10, 1930, pp. 1337-1349.

33. Nur, A., and Byerlee, J. D., "An Exact Effective Stress Law for Elastic Deformation of Rock with Fluids," Journal of Geophysical Research, Vol. 76, No. 26, September 1971, pp. 6414-6419.

34. Olson, R. E., and Mesic, G., "Mechanisms Controlling Compressibility of Clay," Journal of Soil Mechanics and Foundations Division, ASCE, Vol. 96, No. SM6, 1970, pp. 1863-1877.

35. Paaswell, R. E., "The Effect of Temperature on a Fine-Particled Consolidating Soil," Thesis presented to Rutgers, the State University, at New Brunswick, New Jersey, 1965, in partial fulfillment of the requirements for the degree of Doctor of Philosophy.

36. Plum, R. L., and Esrig, M. I., "Some Temperature Effects on Soil Compressibility and Pore Water Pressure," Proceedings of International Conference on Effects of Temperature and Heat on Engineering Behavior of Soils, Special Report No. 103, Highway Research Board, 1969, pp. 231-242.

37. Rubey, W. W., and Hubbert, M. K., "Role of Fluid Pressure in Mechanics of Overthrust Faulting," Bulletin of Geol. Society of America, Vol. 70, February 1959, pp. 167-206.

38. Rubey, W. W., "The Effects of Gravitational Compaction on the Structure of Sedimentary Rock: A Discussion," Bulletin of AAPG, Vol. 11, No. 6, 1927, pp. 621-632.

39. Seed, H. B., Woodard, R. J., and Lundgren, R., "Fundamental Aspects of the Atterberg Limits," Journal of Soil Mechanics and Foundations Division, ASCE, Vol. 90, No. SM6, Nov. 1964, pp. 75-105.

40. Sherman, W. C., and Hadjidakis, C. G., "Engineering Properties of Fine-Grained Mississippi Valley Alluvial Soil, Meander Belt and Backswamp Deposits," U. S. Waterways Experiment Station, Technical Report No. 3-604, Vicksburg, Mississippi, June 1962.

41. Skempton, A. W., "Effective Stress in Soils, Concrete and Rocks," Pore Pressure and Suction in Soils, Butterworths and Co., London, England, 1961, pp. 4-16.

42. Skempton, A. W., "Notes on the Compressibility of Clay," Quarterly Journal of Geology Society of London, Vol. 10, Part 1 and 2, 1943, pp. 119-135.

43. Smith, W. O., and Stallman, R. W., "Measurement of Permeability in Ground-Water Investigations," Symposium on Permeability of Soils, ASTM, Special Technical Publication No. 163, 1954, pp. 56-67.

44. Terzaghi, K., "Simplified Soil Tests for Subgrades and Their Physical Significance," Public Road, Vol. 7, No. 8, October 1926, pp. 153-162.

45. Terzaghi, K., and Peck, R. B., Soil Mechanics in Engineering Practice, John Wiley and Sons, Inc., New York, N.Y., 1948.

46. Thompson, L. J., "Overpressured Marine Sediments," Report for U.S.G.S, Grant No. 14-08-001-G-444, U. S. Geological Survey, Texas A&M Research Foundation, College Station, Texas, July 1979.

47. Thompson, L. J., Chen, Robert H., and Bryant, William R., "Overpressured Marine Sediments," a Research Project for the U. S. Geological Survey, Conservation Branch, Metairie, Louisiana, Texas A&M Research Foundation, College Station, Texas, January 1977.

48. Warkentin, B. P., "Interpretation of the Upper Plastic Limit of Clay," Nature, April 1961, pp. 287-288.

49. Wu, T. H., Soil Mechanics, Allyn and Bacon, Inc., Boston, Mass., 1970.

50. Yong, R. T., Taylor, L., and Warkentin, B. P., "Swelling Pressure of Sodium Montmorillonite at Depressed Temperatures," Proceedings of 11th National Conference on Clay and Clay Minerals, Vol. 1, pp. 268-281.

APPENDIX II

Notation

NOTATION

A = compressibility coefficient,

A_o = experimental constant,

A_t = cross-sectional area of soil,

a = the ratio of grain-to-grain contact area to the total area,

B = compressibility coefficient,

B_o = experimental constant,

C = permeability constant,

C_c = compression index,

C_k = a factor depends on the pore shape, specific surface area, and the ratio of length of actual flow path to soil bed thickness,

C_p = the compressibility of porous material,

C_s = the compressibility of solid substance,

%C = percent clay content,

D = permeability constant,

E = area ratio parameter

e = void ratio,

F = experimental constant reflecting the compressibility,

F_m = force acting on the mineral matrix per unit total cross-section area,

G = experimental constant,

H = sample height,

H_c = the bulk modulus of the solid,

H_m = the intrinsic bulk modulus of the solid,

H_s = height of solid,

H_w = height of water,

i = hydraulic gradient,

K = absolute permeability,

k = permeability,

n = porosity,

P = pressure difference between top and bottom of the sample,

q = flow rate,

u = pore pressure,

V_s = volume of solid,

V_w = volume of water,

W_s = weight of solid,

W_T = total weight of soil,

W_w = weight of water,

w = moisture content,

w_ℓ = liquid limit,

w_p = plastic limit,

α = experimental constant,

β = experimental constant,

γ = unit weight,

γ_s = unit weight of solid,

γ_w = unit weight of water,

λ = parameter due to the shearing resistances,

μ = viscosity,

μ_{20} = viscosity at temperature of 20^oC,

μ_T = viscosity at temperature of T^oC,

$\bar{\sigma}$ = the stress acting on the solid matrix,

σ = total stress,

ϕ' = the angle of shearing resistance of the porous material,

ϕ'_a = the angle of shearing resistance obtained from the normal consolidation undrained test,

ϕ'_b = the angle of shearing resistance obtained from the test with negative pore pressure,

ψ = the angle of intrinsic shearing resistance.

APPENDIX III

Tables of Test Data and Results of
Consolidation and Permeability Tests

TABLE 8 - Permeability Test Data

Test	Sample Height H (in.)	Porosity Ratio	p_T* (psi)	p_B** (psi)	Flow Rate (mℓ/sec x 1000)	Average Permeability (cm/sec)
K-20	0.693	0.449	271	0	1.4	
			362	0	2.0	
			453	0	2.5	4.0×10^{-9}
K-20	0.642	0.405	362	0	1.0	
			543	0	1.5	
			724	0	2.2	2.35×10^{-9}
K-20	0.5751	0.336	904	0	0.7	
			1266	0	1.0	
			1628	0	1.3	6.11×10^{-10}
K-20	0.5199	0.266	1440	0	0.3	
			1980	0	0.4	
			2700	0	0.7	1.74×10^{-10}
K-60	0.709	0.529	47	2.5	0.50	
			93	2.5	1.00	
			137	2.5	2.1	1.05×10^{-8}
K-60	0.65	0.489	92	2.5	0.6	
			137	2.5	1.3	
			183	2.5	2.3	7.68×10^{-9}
K-60	0.604	0.447	182	2.5	1.3	
			363	2.5	3.8	6.36×10^{-9}

TABLE 8 - (Continued)

Test	Sample Height H (in.)	Porosity Ratio n	p_T* (psi)	p_B** (psi)	Flow Rate (mℓ/sec x 1000)	Average Permeability (cm/sec)
K-60	0.550	0.393	182	2.5	0.7	
			363	2.5	1.6	
			542	2.5	2.5	2.77×10^{-9}
K-60	0.51	0.345	365	2.5	0.7	
			542	2.5	1.1	
			722	2.5	1.5	1.20×10^{-9}
K-60	0.469	0.288	542	2.5	0.5	
			962	2.5	0.7	
			1322	2.5	1.1	4.70×10^{-10}
K-60	0.443	0.246	722	2.5	0.3	
			1442	2.5	0.7	
			2162	2.5	0.9	2.33×10^{-10}
K-90	0.774	0.542	104	14	0.7	
			125	14	0.8	4.69×10^{-8}
K-90	0.674	0.474	150	14	3.3	
			195	14	3.8	1.01×10^{-8}
K-90	0.623	0.431	240	14	2.6	
			330	14	4.3	5.49×10^{-9}
K-90	0.537	0.340	558	14	4.0	
			740	14	5.3	3.51×10^{-9}
K-90	0.517	0.313	558	14	1.8	
			738	14	2.3	
			920	14	3.2	1.25×10^{-9}

TABLE 8 - (Continued)

Test	Sample Height H (in.)	Porosity Ratio n	p_T* (psi)	p_B** (psi)	Flow Rate (mℓ/sec x 1000)	Average Permeability (cm/sec)
K-90	0.486	0.270	920	14	1.3	
			1195	14	1.7	
			1458	14	2.2	4.76×10^{-10}
K-90	0.457	0.223	1434	14	0.8	
			2175	14	1.3	
			2894	14	1.6	1.55×10^{-10}
I-20	0.936	0.453	45	0	0.8	2.02×10^{-9}
I-20	0.873	0.413	90	0	0.1	
			135	0	0.2	1.43×10^{-9}
I-20	0.819	0.375	180	0	0.16	
			270	0	0.2	8.86×10^{-10}
I-20	0.773	0.337	360	0	0.16	
			540	0	0.22	4.26×10^{-10}
I-20	0.728	0.297	720	0	0.10	
			1080	0	0.15	1.17×10^{-10}
I-20	0.692	0.26	720	0	0.04	
			1440	0	0.06	4.13×10^{-11}
I-20	0.667	0.233	1080	0	0.05	3.49×10^{-11}
I-60	1.127	0.751	92	2.5	0.19	
			138	2.5	0.39	3.32×10^{-9}
I-60	1.038	0.380	182	2.5	0.20	
			273	2.5	0.38	1.59×10^{-9}

TABLE 8 - (Continued)

Test	Sample Height H (in.)	Porosity Ratio n	p_T* (psi)	p_B** (psi)	Flow Rate (mℓ/sec x 1000)	Average Permeability (cm/sec)
I-60	0.965	0.333	362	2.5	0.20	
			542	2.5	0.28	6.03×10^{-10}
I-60	0.914	0.295	723	2.5	0.17	
			1082	2.5	0.11	1.78×10^{-10}
I-60	0.821	0.215	2883	2.5	0.10	
			4322	2.5	0.09	2.71×10^{-11}
I-60	0.791	0.186	5043	2.5	0.05	1.02×10^{-11}
I-90	0.940	0.441	105	14	0.37	
			150	14	1.11	4.95×10^{-9}
I-90	0.872	0.398	194	14	0.59	
			230	14	0.83	3.65×10^{-9}
I-90	0.805	0.347	375	14	0.42	
			553	14	0.76	1.26×10^{-9}
I-90	0.748	0.298	733	14	0.38	4.15×10^{-10}
I-90	0.707	0.257	1095	14	0.45	
			1455	14	0.2	1.19×10^{-10}
I-90	0.666	0.212	2895	14	0.09	
			4334	14	0.15	2.67×10^{-11}
I-90	0.640	0.180	4330	14	0.02	4.12×10^{-12}
B-20	0.365	0.43	2522	0	0.008	3.97×10^{-12}
B-20	0.343	0.364	901	0	0.005	
			1263	0	0.016	1.25×10^{-12}

TABLE 8 - (Continued)

Test	Sample Height H (in.)	Porosity Ratio n	p_T* (psi)	p_B** (psi)	Flow Rate (mℓ/sec x 1000)	Average Permeability (cm/sec)
B-20	0.324	0.327	3600	0	0.005	5.24×10^{-13}
B-20	0.306	0.287	5044	0	0.004	3.12×10^{-13}
B-60	0.592	0.561	138	2.5	0.053	2.51×10^{-10}
B-60	0.527	0.507	273	2.5	0.028	6.51×10^{-11}
B-60	0.471	0.448	542	2.5	0.01	1.11×10^{-11}
B-60	0.437	0.405	1083	2.5	0.01	5.01×10^{-12}
B-60	0.407	0.361	2162	2.5	0.010	1.60×10^{-12}
B-60	0.383	0.321	3602	2.5	0.069	7.48×10^{-13}
B-90	0.848	0.55	134	14	0.07	6.00×10^{-10}
B-90	0.753	0.493	195	14	0.02	9.73×10^{-11}
B-90	0.682	0.441	655	14	0.015	1.84×10^{-11}
B-90	0.633	0.397	1095	14	0.013	8.80×10^{-12}
B-90	0.598	0.362	175	14	0.011	3.69×10^{-12}
B-90	0.558	0.316	2895	14	0.010	2.34×10^{-12}
B-90	0.529	0.279	4335	14	0.007	1.09×10^{-12}
M-U	1.669	0.430	540	0	1.8	1.71×10^{-9}
M-U	1.506	0.368	720	0	0.42	2.49×10^{-10}
M-U	1.376	0.312	1440	0	0.14	3.55×10^{-11}
M-U	1.273	0.258	2160	0	0.13	1.81×10^{-11}
M-U	1.217	0.218	2880	0	0.042	3.73×10^{-12}
M-R	0.773	0.524	45	0	0.167	3.35×10^{-9}

TABLE 8 - (Continued)

Test No.	Sample Height H (in.)	Porosity Ratio n	p_T* (psi)	p_B** (psi)	Flow Rate (mℓ/sec x 1000)	Average Permeability (cm/sec)
M-R	0.716	0.486	90	0	0.2	
			135	0	0.35	2.01×10^{-9}
M-R	0.662	0.444	180	0	0.23	
			270	0	0.35	9.84×10^{-10}
M-R	0.614	0.401	360	0	0.17	
			540	0	0.28	3.51×10^{-10}
M-R	0.5677	0.3521	720	0	0.133	
			1180	0	0.33	1.54×10^{-10}
M-R	0.533	0.311	1440	0	0.133	5.75×10^{-11}
M-R	0.482	0.236	2880	0	0.044	8.57×10^{-12}
M-R	0.467	0.213	4320	0	0.055	6.95×10^{-12}

* Pressure at the top of the sample.

** Pressure at the bottom of the sample.

TABLE 9 - Test Results for Kaolinite Consolidated at 20°C

Load (psi)	Void Ratio (e)	Porosity (n)	Permeability (cm/sec)	Absolute Permeability (millidarcy)
0	4.475	0.817		
90	1.373	0.578		
724	0.815	0.449	4.00×10^{-9}	4.02×10^{-3}
1448	0.681	0.405	2.35×10^{-9}	2.36×10^{-3}
4320	0.506	0.336	6.11×10^{-10}	6.13×10^{-4}
10080	0.361	0.265	1.74×10^{-10}	1.75×10^{-4}
5761 *	0.376	0.276		
2880 *	0.400	0.286		
1440 *	0.433	0.302		
5761 **	0.387	0.279		
10080	0.346	0.257		
0 *	0.647	0.397		

* unloading

** reloading

TABLE 10 - Test Results for Kaolinite Consolidated at 60°C

Load (psi)	Void Ratio (e)	Porosity (n)	Permeability (cm/sec)	Absolute Permeability (millidarcy)
90	1.343	0.573		
180	1.222	0.529	1.05×10^{-8}	4.98×10^{-3}
360	0.957	0.489	7.68×10^{-9}	3.69×10^{-3}
720	0.810	0.447	6.36×10^{-9}	3.02×10^{-3}
1440	0.647	0.393	2.77×10^{-9}	1.32×10^{-3}
2880	0.527	0.345	1.20×10^{-10}	5.70×10^{-4}
720 *	0.578	0.366		
45 *	0.766	0.434		
720 **	0.638	0.389		
2880 **	0.506	0.336		
5760	0.404	0.288	4.70×10^{-10}	2.23×10^{-4}
10080	0.326	0.246	2.33×10^{-10}	1.11×10^{-4}
4320 *	0.350	0.259		
45 *	0.611	0.3762		

* unloading

** reloading

TABLE 11 - Test Results for Kaolinite Consolidated at 90°C

Load (psi)	Void Ratio (e)	Porosity (n)	Permeability (cm/sec)	Absolute Permeability (millidarcy)
0	5.204	0.839		
13.5	2.039	0.671		
136	1.182	0.542	4.69×10^{-8}	1.53×10^{-2}
271	0.900	0.474	1.01×10^{-8}	3.29×10^{-3}
543	0.756	0.431	5.49×10^{-9}	1.79×10^{-3}
1480	0.515	0.340	3.51×10^{-9}	1.14×10^{-3}
2960	0.456	0.313	1.25×10^{-9}	4.06×10^{-4}
723 *	0.515	0.340		
226 *	0.581	0.368		
0 *	0.800	0.444		
720 **	0.565	0.361		
2880 **	0.431	0.301		
5760 **	0.370	0.270	4.76×10^{-10}	1.55×10^{-4}
10080	0.287	0.223	1.55×10^{-10}	5.05×10^{-5}
2160 *	0.330	0.248		
0 *	0.600	0.375		

* unloading

** reloading

TABLE 12 - Test Results for Illite Consolidated at 20°C

Load (psi)	Void Ratio (e)	Porosity (n)	Permeability (cm/sec)	Absolute Permeability (millidarcy)
0	2.508	0.715		
45	1.001	0.500		
90	0.828	0.453	2.02×10^{-9}	2.03×10^{-3}
180	0.705	0.413	1.43×10^{-9}	1.44×10^{-3}
360	0.599	0.375	8.86×10^{-10}	8.90×10^{-4}
705	0.509	0.337	4.26×10^{-10}	1.32×10^{-4}
1520	0.423	0.297	1.17×10^{-10}	1.17×10^{-4}
3150	0.352	0.260	4.13×10^{-11}	4.15×10^{-5}
1112 *	0.374	0.272		
45 *	0.496	0.332		
1112 **	0.397	0.284		
2334 **	0.357	0.263		
4778 **	0.303	0.233	3.49×10^{-11}	3.49×10^{-5}
10070	0.238	0.193		
1925 *	0.285	0.222		
297 *	0.359	0.264		
1 *	0.457	0.314		

* unloading

** reloading

TABLE 13 - Test Results for Illite Consolidated at 60°C

Load (psi)	Void Ratio (e)	Porosity (n)	Permeability (cm/sec)	Absolute Permeability (millidarcy)
90	0.980	0.495		
180	0.750	0.429	3.32×10^{-9}	1.58×10^{-3}
360	0.612	0.380	1.59×10^{-9}	7.55×10^{-4}
720	0.498	0.333	6.03×10^{-10}	2.86×10^{-4}
1518	0.419	0.295	1.78×10^{-10}	8.46×10^{-5}
3150	0.342	0.255		
1518 *	0.353	0.261		
45 *	0.465	0.318		
1518 **	0.369	0.270		
3557 **	0.318	0.241		
6000	0.274	0.215	2.71×10^{-11}	1.29×10^{-5}
10070	0.229	0.186	1.02×10^{-11}	4.85×10^{-6}
4780 *	0.236	0.191		
303 *	0.340	0.254		
45 *	0.400	0.286		
0 *	0.449	0.309		

* unloading
** reloading

TABLE 14 - Test Results for Illite Consolidated at 90°C

Loading (psi)	Void Ratio (e)	Porosity (n)	Permeability (cm/sec)	Absolute Permeability (millidarcy)
90	1.104	0.525		
180	0.790	0.441	4.95×10^{-9}	1.61×10^{-3}
360	0.660	0.398	3.65×10^{-9}	1.19×10^{-3}
705	0.532	0.347	1.26×10^{-9}	4.10×10^{-4}
1520	0.426	0.298	4.15×10^{-10}	1.35×10^{-4}
3150	0.346	0.257	1.19×10^{-10}	3.88×10^{-5}
702 *	0.385	0.278		
45 *	0.508	0.337		
1110 **	0.398	0.285		
3556 **	0.318	0.241		
5759	0.269	0.212	2.67×10^{-11}	8.70×10^{-6}
10070	0.220	0.180	4.12×10^{-12}	1.34×10^{-6}
2305 *	0.260	0.206		
45 *	0.398	0.285		

* unloading

** reloading

TABLE 15 - Test Results for Bentonite Consolidated at 20°C

Load (psi)	Void Ratio	Porosity (n)	Permeability (cm/sec)	Absolute Permeability (millidarcy)
0				
90	1.712	0.631		
180	1.175	0.540		
360	0.958	0.489		
720	0.830	0.454		
1440	0.693	0.409		
542 *	0.748	0.428		
0 *	1.077	0.519		
720 **	0.780	0.438		
1440 **	0.677	0.403	3.97×10^{-12}	3.98×10^{-6}
2880	0.573	0.364	1.25×10^{-12}	1.26×10^{-6}
5760	0.486	0.327	5.24×10^{-13}	5.26×10^{-7}
10080	0.402	0.287	3.12×10^{-13}	3.13×10^{-7}
4321 *	0.444	0.307		
0 *	0.898	0.473		

* unloading
** reloading

TABLE 16 - Test Results for Bentonite Consolidated at 60°C

Load (psi)	Void Ratio (e)	Porosity (n)	Permeability (cm/sec)	Absolute Permeability (millidarcy)
0	8.4584	0.8943		
90	1.9165	0.6571		
180	1.2765	0.5607	2.51×10^{-10}	1.19×10^{-4}
360	1.0277	0.5608	6.51×10^{-11}	3.09×10^{-5}
720	0.8112	0.4478	1.11×10^{-11}	5.27×10^{-6}
1440	0.6819	0.4054	5.01×10^{-12}	2.38×10^{-6}
2880	0.5642	0.3607	1.60×10^{-12}	7.60×10^{-7}
720 *	0.6392	0.3899		
0 *	0.9657	0.4913		
720 **	0.7242	0.4200		
2880 **	0.5577	0.3580		
5760	0.4727	0.3210	7.48×10^{-13}	3.55×10^{-7}
10080	0.4015	0.2865		
5760 *	0.4230	0.2973		
0 *	0.7638	0.4330		

* unloading

** reloading

TABLE 17 - Test Results for Bentonite Consolidated at 90°C

Load (psi)	Void Ratio (e)	Porosity (n)	Permeability (cm/sec)	Absolute Permeability (millidarcy)
0				
180	1.223	0.550	6.00×10^{-10}	1.96×10^{-4}
360	0.974	0.493	9.73×10^{-11}	3.17×10^{-5}
720	0.788	0.441	1.84×10^{-11}	6.00×10^{-6}
1440	0.659	0.397	8.80×10^{-12}	2.87×10^{-6}
2880	0.568	0.362	3.69×10^{-12}	1.20×10^{-6}
720 *	0.633	0.388		
0 *	0.901	0.474		
1440 **	0.618	0.382		
2880	0.539	0.350		
5760	0.463	0.316	2.34×10^{-12}	7.63×10^{-7}
10080 *	0.387	0.279	1.09×10^{-12}	3.55×10^{-7}
4320 *	0.426	0.299		
0 *	0.825	0.451		

* unloading

** reloading

TABLE 18 - Test Results for Marine Core from Angola Basin (Remolded) Consolidated at 20°C

Load (psi)	Void Ratio (e)	Porosity (n)	Permeability (cm/sec)	Absolute Permeability (milli darcy)
0	4.941	0.832		
45	1.337	0.572		
90	1.102	0.524	3.35×10^{-9}	3.36×10^{-3}
180	0.948	0.487	2.01×10^{-9}	2.02×10^{-3}
360	0.800	0.444	9.84×10^{-10}	9.88×10^{-4}
705	0.670	0.401	3.51×10^{-10}	3.52×10^{-4}
1520	0.543	0.352	1.54×10^{-10}	1.55×10^{-4}
2740	0.450	0.311	5.75×10^{-11}	5.77×10^{-5}
1112 *	0.466	0.318		
297 *	0.521	0.342		
1926 **	0.463	0.316		
3963 **	0.390	0.281		
7629	0.310	0.236	8.57×10^{-12}	8.60×10^{-6}
10070	0.270	0.213	6.95×10^{-12}	6.98×10^{-6}
5593 *	0.275	0.216		
705 *	0.361	0.265		
45 *	0.472	0.320		
0	0.586	0.369		

* unloading
** reloading

TABLE 19 - Test Results for Marine Core from Angola Basin (Undisturbed) Consolidated at 20°C

Loading (psi)	Void Ratio (e)	Porosity (n)	Permeability (cm/sec)	Absolute Permeability (millidarcy)
0				
90	0.962	0.490		
180	0.891	0.471		
360	0.837	0.456		
702	0.754	0.430	1.71×10^{-9}	1.72×10^{-3}
1520	0.583	0.368	2.49×10^{-10}	2.50×10^{-4}
3150	0.457	0.313	3.55×10^{-11}	3.56×10^{-5}
6407	0.349	0.258	1.81×10^{-11}	1.82×10^{-5}
10070	0.279	0.219	3.73×10^{-12}	3.74×10^{-6}
4768 *	0.285	0.222		
297 *	0.353	0.261		
45 *	0.410	0.291		

* unloading

TABLE 20 - Atterberg Limits % Clay Content and Compressibility Coefficients A&B of Test Data Employed in the Computer Analysis

Sample Identification	Origin	Liquid Limit (%)	Plastic Limit (%)	Plasticity Index (%)	% Clay	A (psi)	B	R^2	Maximum Consolidation Pressure (psi)	Porosity Ratio Corresponding to the Max. Pressure
DATA FROM W. R. BRYANT, OCEANOGRAPHY DEPARTMENT, TEXAS A&M UNIVERSITY										
73-3-7	San Diago Canyon	140	50	90	47.64	0.524×10^{-1}	- 14.36	0.97	57	0.62
71-A-4 S38-D10	Caribbean Sea	66	31	35	40.78	0.104	- 10.75	0.95	455	0.45
71-A04 S38-D315	Caribbean Sea	54	32	22	47.39	0.72×10^{-2}	- 13.83	0.94	455	0.44
71-A-1 S35-D380	Campeche Bay	90	43.6	46.4	80.85	0.84×10^{-1}	- 14.37	0.97	455	0.54
71-A-4 S36-D80	Caribbean Sea	67	35	32	56.17	0.12×10^{-2}	- 18.65	0.94	455	0.49
72-2-8	Caribbean Sea	66	35	31	56.7	0.18×10^{-1}	- 13.62	0.85	1820	0.40
71-A-4 S39-D80	Caribbean Sea	76	39	37	41.17	0.266×10^{-1}	- 16.07	0.97	455	0.53
71-A-4 S39-D250	Caribbean Sea	102	44	58	80.66	3.02	- 5.69	0.96	1820	0.305
71-A-4 S39-D430	Caribbean Sea	98	41	57	71.39	0.355	- 7.84	0.98	455	0.39
70-A-8 S7-D60	West Florida Shelf	106	41	65	64.00	0.9×10^{-10}	- 10.88	0.97	455	0.43
70-A-8 S6-D70	Mississippi Fan	90	37	53	73.0	0.358	- 7.63	0.99	455	0.38
70-A-8 S13-D40	West Florida Shelf	115	44	71	62.0	0.528	- 9.7	0.98	455	0.49

TABLE 20 - (CONTINUED)

Sample Identification	Origin	Liquid Limit (%)	Plastic Limit (%)	Plasticity Index (%)	% Clay	A (psi)	B	R^2	Maximum Consolidation Pressure (psi)	Porosity Ratio Corresponding to the Max. Pressure
69-A-8 S7-D55	West Florida Shelf	106	41	65	65.0	0.311	- 8.65	0.98	455	0.44
70-A-8 S7-D145	West Florida Shelf	80	35	45	64.0	0.465	- 7.53	0.98	455	0.39
69-A-5 S3-D55	Mississippi Fan	130	45	85	82.0	0.436	- 9.49	0.98	455	0.47
70-A-8 S7-D140	West Florida Scrap	68	35	33	64.0	0.40	- 7.967	0.94	455	0.39
70-A-8 S13-D120	West Florida Scrap	100	42	58	56.0	0.28	- 11.47	0.98	455	0.52
69-A-5 S81-D40	Caribbean Sea	113	40	73	69.0	2.09	- 5.87	0.98	455	0.39
69-A-5 S4-D130	Mississippi Fan	107	38	69	82.0	0.467×10^{-1}	- 19.08	0.99	455	0.62
69-A-5 S71-D55	Caribbean Sea	104	39	65	65	0.86×10^{-1}	- 13.07	0.99	455	0.53
69-A-4 S6-D180	Mississippi Fan	86	35	51	82.5	0.909	- 5.94	0.97	455	0.34
69-A-4 S7-D85	Mississippi Fan	77	35	42	74.3	0.233	- 9.20	0.99	455	0.43
69-A-4 S7-D270	Mississippi Fan	94	40	54	81.3	0.310	- 8.52	0.98	455	0.41
69-A-4 S5-D265	Mississippi Fan	74	31	43	68.0	0.167	- 8.76	0.99	455	0.40
4-11-72 leg 24	Indian Ocean	148	46	102	81.3	0.139×10^{-1}	- 16.45	0.94	228	0.55

TABLE 20 - (CONTINUED)

Sample Identification	Origin	Liquid Limit (%)	Plastic Limit (%)	Plasticity Index (%)	% Clay	A (psi)	B	R^2	Maximum Consolidation Pressure (psi)	Porosity Ratio Corresponding to the Max. Pressure
2-11-72 leg 24	Indian Ocean	68	38	30	48.4	0.219	- 6.65	0.94	455	0.30
69-5-8S 35 cm	Abyssel Plain	113	40	73	65.0	1.334	- 5.85	0.97	9720	0.21
71-4-35S 100 cm	Caribbean Sea	90	44	46	84	0.124	- 12.08	0.97	6944	0.40
69-5-6S 65 cm	Mississippi Fan	91	40	51	76	0.222	- 11.07	0.99	455	0.50
69-4-7P 270 cm	Mississippi Fan	77	35	42	74.2	0.558	- 7.22	0.99	9720	0.39
70-8-16S 16 cm	Mississippi Fan	90	37	53	37.4	2.04	- 5.12	0.96	9720	0.18
leg 24-3	Indian Ocean	68	38	30	49	0.13	- 11.33	0.96	9720	0.37
leg 24-5	Indian Ocean	143	46	97	87	0.88×10^{-1}	- 8.41	0.93	9720	0.24
DATA FROM C.C. MATHEWSON, GEOLOGY DEPARTMENT, TEXAS A&M UNIVERSITY										
VB-1	Vicksburg	67	24	43	68	1.603	- 3.88	0.95	569	0.20
MI-901-10M	10% Wyoming Bentonite 90% Illite (NY)	70	18	52	50	0.803	0 5.24	0.96	569	0.27
VL-1	Vicksburg	38	24	14	54	0.257	- 5.36	0.98	568	0.26
IL-1	New York	29	18	11	47	0.39	- 5.36	0.90	568	0.25
KA-1	Wrens, Ga.	70	29	41	93	0.148×10^{-1}	- 12.83	0.97	568	0.42
CH-1	Chenaoult	45	15	30	36	0.337×10^{-1}	- 7.66	0.98	568	0.27

TABLE 20 - (CONTINUED)

Sample Identification	Origin	Liquid Limit (%)	Plastic Limit (%)	Plasticity Index (%)	% Clay	A (psi)	B	R^2	Maximum Consolidation Pressure (psi)	Porosity Ratio Corresponding to the Max. Pressure
GM	Grimes, Tex.	47	20	27	33	0.1433	- 6.066	0.97	568	0.24
DATA FROM AKAJI ( )										
Cl-1	Cleveland	34	18	16	35	2.242	- 4.312	0.98	20,800	0.09
DATA FROM THOMPSON ( )										
Vir-1	Virginia	59	39	20	70	1.799	- 5.5	0.99	1,716	0.24
Mis-1	Mississippi	113	33	80	85	0.348	- 11.21	0.97	10,500	0.31
Camp-1	Campechi	61	26	35	80	2.728	- 6.21	0.92	10,500	0.23
Hawaii	Hawaii	93	35	58	87	3.59	- 5.71	0.96	2,300	0.28
South China	South China Sea	69	32	37	81	0.372	- 10.1	0.98	10,500	0.28
DATA FROM THE TEST PERFORMED BY THE AUTHOR										
Kaolinite	Kossee, Tex.	55	35	20	99	15.17	- 4.99	0.98	10,080	0.25
Illite	Illinois	46	24	22	77	1.06	- 5.78	0.99	10,080	0.19
Bentonite	Wyoming	388	33	355	85	4.48	- 6.32	0.99	10,080	0.28
Mu-20	Angola Basin	72	26	46	87	28.41	- 3.94	0.99	10,080	0.28

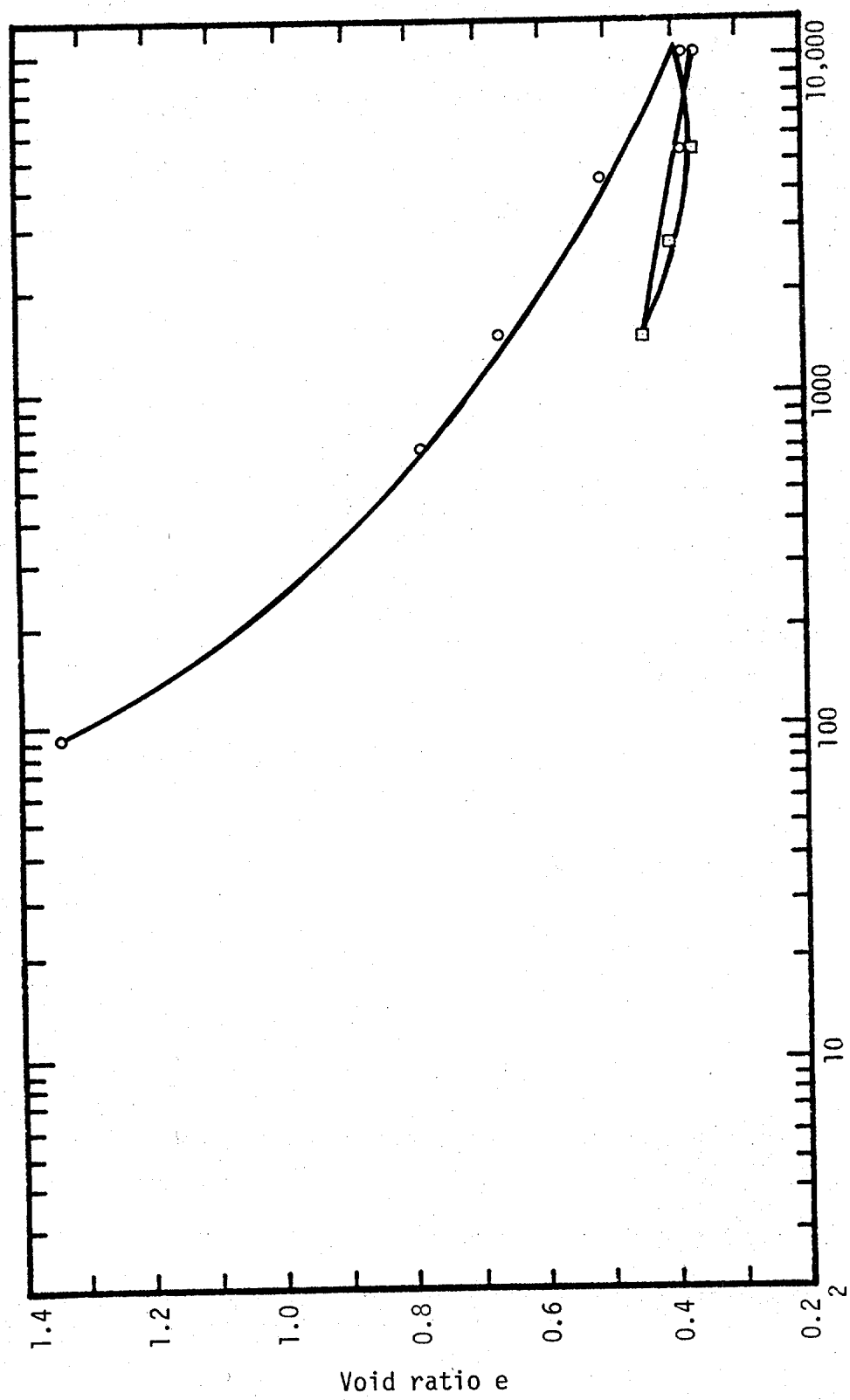

Fig. 25 - Graph of Void Ratio versus Consolidation Pressure for Kaolinite Tested at 20°C

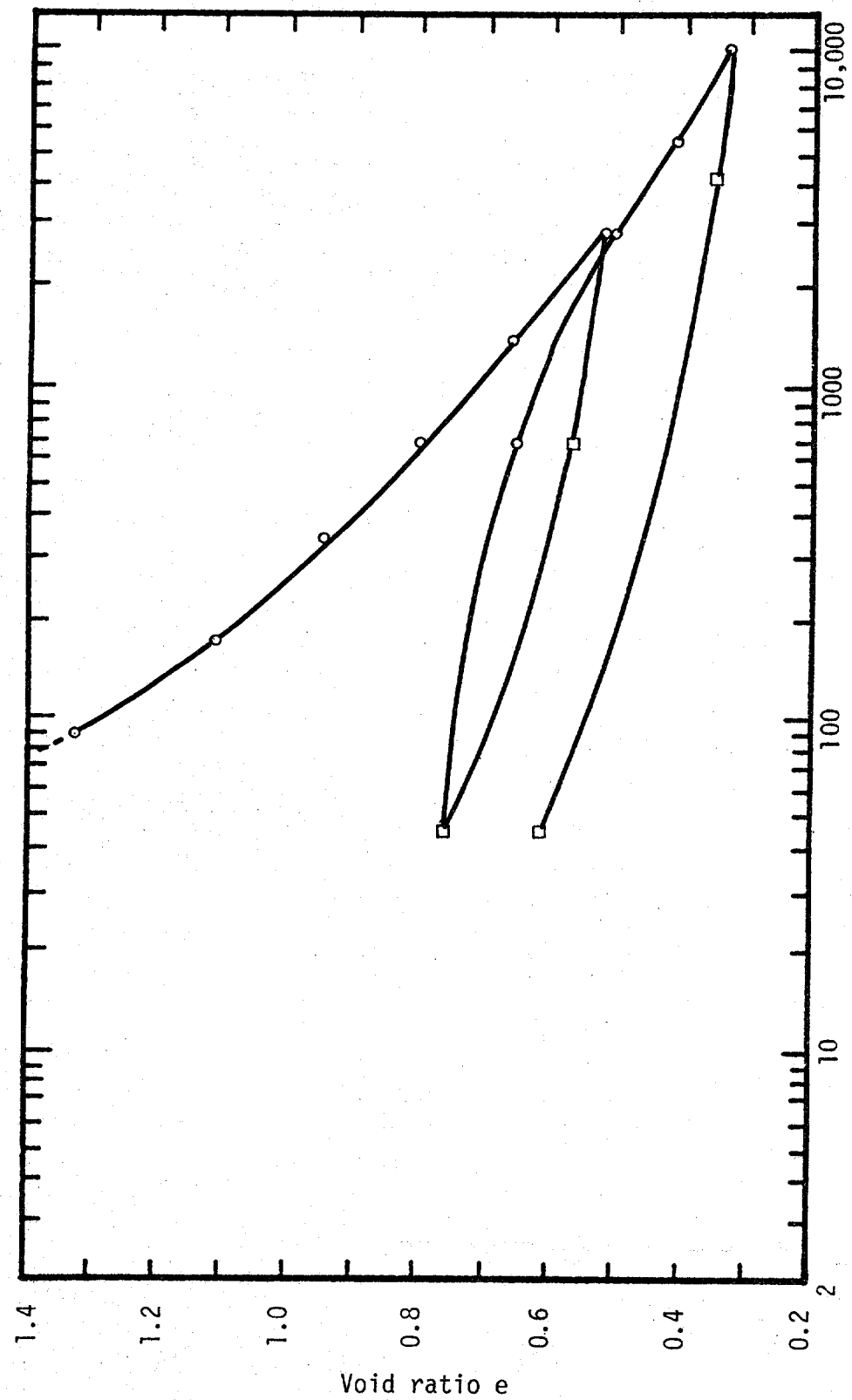

Fig. 26 - Graph of Void Ratio versus Consolidation Pressure for Kaolinite Tested at 60°C

TABLE 21 - Liquid Limit, Plastic Limit, and Permeability Constants C and D of Test Data Employed in the Computer Analysis

Sample	C cm/sec	D	Liquid Limit (%)	Plastic Limit (%)
Kaolinite	0.52×10^{-6}	6.07	55.0	34.8
Illite	0.546×10^{-6}	6.79	45.6	23.5
Bentonite	0.273×10^{-8}	7.43	338.0	32.5
Marine Core Angola Basin	0.163×10^{-7}	8.63	72.0	25.8
Virginia Sediment	0.177×10^{-1}	18.41	59.3	39.3
Mississippi Delta Sediment	0.25×10^{-4}	18.17	113.2	32.8
Campeche	0.723×10^{-6}	6.61	61.4	26.3
Hawaii	0.823×10^{-7}	6.53	92.5	37
China Sea	0.464×10^{-5}	10.18	69	37

LL is the liquid limit

PL is the plastic limit

%C is the % clay content

APPENDIX IV

Graphs of Consolidation Tests

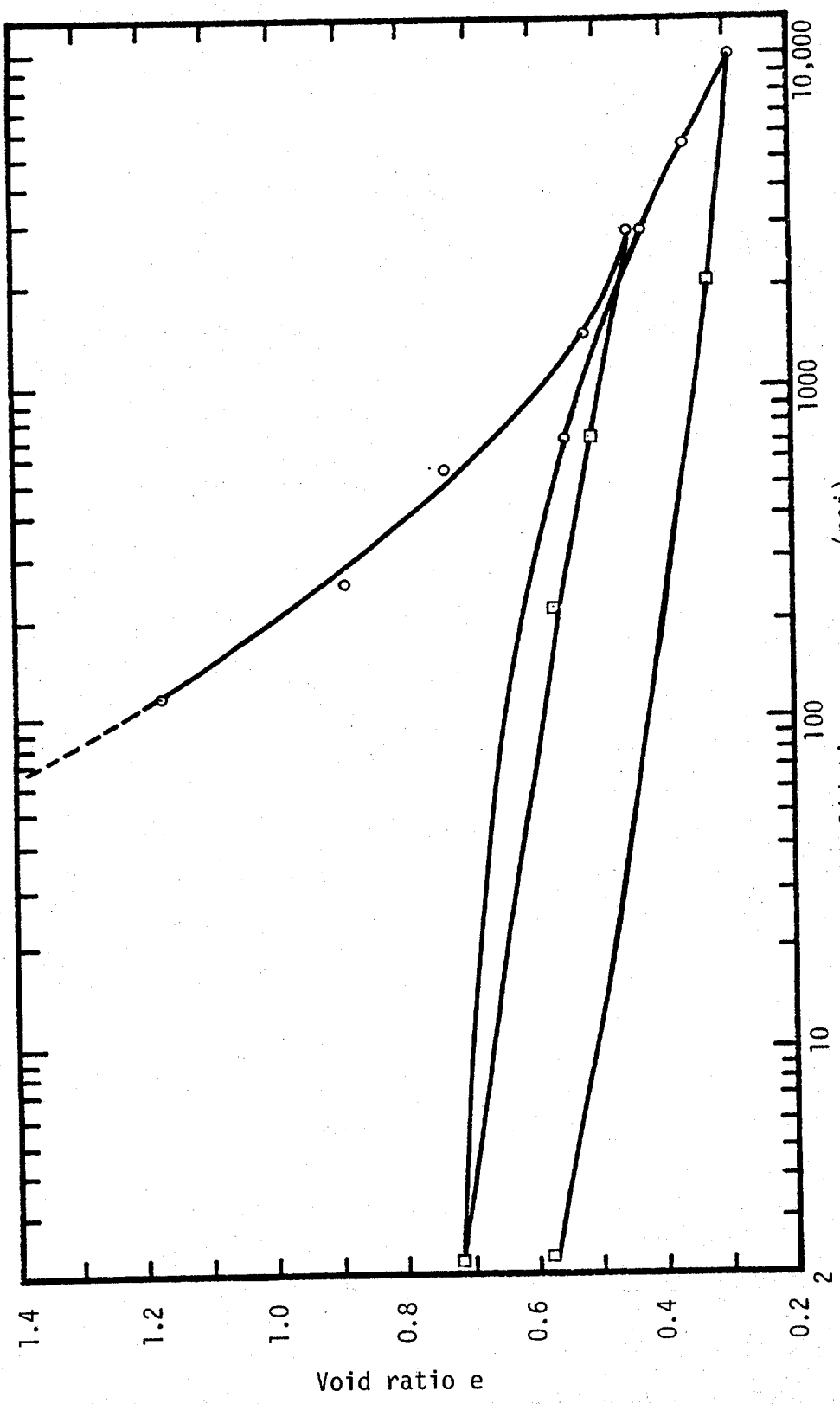

Fig. 27 - Graph of Void Ratio versus Consolidation Pressure for Kaolinite Tested at 90°C

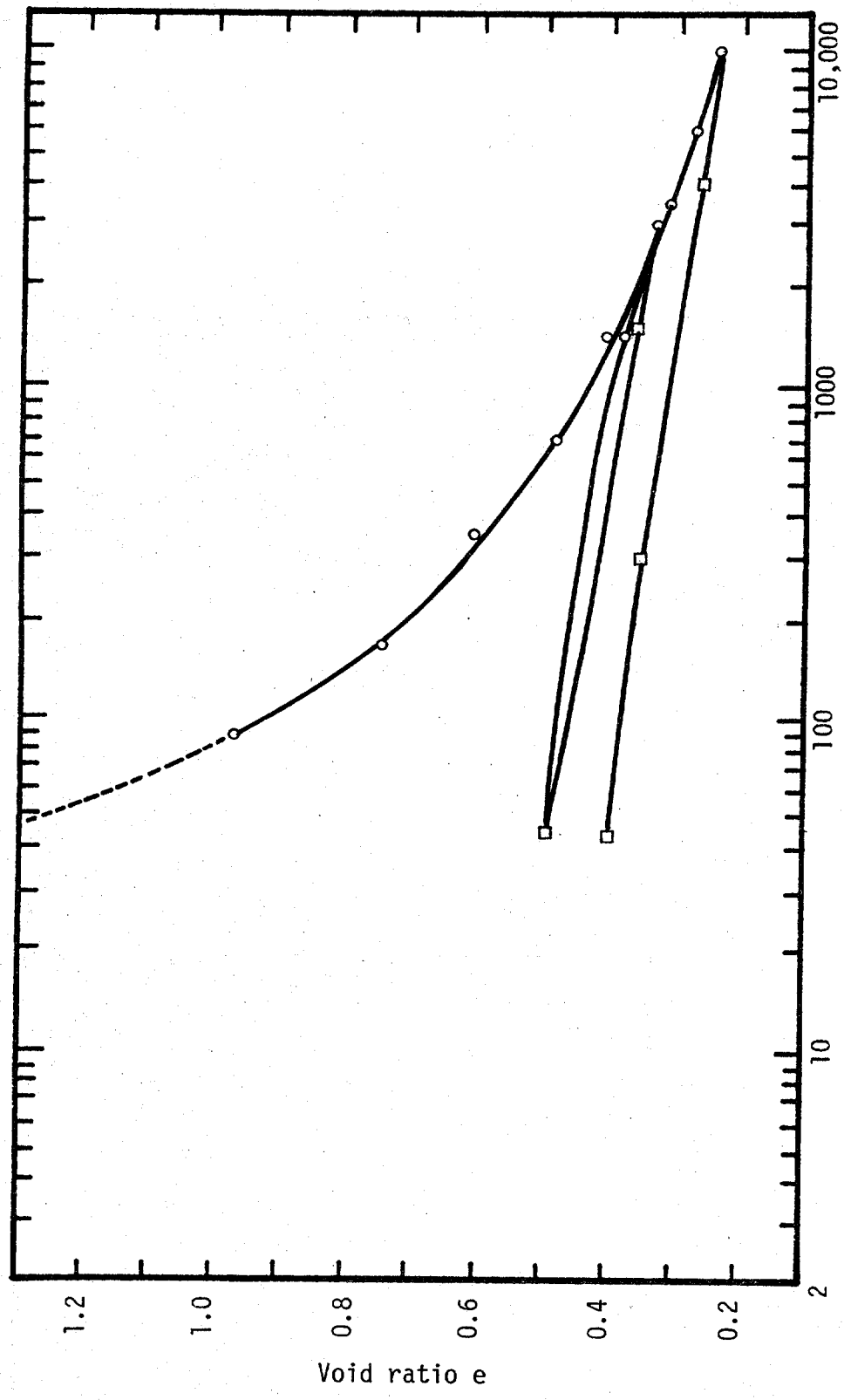

Fig. 28 - Graph of Void Ratio versus Consolidation Pressure for Illite Tested at 60°C

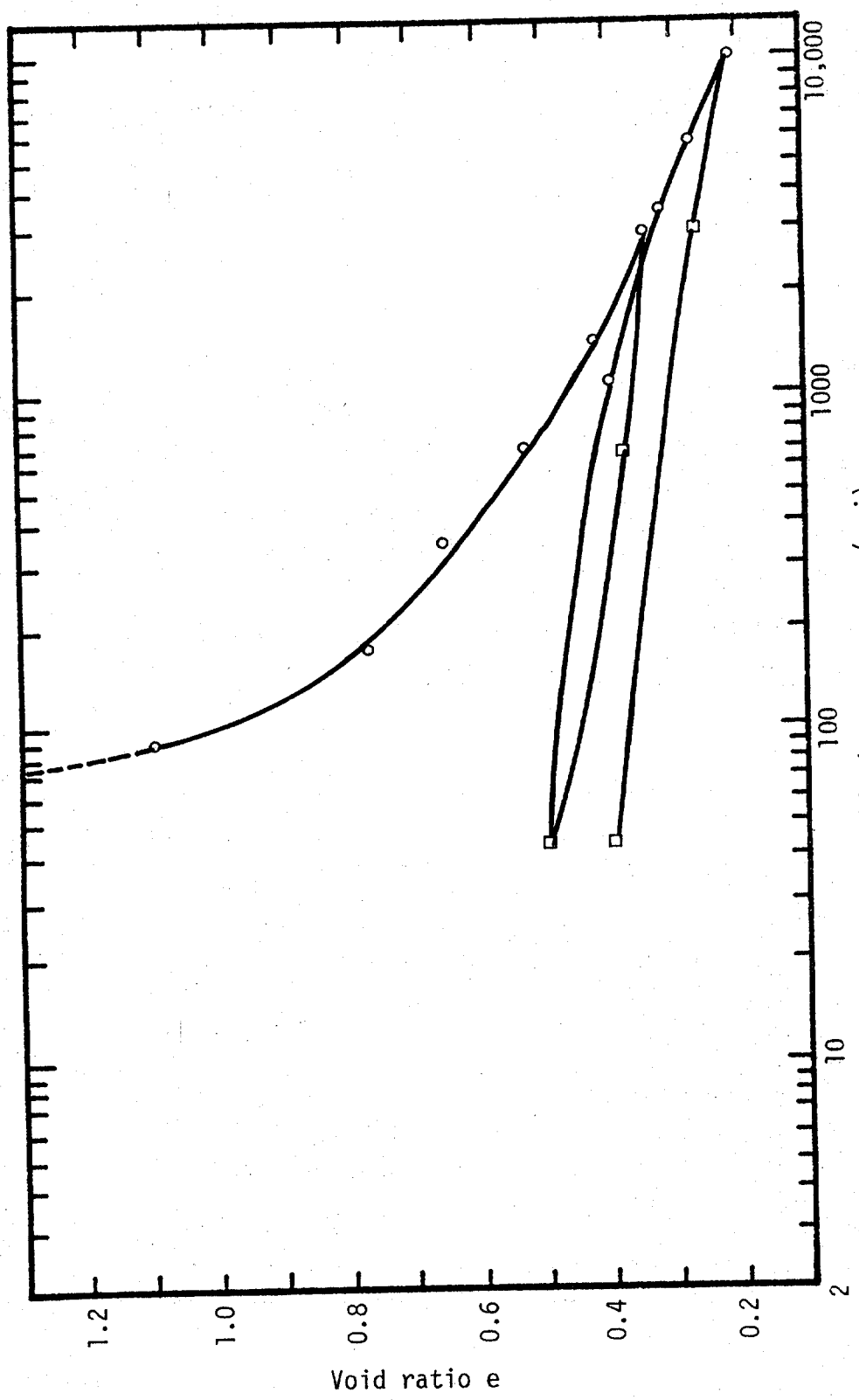

Fig. 29 - Graph of Void Ratio versus Consolidation Pressure for Illite Tested at 90°C

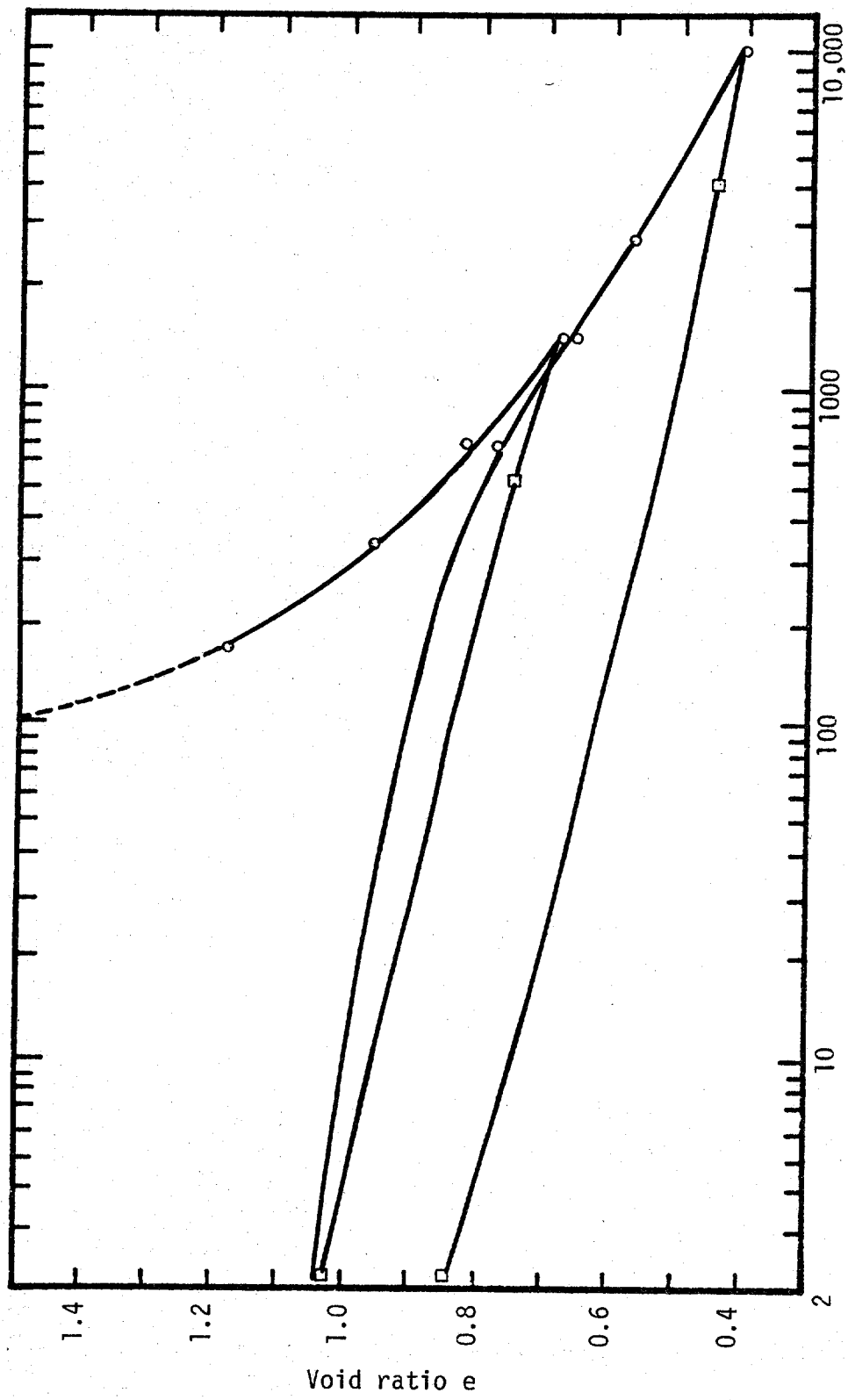

Fig. 30 - Graph of Void Ratio versus Consolidation Pressure for Bentonite Tested at 20°C

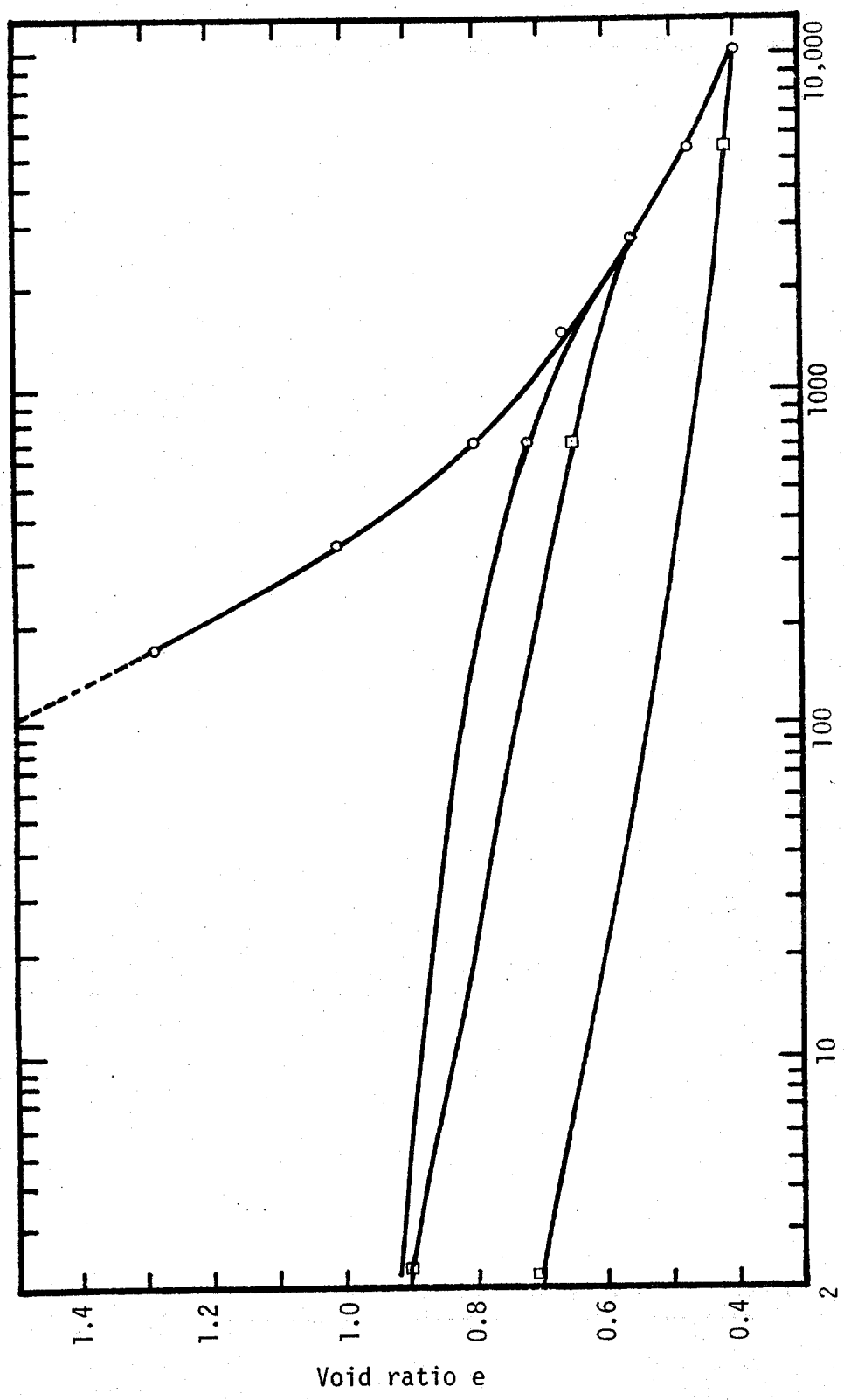

Fig. 31 - Graph of Void Ratio versus Consolidation Pressure for Bentonite Tested at 60°C

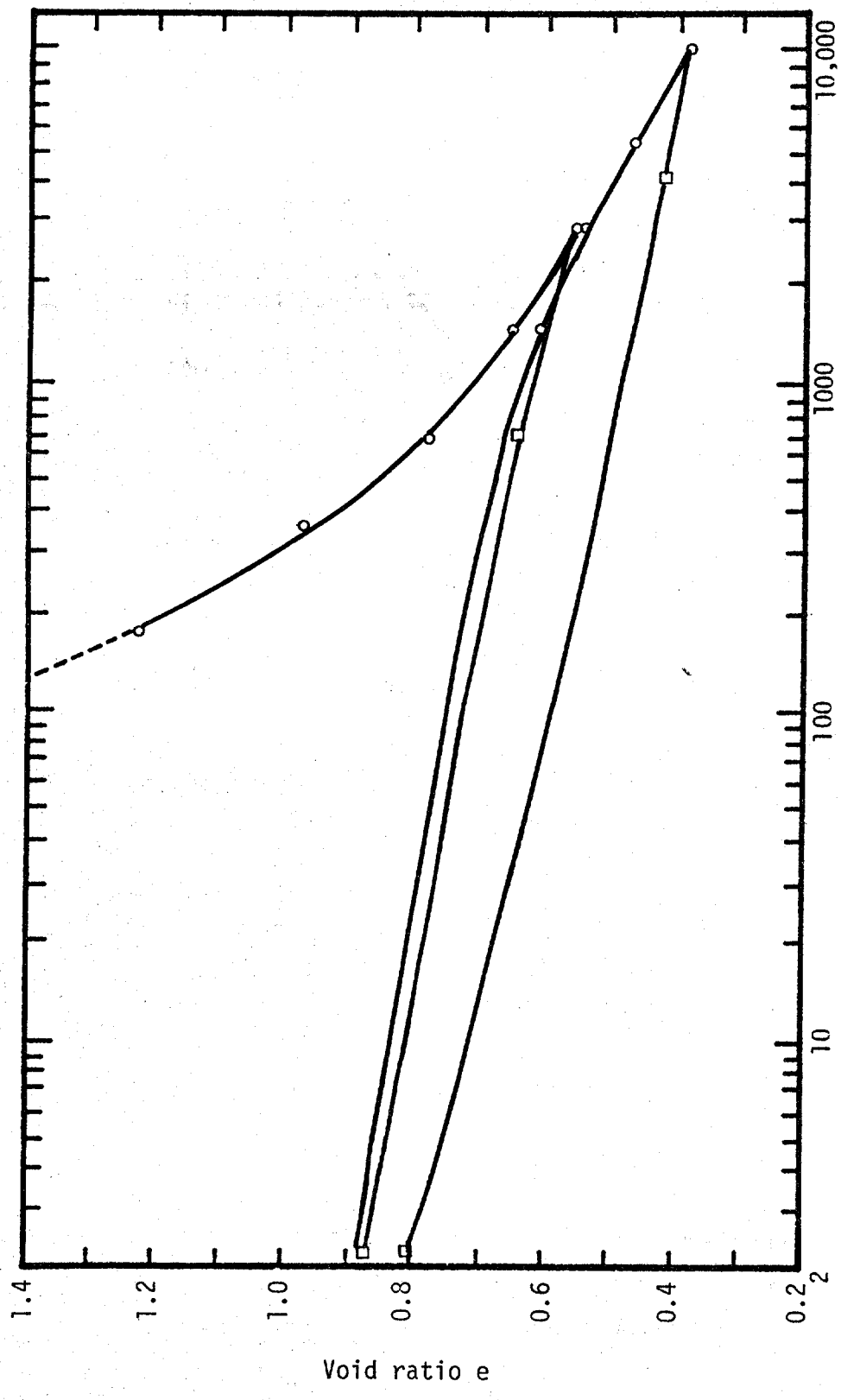

Fig. 32 - Graph of Void Ratio versus Consolidation Pressure for Bentonite Tested at 90°C

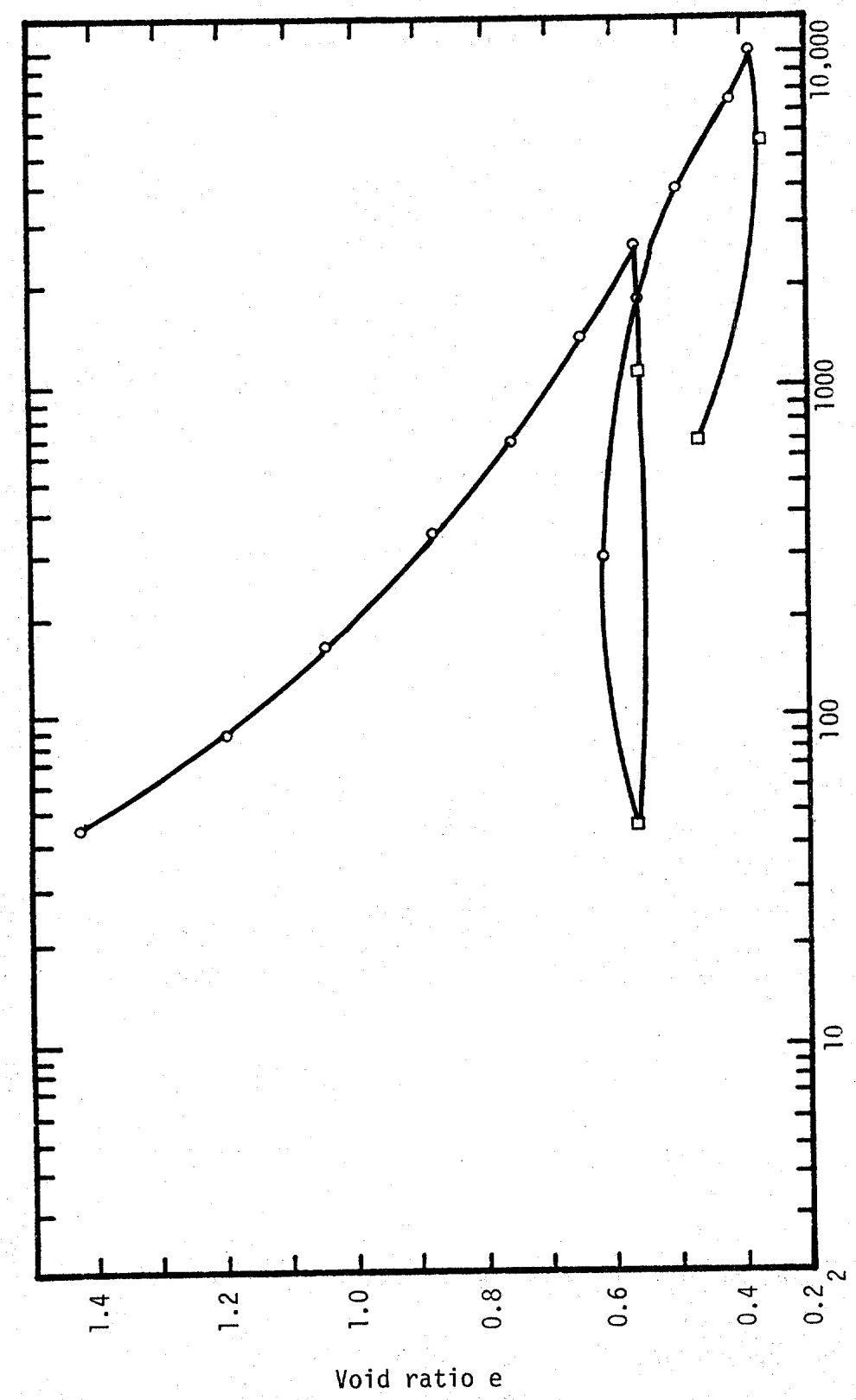

Fig. 33 - Graph of Void Ratio versus Consolidation Pressure for Remolded Marine Core from Angola Basin Tested at 20°C.

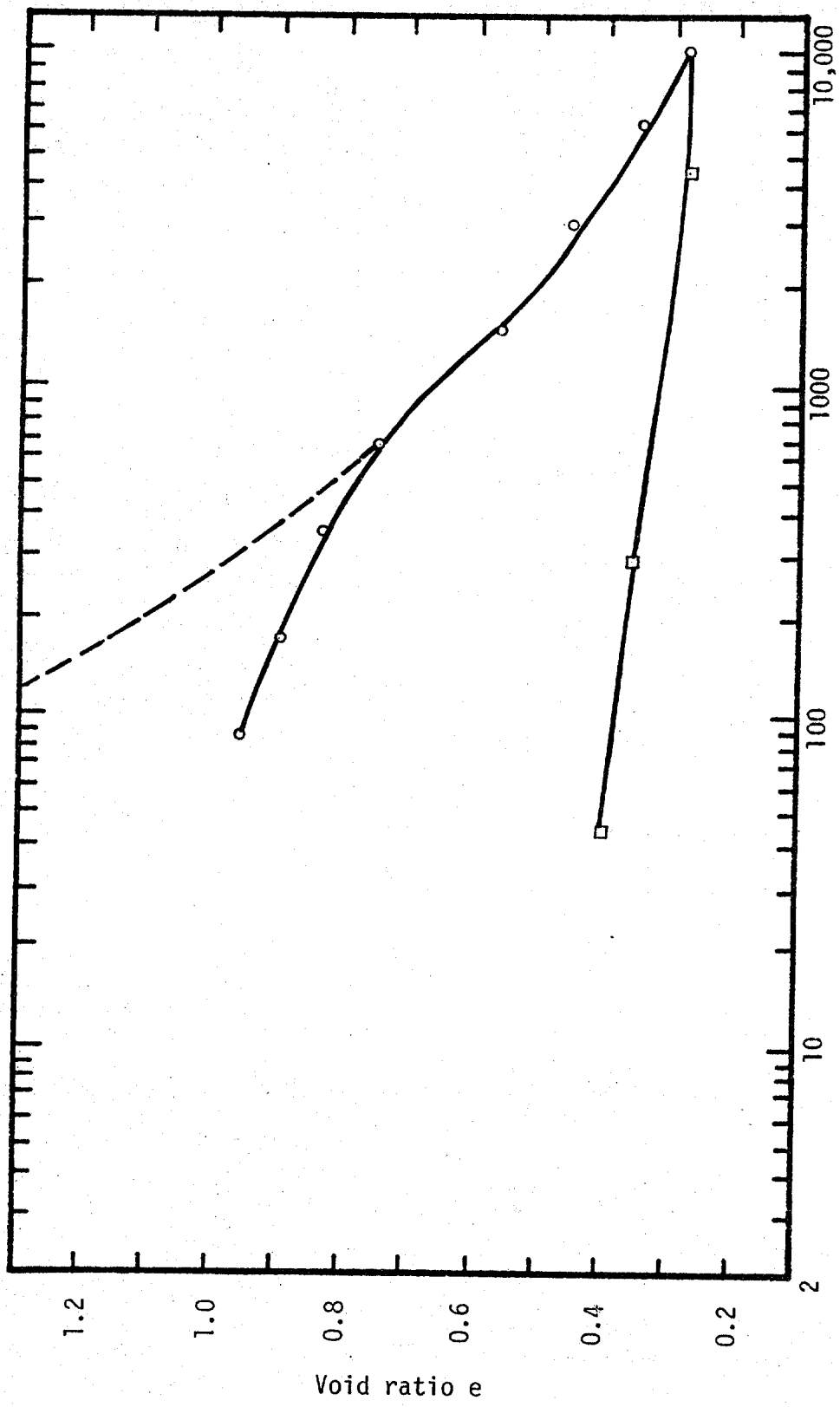

Fig. 34 - Graph of Void Ratio versus Consolidation Pressure for Undisturbed Marine Core from Angola Basin Tested at 20°C

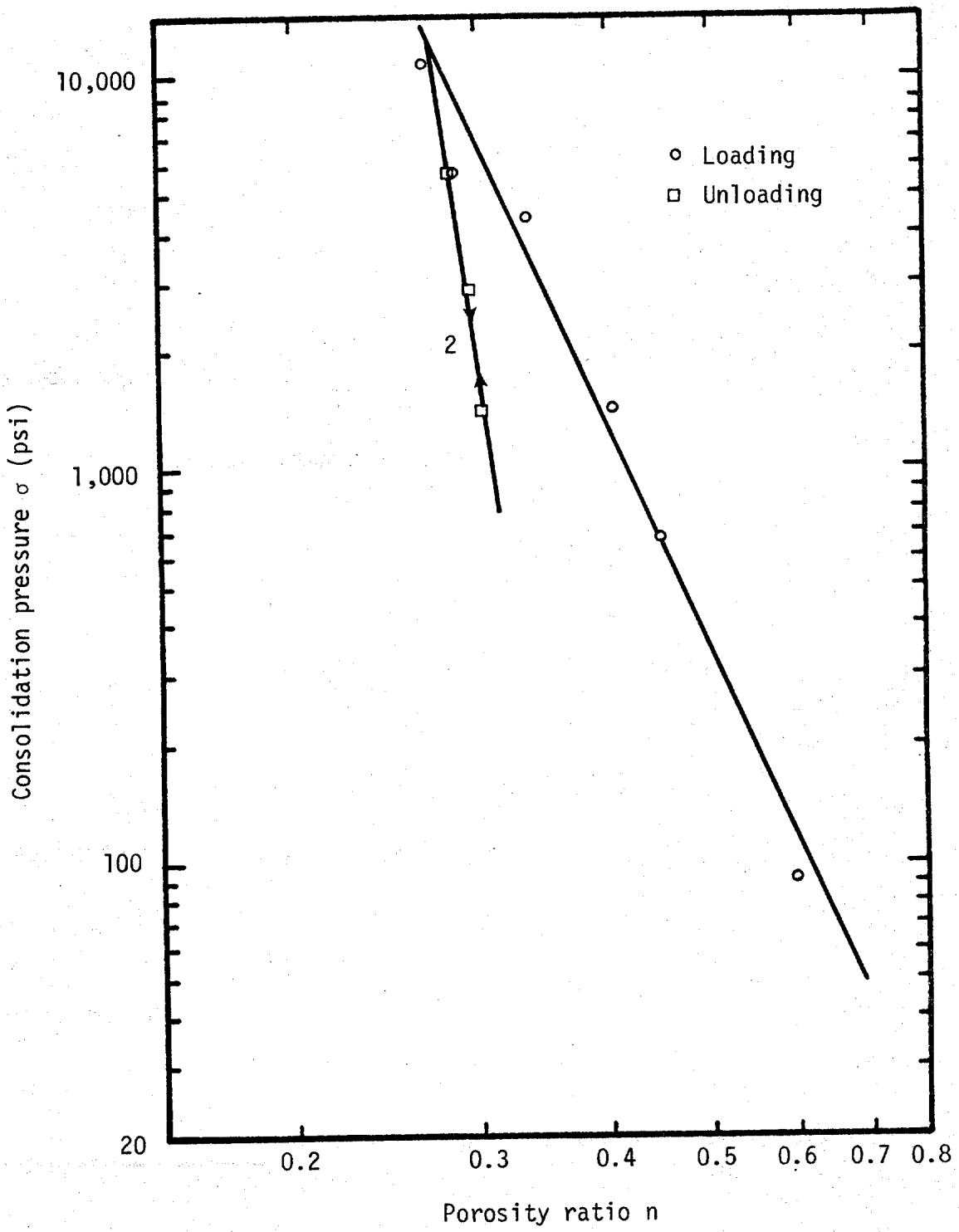

Fig. 35 - Graph of Consolidation Pressure versus Porosity Ratio for Kaolinite Tested at 20°C

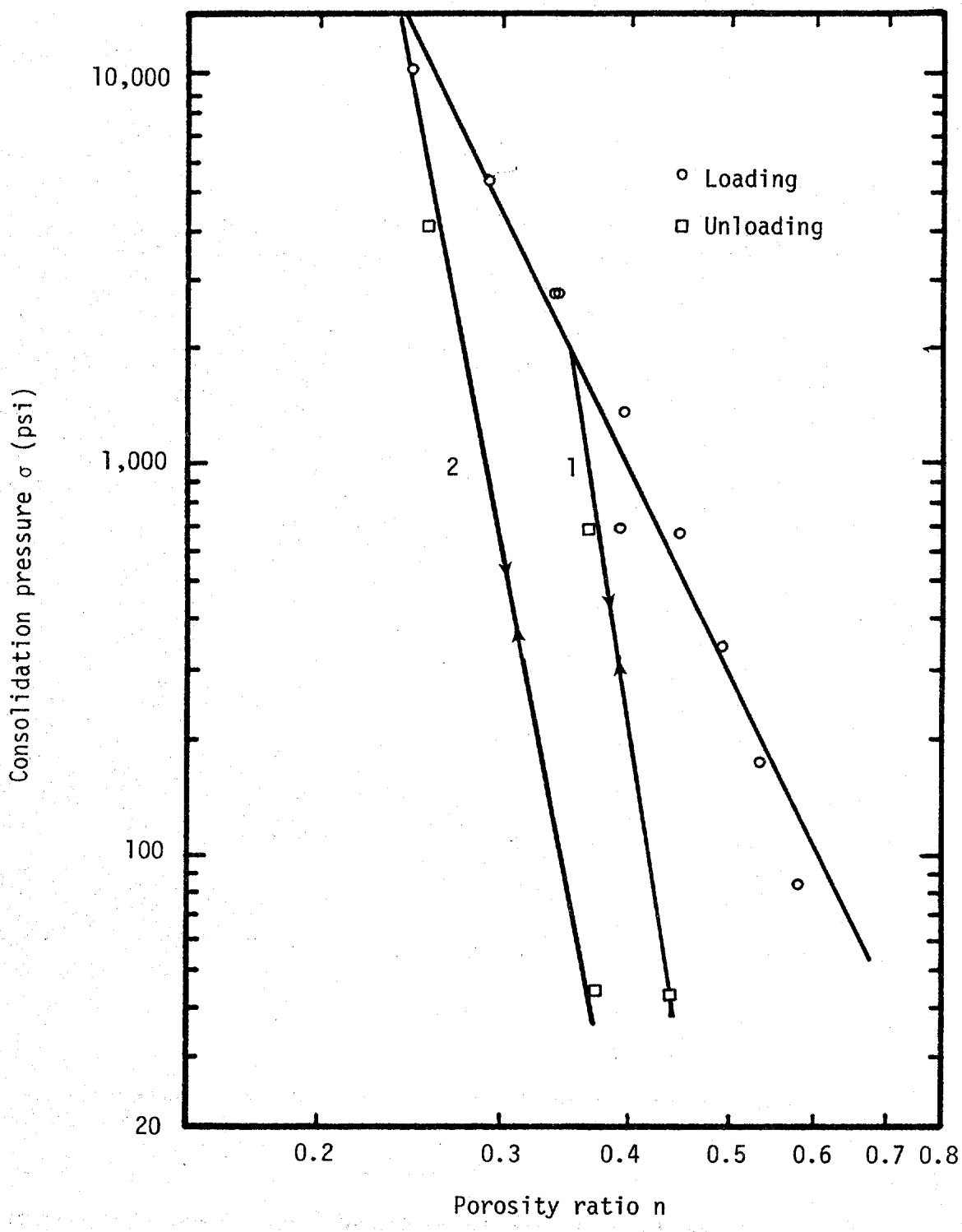

Fig. 36 - Graph of Consolidation Pressure versus Porosity Ratio for Kaolinite Tested at 60°C

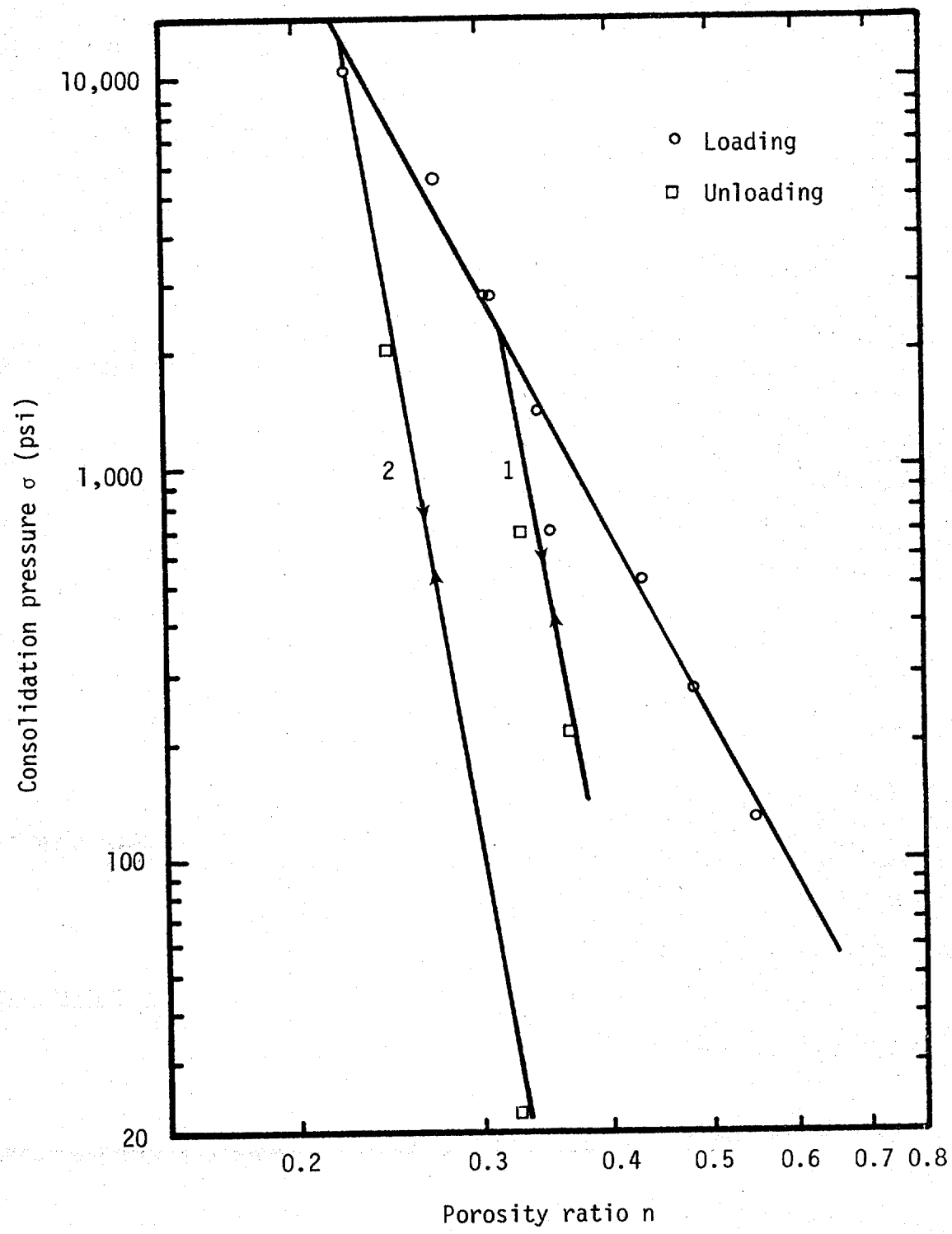

Fig. 37 - Graph of Consolidation Pressure versus Porosity Ratio for Kaolinite Tested at 90°C

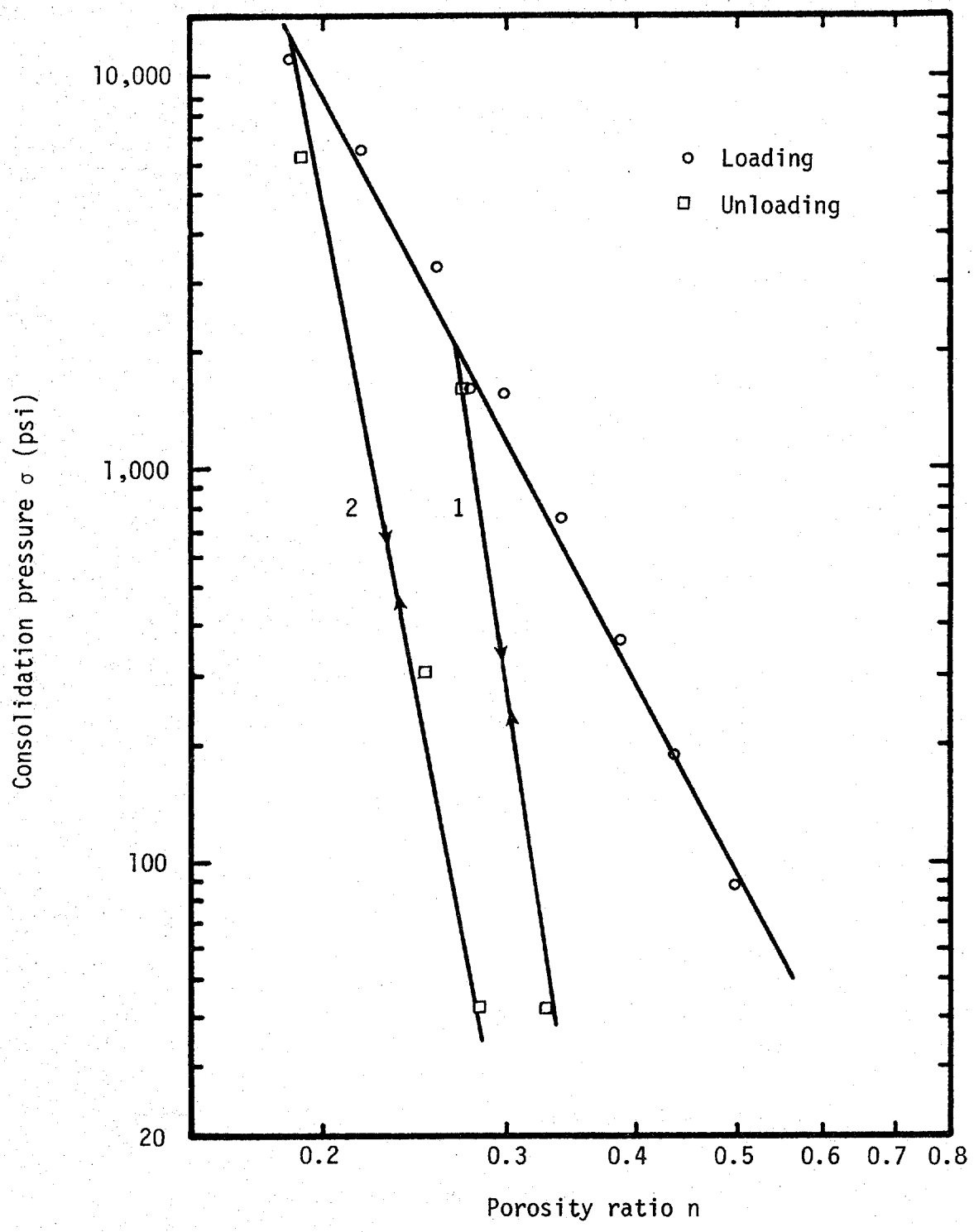

Fig. 38 - Graph of Consolidation Pressure versus Porosity Ratio for Illite Tested at 60°C

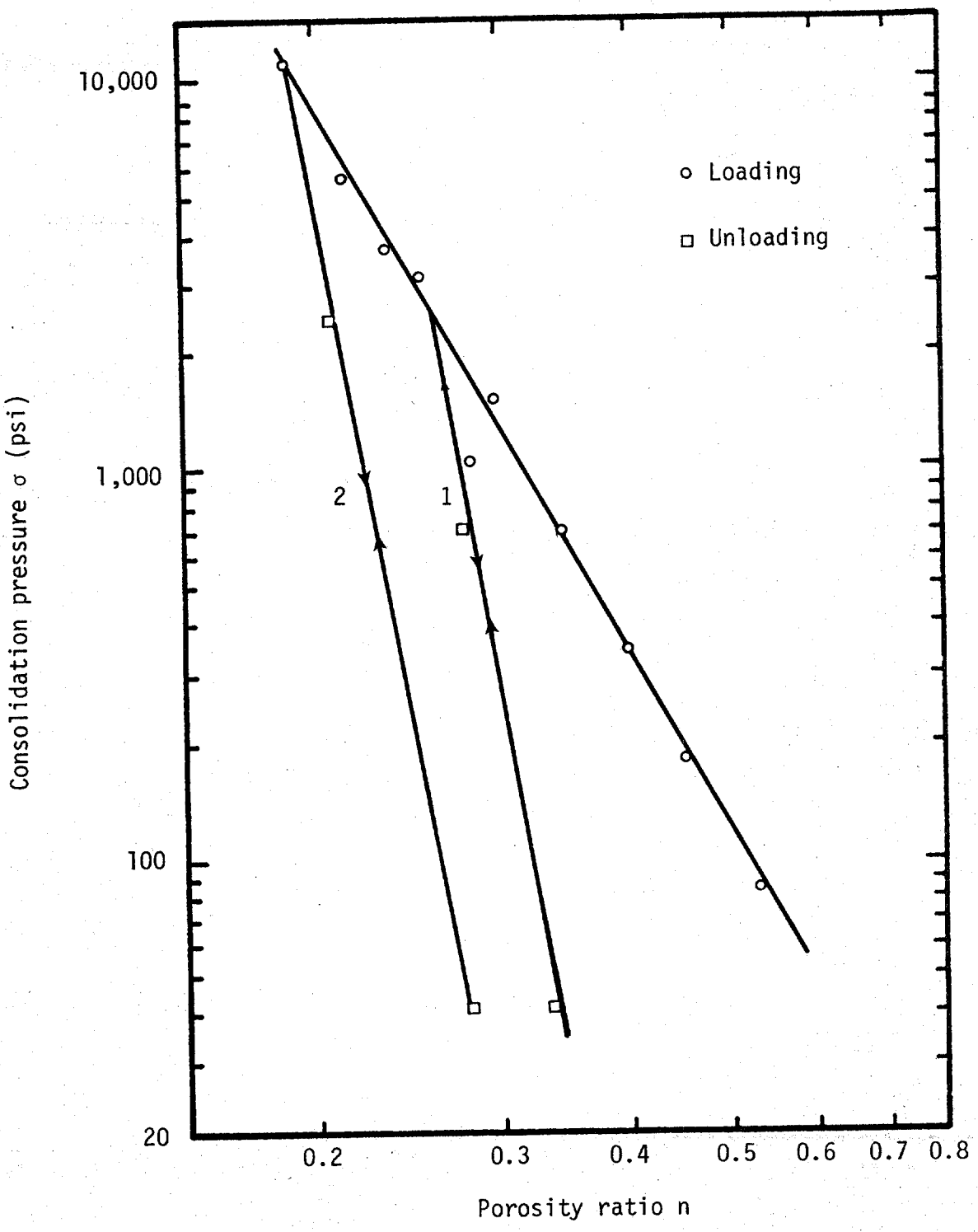

Fig. 39 - Graph of Consolidation Pressure versus Porosity Ratio for Illite Tested at 90°C

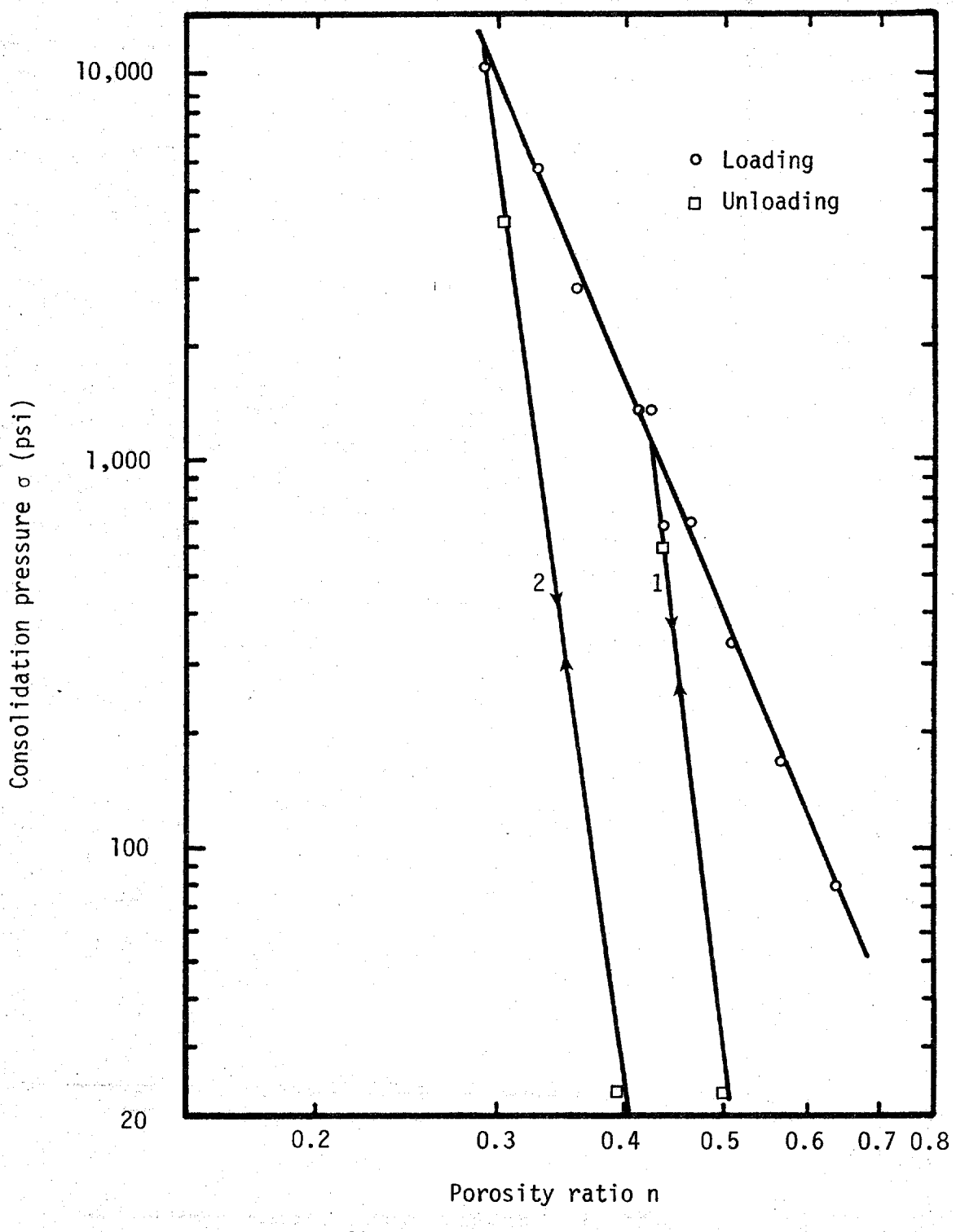

Fig. 40 - Graph of Consolidation Pressure versus Porosity Ratio for Bentonite Tested at 20°C

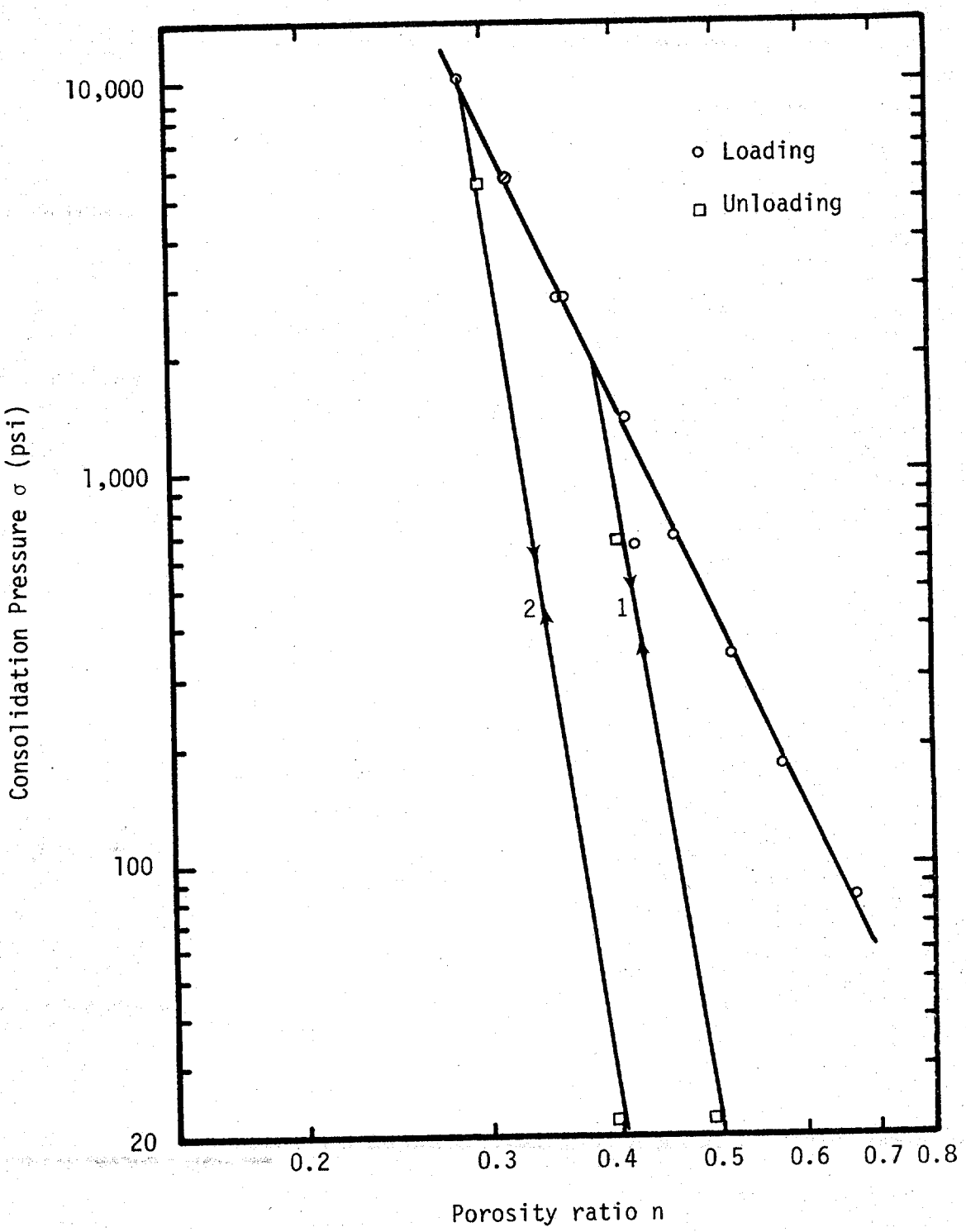

Fig. 41 - Graph of Consolidation Pressure versus Porosity Ratio for Bentonite Tested at 60°C

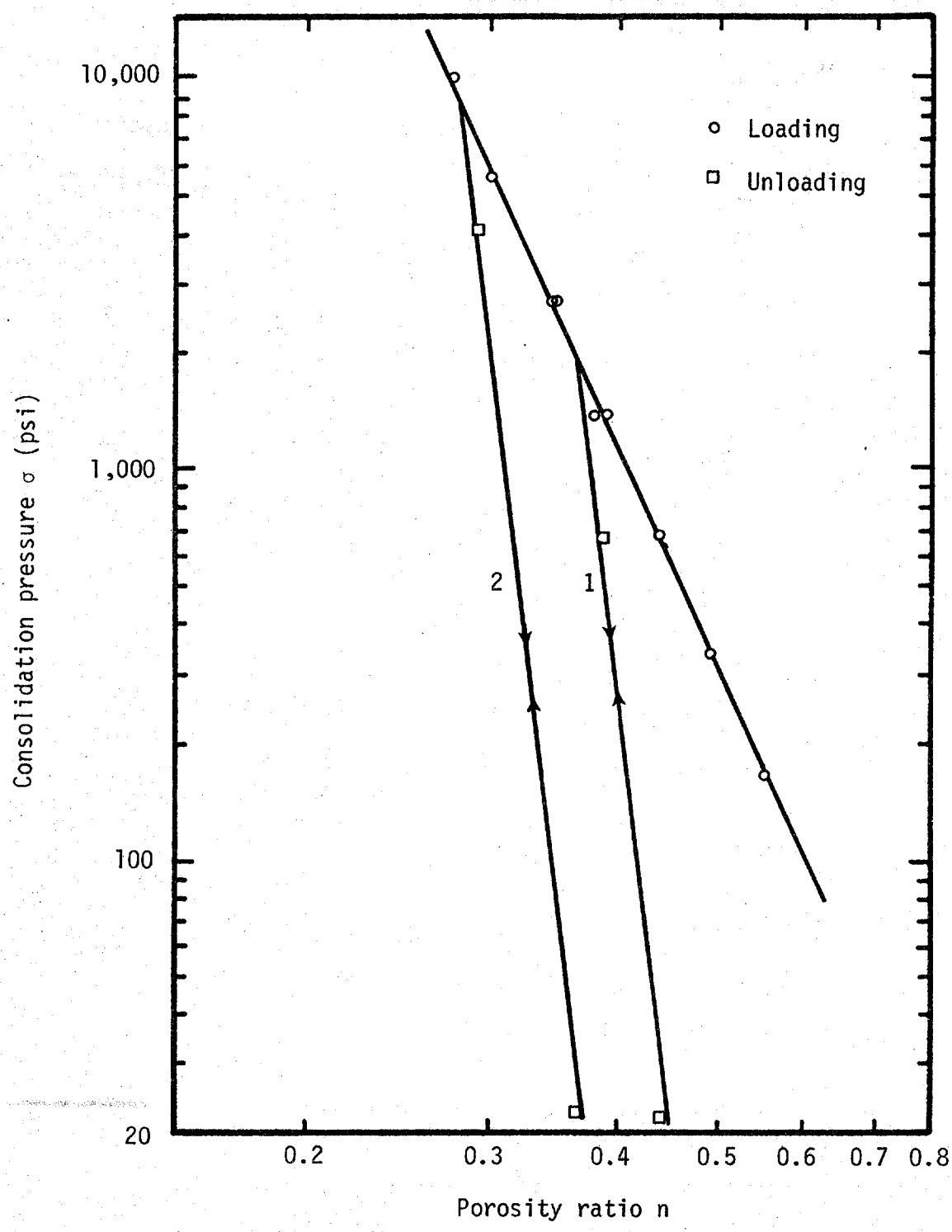

Fig. 42 - Graph of Consolidation Pressure versus Porosity Ratio for Bentonite Tested at 90°C

APPENDIX V

Sample Calculations

Determination of the height of water

$$W_w = W_T \left(\frac{w}{1+w}\right)$$

$$V_w = \frac{W_w}{\gamma_w}$$

$$H_w = \frac{V_w}{A_t}$$

Determination of the height of solid

$$W_s = W_T - W_w$$

$$V_s = \frac{W_s}{\gamma_s}$$

$$H_m = \frac{V_s}{A_t}$$

For saturated soil

$$H = H_s + H_w$$

w = moisture content

W_w = weight of water

W_T = weight of soil

V_w = volume of water

γ_w = unit weight of water

H_w = height of water

A = area of the consolidometer

W_s = weight of solid

V_s = volume of solid

γ_s = unit weight of solid

H_m = height of solid

H = height of soil

$$\text{Void ratio (e)} = \frac{\text{vol. of void}}{\text{vol. of solid}} \text{ or } \frac{\text{vol. of water}}{\text{vol. of solid}}$$

$$= \frac{H_w \cdot A_t}{H_s \cdot A_t}$$

$$= \frac{H_w}{H_s} \text{ or } \frac{H - H_s}{H_s}$$

$$\text{Porosity ratio (n)} = \frac{\text{vol. of water}}{\text{vol. of soil}} = \frac{H_w \cdot A_t}{H \cdot A_t}$$

$$= \frac{H - H_s}{H}$$

Sample calculations are based on the results obtained from experiment #I-60 (Illite consolidated at 60°C).

$w = 0.1664$

$W_T = 168.07$ g

$w_s = 2.79$ g/ce

$w = 1.026$ g/cc

$W_w = 168.07 \left(\frac{0.1664}{1 + 0.1604}\right) = 23.83$ g

$V_w = \frac{23.83}{1.026} = 23.23$ cm^3

$H_w = \frac{23.23 \text{ cm}^3}{31.68 \text{ cm}^2} \frac{1}{2.54} \frac{\text{in}}{\text{cm}} = 0.289$ in.

$W_s = (168.07 - 23.83)$ g $= 144.24$ g

$V_s = \frac{144.24}{2.79} = 51.70$ cm^3

$H_s = \frac{51.70 \text{ cm}^3}{31.68 \text{ cm}^2} \frac{1}{2.54} \frac{\text{in}}{\text{cm}} = 0.644$

$H = (0.289 + 0.644)$ in. $= 0.933$

Void ratio (e) $= \frac{0.289}{0.644} = 0.449$

Porosity ratio (n) $= \frac{0.289}{0.933} = 0.309$

Determination of coefficient of permeability.

$$k = \frac{q}{iA_t} \quad \text{. . . . . Darcy's law}$$

$$i = \frac{P}{H_w}$$

k is the coefficient of permeability

q is the flow rate

i is the pressure gradient

A_t is the cross-sectional area of the sample

P is the pressure difference between the top and bottom of the sample

H is the height of soil

γ_w is the unit weight of permeant

$$K = \frac{k \cdot \mu}{\gamma}$$

K is the absolute permeability

μ is the viscosity of the permeant @ at test temperature

γ is the unit weight of permeant @ test temperature

Sample calculation is based on the results obtained from experiment #I-60 (Illite consolidated at $60^{o}C$) at porosity ratio = 0.186.

$H = 0.7914$ in.

$P = 5040$ psi

$q = 0.55 \times 10^{-4}$ cm^3/sec

$A = 31.68$ cm^2

$$\gamma_w = 0.037 \text{ \#/in.}^3$$

$$i = \frac{5041 \text{ \#/in.}^2}{0.037 \text{ \#/in.}^3 \times 0.7914 \text{ in.}} = 1.721 \times 10^5$$

$$k = \frac{0.55 \times 10^{-4} \text{ cm}^3/\text{sec}}{31.68 \text{ cm}^2 \times 1.721 \times 10^{-5}} = 1.02 \times 10^{-11} \text{ cm/sec}$$

$$\mu \text{ @ } 60^{\circ}\text{C} = 4.8 \times 10^{-6} \text{ g-sec/cm}^2$$

$$\gamma \text{ @ } 60^{\circ}\text{C} = 1.016 \text{ g/cm}^3$$

$$K = \frac{1.02 \times 10^{-11} \text{ cm/sec} \times 4.8 \times 10^{-6} \text{ g-sec/cm}^2}{1.016 \text{ g/cm}^3}$$

$$= 4.81 \times 10^{-17} \text{ cm}^2$$

$$= 4.81 \times 10^{-17} \text{ cm}^2 \times 1.01 \times 10^{11} \text{ millidarcy/cm}^2$$

$$= 4.85 \times 10^{-6} \text{ millidarcy}$$

APPENDIX VI

Computer Program

SIMPLE MULTIPLE REGRESSION

The program used in the analysis is written by C. H. Michalak, system analyst of Texas Transportation Institute. It is a simplified version of the Wilson-Goodlatt multiple regression. The program groups the data into a sum of squares and cross products matrix. The matrix is inverted to solve for the coefficients which are used to determine the predicted values. The coefficient of determination (R^2) is also calculated to evaluate how well the function describes the data. The program is as follows:

Input Data Guide

Identification Card (20A4)		One card per problem
		Title of the problem
Basic Parameter (215)		One Card per problem
CC 1-5	NOBS	Total number of observations
CC 6-10	NVAR	Number of terms in the function

Compressibility coefficients or permeability constants and material properties (F10.6, T15, F9.4, T29, F9.2, T45, F9.5, T55, F9.5) NOBS cards per problem.

CC 1-10	Y_1	Compressibility coefficient A or permeability constant C
CC 15-24	Y_2	Compressibility coefficient B or permeability constant D
CC 29-38	X_1	Liquid limit
CC 45-54	X_2	Plastic limit
CC 55-64	X_3	% clay content

Input for the Function

The function may have a maximum of 20 terms. Each term is expressed in terms of liquid limit, plastic limit, and % clay content, which is represented by symbols X_1, X_2, and X_3 respectively. The input terms are placed in the main program following card no. 22 in the sequence of X MAT (M,1), X MAT (M,2), . . . etc. The last term, X MAT(M,NVAR) is used to define the function as the compressibility coefficients or permeability constants A, B, C, or D.

Additional Note

The constant coefficient in the function computed by the program for the compressibility coefficient B are in opposite signs. The functions for permeability constants C and D are expressed in terms of liquid limits and plastic limits only.

The program enclosed gives an example for analysing the following function:

$$A = C_o + C_1 \cdot W_\ell + C_2 \cdot W_p + C_3 \cdot \log W_\ell + C_4 - \log W_p$$

$$+ C_5 \cdot \log \%C + C_6 \cdot \%C$$

C_n, n = 0, 1, 2, . . ., are the constant coefficients.

W_ℓ is the liquid limit

W_p is the plastic limit

%C is the percent clay content.

```
C
C
C      MAIN PROGRAM  --  SIMPLE MULTIPLE REGRESSION  --
C
C
       IMPLICIT  PEAL  *  8   ( A-H,0-Z )
C
C
       DIMENSION BITA(25), VAR(25), AVG(25), HEAD(20),
     = XMAT(4J0,25), YHAT(400), YORG(400), DELTA(400)
C
C
C
     1 CONTINUE
C
C      READ & WRITE HEADER CARD
C
       READ(5,105,END=50)  ( HEAD(I), I = 1, 20 )
   105 FORMAT(  20A4  )
       WRITE(6,206)
   206 FORMAT( '1', T54, 'SIMPLE MULTIPLE REGRESSION'/)
       WRITE(6,202)  (  HEAD(I), I= 1, 20  )
   202 FORMAT( 1X, 23('*'), 2X, 20A4, 2X, 23('*')  /   )
C
       READ(5,101)  NOBS, NVAR
   101 FORMAT(  2I5  )
       NVAR=NVAR+1
       IORG =0
       KNT = 0
       M = 0
       WRITE(6,200)
   200 FORMAT(     55X,  'SUMMARY OF INPUT DATA' /   )
       DO 2 I = 1,NOBS
       M = M + 1
       READ (5,103) Y1,Y2,X1,X2,X3
   103 FORMAT (F10.6,T15,F9.4,T29,F9.2,T45,F9.5,T55,F9.5)
       Y2=0.0-Y2
       XMAT(M,1)=X1
       XMAT(M,2)=X2
       XMAT(M,3)=DLOG10(X1)
       XMAT(M,4)=DLOG10(X2)
       XMAT(M,5)=DLOG10(X1-X2)
       XMAT(M,6)=X3
       XMAT(M,NVAR)=Y1
     2 CONTINUE
     3 CONTINUE
       CALL  ERROR ( NOBS,    NVAR, IORG, BITA, ER, AVG,
     * XMAT )
       WRITE(6,211)
C
    45 CONTINUE
       WRITE(6,209) NVAR
   209 FORMAT(T53, 'COEFFICIENTS, C(I), I = 1, ', I2 /  )
C
       DO 34 II=1,NVAR
       KN=II-1
       WRITE(6,300) KN,BITA(II)
```

```
 300 FORMAT (T53, 'C(' ,I2,') = ',G13.6)
  34 CONTINUE
C
      NVR1  =  NVAR  -  1
      YBAR  =  AVG( NVAR )
      SDHAT  =  0.0D0
      SDVAR  =  0.0D0
      ESS  =  0.0D0
      DO  7  K  =  1 ,  NOBS
      YHAT(K)  =  BITA( 1)
      DO  66  M  =  1 ,  NVAR
      VAR( M )  =  XMAT(K,M)
  66 CONTINUE
      DO  6  M  =  1 ,  NVR1
      YHAT(K)  =  YHAT(K)  +  BITA(M+1)  *  VAR(M)
   6 CONTINUE
      YORG(K)  =  VAR(NVAR)
      SDHAT  =  SDHAT  +  ( YHAT(K)  -  YBAR )  **  2
      SDVAR  =  SDVAR  +  ( YORG(K)  -  YBAR )  **  2
      DELTA(K) = YORG(K) - YHAT(K)
      ESS  =  ESS  +  DELTA(K)  **  2
   7 CONTINUE
      IDF  =  NOBS  -  NVR1  -  1
      DF  =  DFLOAT( IDF )
      XSER  =  ESS  /  DF
      RMSR  =  DSQRT( XSER )
      RSQ  =  SDHAT  /  SDVAR
      IF( IORG .EQ. 0 ) GO TO 15
      RSQ = ( SDVAR - ESS ) / SDVAR
  15 CONTINUE
      RR =  DSQRT( RSQ )
      WRITE(6,203)RR, RSQ, XSER, RMSR
 203 FORMAT(     35X,'* R -- VALUE *   * R - SQUARE * ',
     ' ' MEAN SQ RESID.    ****  RMSR ****' //35X,
     * 4( G14.7, 2X) / )
      WRITE(6,204)
 204 FORMAT(53X, 'FEEDBACK SUMMARY OF DATA'//43X,
       '*** Y(OBS) ***   *** Y(HAT) ***   *** ERROR ***'/)
      WRITE(6,210)    (  YORG(K),  YHAT(K),  DELTA(K),
     * K=1, NOBS )
 210 FORMAT(  (  T44, 3( G14.7, 2X ) ) )
      WRITE(6,211)
 211 FORMAT(  '0'  )
      KNT = KNT + 1
      IF( KNT .NE. 2 ) GO TO 49
      WRITE(6,206)
      KNT= 0
  49 CONTINUE
      GO TO  1
  50 WRITE(6,250)
 250 FORMAT( '1' )
      STOP
      END
C

      SUBROUTINE  ERROR ( NOBS,     NVAR, IORG, BITA,
     * ER,AVG,XMAT )
C
      IMPLICIT  REAL  *  8  ( A-H,O-Z )
      DIMENSION  VAR(25), AMAT(26,26), BITA(25),
     = XMAT(400,25), YHAT(400), YORG(400), DELTA(400),
```

```
      = SUM(26), AVG(25), RHS(25)
C       INITIALIZE  MATRIX & SUM VECTOR TO ZERO
        N1  =  NVAR  +  1
        DO   1  M  =  1 ,  N1
        SUM(M)  =  0.0D0
        DO   1  N  =  1 ,  N1
        AMAT(M,N)  =  0.0D0
      1 CONTINUE
        OBS  =  DFLOAT( NOBS )
        DO  3  K  =  1 ,  NOBS
        DO  22  M  =  1 ,  NVAR
        VAR( M )  =  XMAT( K,M )
     22 CONTINUE
C       BUILD MATRIX & SUM VECTOR
        DO   2  M  =  1 ,  NVAR
        SUM(M)  =  SUM(M)  +  VAR(M)
        DO   2  N  =  1 ,  NVAR
        AMAT(M,N)  =  AMAT(M,N)  +  VAR(M)  *  VAR(N)
      2 CONTINUE
      3 CONTINUE
C       CALCULATE AVERAGE & RIGHT HAND SIDE
        DO   4  N  =  1 ,  NVAR
        RHS(N)  =  AMAT(N,NVAR)
        AVG(N)  =  SUM(N)  /  OBS
      4 CONTINUE
C       DO NOT CORRECT MATRIX IF GOING THRU ORIGIN
        NVR1  =  NVAR  -  1
        IF( IORG  .EQ.  1 )  GO  TO  7
C       CORRECT MATRIX
        DO   5  M  =  1 ,  NVAR
        DO   5  N  =  1 ,  NVAR
        AMAT(M,N)=AMAT(M,N)-(SUM(M)*SUM(N) )/OBS
      5 CONTINUE
C       CORRECT RIGHT HAND SIDE
        DO   6  M  =  1 ,  NVAR
        RHS(M)  =  AMAT(M,NVAR)
      6 CONTINUE
C       INVERT THE MATRIX
      7 CONTINUE
        CALL  DIMEQN ( AMAT, NVR1, 0.1D-37, DET  )
        IF( DET  .NE.  0.0D0 )  GO  TO  8
        WRITE(6,200)
    200 FORMAT(  /  10X,  '*** ILL CONDITIONED MATRIX',
     * ' -OEFFICIENTS QUESTIONABLE' // )
        ER  =  99.0D25
        RETURN
      8 CONTINUE
        BETA0  =  AVG( NVAR )
        DO 16 M=1,NVR1
        BETA0  =  BETA0  -  AMAT(M,NVAR)  *  AVG(M)
     16 CONTINUE
        BITA( 1)  =  BETA0
        DO  11  M  =  2 ,  NVAR
        BITA(M)  =  AMAT(M-1,NVAR)
     11 CONTINUE
        IF( IORG  .EQ.  1 )  GO  TO  10
C       CALCULATE ERROR = AMSD
        SSREG  =  0.0D0
        DO   9  L  =  1 ,  NVR1
        SSREG  =  SSREG  +  RHS(L)  *  AMAT(L,NVAR)
      9 CONTINUE
```

```
142           SSER   =  RHS(NVAR)  -  SSREG
143           DFER   =  OBS  -  NVR1  -  1.0D0
144           ASQER  =  SSER  /  DFER
145           IF( ASQER  .LE.  0.0D0 )  GO  TO  14
146           ER  =  DSQRT( ASQER )
147           RETURN
      C       CALCULATE ERROR IN FEEDBACK
148        10 BITA ( 1 )  =  0.0D0
149           YBAR   =  AVG(NVAR)
150           SDHAT  =  0.0D0
151           ESS    =  0.0D0
152           DO  13  K  =  1 ,  NOBS
153           YHAT(K)  =  BITA( 1 )
154           DO  15  M  =  1 ,  NVAR
155           VAR( M )  =  XMAT( K,M )
156        15 CONTINUE
157           DO  12  M  =  1 ,  NVR1
158           YHAT(K)  =  YHAT(K)  +  BITA(M+1)  *  VAR(M)
159        12 CONTINUE
160           YORG(K)  =  VAR( NVAR )
161           SDHAT  =  SDHAT  +  ( YHAT(K)  -  YBAR )  **  2
162           DELTA(K)  =  YHAT(K)  -  YORG(K)
163           ESS  =  ESS  +  DELTA(K)  **  2
164        13 CONTINUE
165           DF  =  OBS  -  1.0D0  -  DFLOAT( NVR1 )
166           ER  =  DSQRT( ESS  /  DF )
167           RETURN
168        14 WRITE(6,201)
169       201 FORMAT(/ 10X,'NEGATIVE SSER DUE TO ROUND OFF'/)
170           ER  =  99.0D25
171           RETURN
172           END

173           SUBROUTINE DIMEQN ( A, N, EPS, DET  )
      C
      C     SUBROUTINE DIMEQN IS A DOUBLE  PRECISION MATRIX
      C     INVERSION ROUTINE THAT SEEKS MAXIMUM PIVIOT ELEMENTS
      C     AND INVERTS IN PLACE
      C     A = ARRAY CONTAINING MATRIX OF COEFFICIENTS TO BE
      C     INVERTED
      C     N = ORDER OF A
      C     EPS = MINIMUM ALLOWABLE VALUE OF MAXIMUM PIVIOT
      C     BEFORE MATRIX IS TERMED SINGULAR
      C     DET = VALUE OF DETERMINANT OF THE MATRIX
      C
174           IMPLICIT  REAL  *  8  ( A-H,O-Z )
175                INTEGER*2  IPIV, ICJ
176           DIMENSION Y(50), ICJ(50), IPIV(2,50), A(26,26)
177           M  =  N  +  1
178                 IF(N .EQ. 1)  GO TO 1
179                  M = N + 1
180                  NX = N + 1
181           DET=1.0
182                ASSIGN 205 TO IZERO
183                   DO 1000  K=1,N
184           KM1=K-1
185                IF(KM1 .GT. 0)  ASSIGN 95 TO IZERO
186           BIGA=0.0
187           DO 101 I=1,N
188           DO 101 J=1,N
189                GO TO IZERO, (95,205)
```

* R -- VALUE *	* R - SQUARE *	MEAN SQ RESID,	**** RMSR **
0.4257544	0.1812668	18.84149	4.340679

FEEDBACK SUMMARY OF DATA

*** Y(OBS) ***	*** Y(HAT) ***	*** ERROR ***
0.5240000D-01	-2.625766	2.678166
0.1040000	-0.8283783	0.9323783
0.7200000D-02	0.6462023	-0.6390023
0.8400000D-01	1.683978	-1.599978
0.1200000D-02	0.4234700	-0.4222700
0.1800000D-01	0.4743614	-0.4563614
0.2660000D-01	-1.494165	1.520765
3.020000	1.448114	1.571886
0.3550000	0.9264971	-0.5714971
0.9000000D-01	0.2471159	-0.1571159
0.3580000	1.607062	-1.249062
0.5280000	-0.3626712	0.8906712
0.3110000	0.3438066	-0.3280658D-01
0.4650000	0.9538556	-0.4888556
0.4360000	1.489019	-1.053019
0.4000000	1.136259	-0.7362590
0.2800000	-0.6907120	0.9707120
2.090000	0.1286796D-01	2.077132
0.4670000D-01	2.533924	-2.487224
0.8600000D-01	0.6590234	-0.5730234
0.9090000	2.794419	-1.885419
0.2330000	1.950491	-1.717491
0.3100000	2.012142	-1.702142
0.1670000	1.901154	-1.734154
0.1390000D-01	-0.4674304	0.4813304
0.2190000	-0.3305571	0.5495571
1.334000	0.5930123	0.7409877
0.1240000	1.966410	-1.842410
0.2220000	1.506351	-1.284351
0.5580000	1.940821	-1.382821
2.040000	-1.835128	3.875128
0.1300000	-0.2744765	0.4044765
0.8800000D-01	1.872456	-1.784456
1.603000	3.185270	-1.582270
0.8030000	4.040968	-3.237968
0.2570000	2.302264	-2.045264
0.3900000	1.746762	-1.356762
0.1480000D-01	4.489158	-4.474358
0.3370000D-01	1.863340	-1.829640
0.1433000	-0.2497471	0.3930471
2.242000	-0.2601937D-01	2.268019
1.799000	5.667187	-3.868187
0.3480000	4.152768	-3.804768
2.728000	3.595404	-0.8674040
3.592000	4.289929	-0.6979291
0.3720000	2.945628	-2.573628
15.17000	5.870360	9.299640
1.060000	3.494664	-2.434664
4.480000	4.254850	0.2251501
28.41000	4.716485	23.69352

```
      95 DO 102 II=1,KM1
         IF(I.EQ.IPIV(1,II).OR.J.EQ.IPIV(2,II)) GO TO 101
102   CONTINUE
205      CONTINUE
         IF(DABS(A(I,J)).LT.BIGA) GO TO 101
         BIGA=DABS(A(I,J))
         IPIV(1,K)=I
         IPIV(2,K)=J
101   CONTINUE
         IF(BIGA.GE.EPS) GO TO 201
         DET = 0.0
         GO TO 200
201   IR=IPIV(1,K)
         JC=IPIV(2,K)
         BIGA=A(IR,JC)
         DET=DET*BIGA
         DO 103 LL=1,M
103   A(IR,LL)=A(IR,LL)/BIGA
         A(IR,JC)=1.0/BIGA
         DO 100 LLL=1,N
         AJCK=A(LLL,JC)
         IF(LLL.EQ.IR) GO TO 100
         A(LLL,JC)=-AJCK/BIGA
         DO 104 L4=1,M
         IF(L4.EQ.JC) GO TO 104
         A(LLL,L4)=A(LLL,L4) -AJCK*A(IR,L4)
104   CONTINUE
100   CONTINUE
1000     CONTINUE
         DO 105 I=1,N
         IR=IPIV(1,I)
         ICJ(IR)=JC
105   CONTINUE
         ICT=0
         NM1=N-1
         DO 106 I=1,NM1
         IP1=I+1
         DO 106 J=IP1,N
         IF(ICJ(J).GE.ICJ(I)) GO TO 106
         ITEMP=ICJ(J)
         ICJ(J)=ICJ(I)
         ICJ(I)=ITEMP
         ICT=ICT+1
106   CONTINUE
         IF((ICT/2)*2.NE.ICT.AND.N.NE.1) DET=-DET
         DO 107 J=1,M
         DO 108 I=1,N
         JC=IPIV(2,I)
         IR=IPIV(1,I)
108   Y(JC)=A(IR,J)
         DO 107 K=1,N
107   A(K,J)=Y(K)
         DO 110 I=1,N
         DO 111 J=1,N
         IR =IPIV(1,J)
         JC=IPIV(2,J)
111   Y(IR)=A(I,JC)
         DO 110 K=1,N
110   A(I,K)=Y(K)
200   RETURN
        1     DET = A(1,1)
```

```
251                     A(1,2)  =  A(1,2)  /  A(1,1)
252                     A(1,1)  =  1.0D0  /  A(1,1)
253                     RETURN
254             END
        //$DATA
```

SIMPLE MULTIPLE REGRESSION

ATTERBERY LIMITS-COMPRESSIBILITY

SUMMARY OF INPUT DATA

COEFFICIENTS, C(I), I = 1, 7

```
C( 0) =   -22.6378
C( 1) = -0.533951D-01
C( 2) = -0.201090D-01
C( 3) =    63.9880
C( 4) =   -32.1167
C( 5) =   -30.1265
C( 6) =   0.966907D-01
```